Entropic Segregation at Surfaces of Polymer Melts

by

Pendar Mahmoudi

A thesis
presented to the University Of Waterloo
in fulfillment of the
thesis requirement for the degree of
Doctor of Philosophy
in
Chemical Engineering

Waterloo, Ontario, Canada, 2018

Examining Committee Membership

The following served on the Examining Committee for this thesis. The decision of the Examining Committee is by majority vote.

Supervisor :	Dr. Mark W. Matsen, Professor, Dept. of Chemical Engineering, University of Waterloo
External Examiner:	Dr. An-Chang Shi, Professor, Dept. of Physics & Astronomy, McMaster University
Internal Member :	Dr. Nasser M. Abukhdeir, Associate Professor, Dept. of Chemical Engineering, University of Waterloo
Internal Member :	Dr. Leonardo Simon, Professor, Dept. of Chemical Engineering, University of Waterloo
Internal-External Member :	Dr. Russell Thompson, Associate Professor, Dept. of Physics & Astronomy, University of Waterloo

Author's Declaration

This thesis consists of material all of which I authored or co-authored: see Statement of Contributions included in the thesis. This is a true copy of the thesis, including any required final revisions, as accepted by my examiners.

I understand that my thesis may be made electronically available to the public.

Statement of Contributions

The majority of findings in this work have been published in co-authored papers, for which unless stated otherwise, all results were obtained by me. The material presented in chapters 3 and 4 have been published in three separate papers. All that is shown in the concluding section pertaining to future studies, is from a work in progress. The contributions for the aforementioned works, are as follows.

The simulation results shown in this work were obtained in collaboration with William S. R. Forrest and Dr. Thomas M. Beardsley.

The worm-like chain results presented in the outlook chapter are from a collaboration with Steven Blaber.

The Gaussian chain model results were provided by Dr. Russell K. W. Spencer.

All of the work mentioned above has been under the guidance and supervision of Prof Mark W. Matsen.

Abstract

Throughout recent years, polymers have been one of the most widely used materials in industry due to their suitability to a vast variety of fields from construction to biomedical and technological utilities. Their extensive and broad range of applications, demands the ever increasing necessity for extensive insight into the behavior and properties of this group of materials. Whilst some aspects of this demand can be addressed through experiments, the inherent difficulties and restrictions of studying polymeric systems with greater degrees of complexity, have motivated researchers to discover alternative means of examining these cases of interest effectively. The advent of polymer theory as well as the development of appropriate computer simulation techniques have proven to be invaluable sources of new insight. With the ever increasing use of polymeric materials in industrial applications, such as highly efficient coatings and adhesives, an in-depth knowledge of their behavior close to surfaces is needed. Moreover, for the development of effective materials, an accurate understanding of their physical properties such as their surface tension is also required.

In this light, our goal is to study the surface behavior of polymers melts, whether they be monodisperse or polydisperse. The study of the former system, which is a melt composed of chains of a single length, is more attractive theoretically as a basis for a comprehensive study of influential parameters. However, in reality, most polymeric materials are polydisperse, hence motivating the detailed assessment of both. Surfaces behave as reflecting boundaries for the most part but violations are seen to occur due to a number of parameters such as the finite width of surface profiles, discreteness of chains as well as excluded volume effects. These result in an excess of end monomers being observed at the surfaces of monodisperse melts and shorter chains segregating to the surfaces of polydisperse ones, from which the surface tension is seen to be affected as well. The source of these migrations could either be enthalpic, with a preference for ends to be closer to surfaces, but also purely entropic which is the case studied here. With the inherent difficulties of experimentally isolating these entropic phenomena, a more successful outcome is obtained through their theoretical study. Hence, for both of the aforementioned systems, we shall be performing mean-field calculations as well as Monte Carlo simulations, in addition to comparing them with universal predicted forms to test their accuracy.

Acknowledgements

First and foremost a sincere thanks for the mentorship and guidance of my supervisor, Prof. Mark Matsen as well as his patience while introducing me to the vast and intriguing field of polymer physics. The variety of topics explained and characterized by the awe-inspiring field of physics, never ceases to amaze me and the concepts I learned throughout this project were no exception. Lessons offered in conducting research, critical thinking and collaborations with fellow scientists convey a small portion of what I have been taught under his supervision.

It goes without saying that many of the successes I have obtained thus far would not have been possible, without Prof Nasser Abukhdeir believing in my abilities and providing me with this wonderful opportunity. His guidance, whether it be study or life related, has been invaluable. This journey started with my fascination with the field of Chemical Engineering and the path I have undertaken at the University of Waterloo, which would not have been possible without being given this chance, has only strengthened this belief.

My gratitude extends to Prof. Simon who gave me new insight into the industrial aspects of polymer research through his lectures. Needless to say the comments and observations provided by him as well as Prof. Thompson, as members of my committee, have taught me to be critical of my work and see it in new light, which is greatly appreciated.

It would be remiss of me to not recall the vast number of insightful conversations I have had with fellow members of my group, Dr Spencer and Dr Beardsley. There was never a dull moment with you there.

Having spent this time away from my country, there have been many who have made this place a home away from home. To all my friends, your support has made all the difference.

Last but not least, my sincere gratitude to my family who have always been pillars of strength. I thank you for your optimism, encouragement, advice and willingness to skype no matter the time difference. It has made all of this possible and for that I am forever grateful.

Dedication

To my family for their unconditional, unwavering support.

Also for those we lost, who inspired my love of science. You are remembered.

Table of Contents

List of Figures xi

List of Symbols xiv

1 Introduction 1

1.1 Polymer bulk behavior . . . 3

1.1.1 Average size of a polymer chain . . . 5

1.2 Polymer surface behavior . . . 7

1.2.1 Silberberg Hypothesis . . . 8

1.3 Methods used in theoretical studies . . . 10

1.4 Literature review . . . 12

1.4.1 Monodisperse melts . . . 12

1.4.2 Polydisperse melts . . . 16

1.5 Outline of thesis . . . 18

2 Theory and simulation 19

2.1 Off-lattice model . . . 19

2.1.1 Chain in an external field . . . 20

2.1.2 Self-consistent field theory for polydisperse melts . . . 25

2.1.3 Semi-analytical calculation for polydisperse melts . . . 29

2.2 Lattice model . . . 35

2.2.1 Self-consistent field theory for polydisperse melts 35
2.2.2 Semi-analytical calculation for polydisperse melts 37
2.2.3 Monte Carlo simulations 38

3 Monodisperse melts **44**
3.1 Off-lattice model 45
3.1.1 Theory 45
3.1.2 Results 47
3.1.3 Discussion 57
3.2 Lattice model 60
3.2.1 Theory and simulation 60
3.2.2 Results 61
3.2.3 Discussion 64

4 Bidisperse Melts **65**
4.1 Off-lattice model 67
4.1.1 Theory 67
4.1.2 Results 70
4.1.3 Discussion 77
4.2 Lattice model 78
4.2.1 Theory and simulation 78
4.2.2 Results 80
4.2.3 Discussion 84

5 Conclusions **86**
5.1 Summary 87

References **90**

Appendices **103**

A Convolution integral for infinitely long chains **104**

B Wormlike Chain model **105**

B.1 Literature review 106

B.2 Theory 109

List of Figures

1.1 A generic pair correlation function from [1] 4

1.2 Polymer chain with N beads and N-1 bonds 5

1.3 Illustration of the Silberberg argument [2]. (a) shows a polymer taken from the bulk, while (b)-(d) show configurations of equivalent energy (and thus probability) obtained by reflections about the plane $z = 0$. The surface is created by removing (a)-(c) and doubling the probability of (d). 8

2.1 Illustration of the (a) slithering snake move and the (b) crankshaft move. . 41

3.1 (a) Concentration of ends, $\phi_e(z)$, and (b) self-consistent field, $w(z)$, for the sigmoidal polymer profile, eq. (3.5), of width $\xi = a$, as shown by the dashed curve in plot (a). The red curves denote the infinite molecular weight limit while the finite length results are shown by the black curves. 47

3.2 Analogous plots to those of fig. 3.1, but calculated for a linear polymer profile, eq. (3.6), of width $\xi = a$. 48

3.3 The surface excess of ends per unit area, $\Delta\sigma_e$, plotted in terms of the width, ξ, of the concentration profile in the infinite molecular-weight limit. The ratio appearing in the vertical axis is precisely the A appearing in eqs. (3.10), (3.11), (3.13) and (3.20). 49

3.4 Correction to $G_N^0(z) \approx G_\infty(z)$ plotted on the (a) monomer and (b) molecular length scales for different values of N. The red curves show $A\sqrt{6/\pi}G_\infty(z)$ and $A\sqrt{6/\pi}\exp(-3z^2/2a^2N)$, depicting the short and long range parts of equation 3.10, respectively. 51

3.5 Correction to $\phi^0(z) \approx \phi(z)$ plotted on the (a) monomer and (b) molecular length scales for different polymerizations, N. The red curves denote $4A\sqrt{6/\pi}\phi(z)$ and $4A\sqrt{6/\pi}f(z/aN^{1/2})$, depicting the short and long range parts of equation 3.11, respectively. 52

3.6 Correction to $\phi_e(z) \approx G_\infty(z)$ plotted on the (a) monomer and (b) molecular length scales for polymers of various lengths N, calculated for a sigmoidal surface profile of width $\xi = a$. The red curves denote $AB(0)G_\infty(z)$ and $AB(z/aN^{1/2})$, verifying both length scales of the semi-analytical formulation as proposed by equation 3.13, respectively. 53

3.7 Analogous plots to those in figure 3.6, but calculated for a linear surface profile of width $\xi = a$. 54

3.8 Entropic contribution to the surface tension, γ_{en}, as a function of the width, ξ, of the concentration profile in the infinite molecular-weight limit. The dimensionless ratio plotted on the vertical axis equates to the Γ_∞ appearing in equation 3.20. 55

3.9 Entropic contribution to the surface tension, γ_{en}, as a function of polymerization, N. The symbols denote the full SCFT calculation while the red curves denote the approximation from equation 3.20. 57

3.10 (a) Total concentration, $\phi(z)$, for a monodisperse melt of $N = 80$ polymers from simulation without (blue curve) and with (black curve) an external field, $w(z)$. The inset shows the field for the step profile. (b) distribution of end monomers, $\phi_e(z)$, from the simulation for the step profile (solid curve) compared to SCFT (dashed curve). 62

3.11 (a) Depletion of end monomers in monodisperse melts of various polymerizations, N, obtained from simulation (solid curves) and SCFT (dashed curves). (b) scaling plot comparing the results to the semi-analytical prediction in equation 3.13 (red curve). 63

4.1 Numerical values of A and Γ_∞ evaluated using eqs. (3.9) and (3.17), respectively. The dashed curves give approximate values corresponding to the Gaussian chain model from [3]. 69

4.2 Polymer concentrations, $\phi_\nu(z)$ ($\nu = s$ or l), in a 50:50 mixture of $N_s = 40$ and $N_l = 320$ polymers, calculated for a surface profile, $\phi(z)$, of width $\xi = a$. The dashed curve denotes the reference concentration, $\phi(z)/2$, corresponding to zero surface segregation. 70

4.3 Dependence of $C(\zeta)$ on $\alpha \equiv N_l/N_s$ and $\bar{\phi}_s = 1 - \bar{\phi}_l$. Plot (a) demonstrates the dependence of its magnitude on the parameters, while plots (b) and (c) show how its shape changes with α and $\bar{\phi}_s$, respectively. 71

4.4 Excess concentration of short polymers, $\delta\phi_s(z) \equiv \phi_s(z) - \bar{\phi}_s\phi(z)$, plotted on the (a) monomer and (b) molecular length scales for $\alpha = 8$ and $\bar{\phi}_s = 0.5$. Dashed curves denote SCFT results and solid curves correspond to the approximation in equation (4.12). 72

4.5 (a) Surface excess of short polymers, θ_s, as a function of the surface width, ξ, calculated for different chain lengths, N_s. (b) Entropic surface tension, γ_{en}, as a function of N_s calculated for different values of ξ. All results are for fixed values of $\alpha \equiv N_l/N_s = 8$ and $\bar{\phi}_s = \bar{\phi}_l = 0.5$. The SCFT calculations are denoted by symbols and the semi-analytical approximations, equations 4.15 and 4.16, are plotted with continuous curves. 74

4.6 Analogous plots to those of figure 4.5 examining the dependence of θ_s and γ_{en} on α for fixed values of $\xi = a$ and $\bar{\phi}_s = \bar{\phi}_l = 0.5$. 75

4.7 Analogous plots to those of figure 4.5 examining the dependence of θ_s and γ_{en} on $\bar{\phi}_s$, for fixed values of $\xi = a$ and $\alpha = 8$. 76

4.8 (a) Concentration of short chains, $\phi_s(z)$, for bidisperse melts of different polymerizations with fixed $\alpha \equiv N_l/N_s = 8$ and $\bar{\phi}_s = 0.5$, obtained from simulation (solid curves) and SCFT (dashed curves). (b) scaling plot comparing the results to the semi-analytical prediction in eq 4.22 (red curve). (c) integrated excess of short polymers, θ_s, from simulations (crosses) and SCFT (circles) compared to the semi-analytical prediction in equation 4.15 (red line). 80

4.9 (a) Plot of the excess concentration of short chains in a bidisperse melt for $N_l = 80$ and 320 with fixed $N_s = 20$ and $\bar{\phi}_s = 0.5$, obtained from simulation (solid curves) and SCFT (dashed curves). (b) Integrated excess of short polymers from simulation (crosses) and SCFT (circles). The red curves denote the semi-analytical predictions. 82

4.10 Analogous plots to those of figure 4.9 showing the dependence on $\bar{\phi}_s$ for $N_s = 20$ and $N_l = 160$. 83

B.1 Schematic of the (a) Gaussian and the (b)worm-like chains 109

B.2 Depletion of ends in the bulk for (a) constant persistence length $l_p = 0.25$ and (b) constant end-to-end length $R_0 = 8$ 118

List of Symbols

n	number of polymer chains
N	number of monomers in polymer chains
ρ_0	monomer concentration
V	total volume
$\mathcal{A}$	surface area
L	characteristic system size
$\mathbf{r}$	position vector
$\mathbf{R}$	bond vector
$\mathbf{u}$	tangent vector
s	position along chain contour
a	statistical segment length
b	bond length
R_0	rms end-to-end length
l_c	contour length
l_p	persistence length
ξ	interfacial width
κ	compressibility of melt
N_n	number average degree of polymerization
N_w	weight average degree of polymerization
θ_N	integrated amount for chains of length N
k_B	Boltzmann constant
T	temperature
H	Hamiltonian

$w(\mathbf{r})$	self-consistent field
$u_b(\mathbf{R})$	bond potential
Q	partition function
G	forward propagator
$G^\dagger$	backward propagator
$w_\infty(z)$	field for infinitely long chains
$G_\infty(z)$	propagator for infinitely long chains
$\phi_N(z)$	concentration for chains of length N
$\phi_N^0(z)$	concentration for chains of length N in w_∞
$\phi(z)$	total concentration
$\phi_e(z)$	concentration of end monomers
$\bar{\phi}_N$	bulk volume fraction for chains of length N
μ	chemical potential
γ_{en}	entropic contribution to surface tension
A	surface excess of ends per unit area for infinitely long chains
Γ_∞	entropic contribution to surface tension for infinitely long chains
$C(\zeta)$	universal function for excess of short chains in bidisperse melts
$B(\zeta)$	universal function for depletion of ends in monodisperse melts
α	ratio of lengths in bidisperse melts
η	ratio of volume fractions in bidisperse melts
λ	simple mixing parameter
$\mathcal{K}$	bending rigidity

Chapter 1

Introduction

From the introduction of the macromolecular hypothesis by Staudinger in 1920 [4], which claimed polymers are made up of covalently bonded elementary units called monomers, the field of polymer science has advanced greatly [5, 6]. The following thirty years saw the establishment of fundamental polymer physics concepts as well as the production of polymer synthesis tools. Today, polymers are of vital importance in many commercial and industrial sectors, in light of their ability to be geared towards specific requirements, due to their customizable constituent molecules [7]. They are widely used in manufacturing products such as adhesives, protective coating and lubricants [8] for which most of the processing is carried out in the molten state. The industrial importance and relevance of these polymer melts, which are liquid polymers in the absence of solvents, resulted in an increased interest in their study to aid the development of the aforementioned applications. More specifically, the presence of polymer melts in proximity of solid surfaces is inherent in these utilities for which a detailed understanding is undeniably required.

The placement of polymer melts near surfaces affects their conformations, which will result in differences in bulk and surface behavior. With our focused interest devoted to the latter, we will present the general aspects of the bulk behavior before noting the differences among the two. The conformations of polymer chains in melts, in other words the way the monomers are arranged in space which in turn determines the spatial structure of the chain, are inherently simpler than real chains due to the fact that they are ideal chains. That is to say, the correlations between various chains are suppressed which makes the conformations of one to be almost independent of all others [9, 10]. This ideal chain behavior is realized because of excluded volume interactions between the segments being canceled out due to an effect called screening, which is best explained for the bulk behavior of polymers. Our first focus here will be to demonstrate one result of the screening effect in the bulk of

polymer melts, which is a universal scaling for the end-to-end distances of these chains, before focusing on their surface behavior.

Before the consideration of the surface of polymer melts, a review of previous literature looking at these systems will motivate the significance of our findings. In terms of experimental studies, the majority of preceding attempts convey difficulties encountered in these methods. This is both due to the multi-scale nature of these systems in addition to the level of accuracy desired for some topics of interest, which may become unfeasible using experiments. In this light, we owe a great portion of the current knowledge in this topic to theory as well as simulations. Hence, we shall review these approaches to highlight their triumphs in addition to their downfalls. With the methodology of the work at hand being a theoretical one and our focus being on polymer melt behavior, a detailed literature review on previous developments in this field shall be presented. This review will be considered in two sections, one aimed toward studies implemented on melts containing chains of the same length and the other considering melts consisting of chains of different lengths, which are denoted as monodisperse and polydisperse melts respectively. The monodisperse melt is a good foundation to consider the basics of the theory, but most polymeric materials are polydisperse and as such it is of great importance to characterize their behavior. The introduction shall be concluded by an outline of the thesis to provide a general scope and structure for the reader.

1.1 Polymer bulk behavior

With the large number of monomers in a polymer, one would think that gaining knowledge on the conformations of individual chains would be a daunting task [11]. However the opposite is seen to be true where the large molecular weight of these molecules, for which Staudinger first used the appropriate term of "macromolecules", makes the atomic detail less noticeable and bestows universal behavior on different polymer types [10, 12]. An important property of this nature was first mentioned as part of the Flory hypothesis in 1949 [6, 13]. In the aforementioned work, it was stated that the conformations of a polymer molecule situated in a medium of similar polymer molecules would be undistorted by interference effects. In other words, Flory noted that the scaling of the random flight model as stated by Kuhn [14] would be restored for these chains.

The random flight approximation stated the configuration of a chain to be equal to a particle going through an unrelated series of displacements, the directions of which are entirely random and independent of one another [15]. This approximation gave the distance between two ends of such a path as proportional to the length of each step (segment length) as well as the square root of the number of steps taken (the number of monomers). For solutions of melts in good solvents, chains are seen to expand to larger sizes than the aforementioned scale, since it would grant higher degrees of configurational freedom. Flory's hypothesis for this type of scaling for the end-to-end distances of polymer chains being restored for melts was reliant on the fact that no benefit would come from their expansion. That is to say for melts, should these chains expand, the configurational freedom of the system as a whole would not improve since it would result in increased interference with surrounding molecules. As such, the scaling mentioned before is restored for polymer melts where their size is seen to universally scale as their degree of polymerization to the power of an exponent which is not dependent on their chemical details. The underlying cause for this behavior can be better described in terms of an effect called screening which is seen to be present in these systems.

Polymer melts differ from simple liquids due to the existing connectivity that they have among their monomers. This connectivity results in long range entropic effects, however it is effectively screened in these systems [9]. The reason for this can be explained by the pair correlation function, $g(r)$, seen in figure 1.1, which shows the probability of one particle being found a distance r away from another placed at the origin. For polymer liquids, the oscillations in the correlation function are small and they dampen out fairly rapidly [16], which is the essence of the screening effect seen in melts. That is to say, a monomer belonging to a polymer chain will not be greatly affected by another monomer at a certain correlation length away, which typically will be on the order of a monomer

size. The simplifications arising from this screening effect are key to the study of polymer melts.

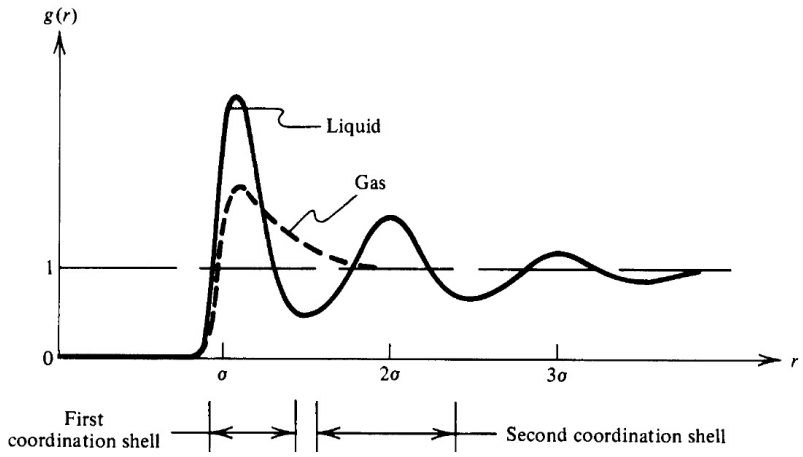

Figure 1.1: A generic pair correlation function from [1]

One notable effect stemming from this screening is the random walk behavior of polymer chains exhibited in the bulk, seen as the end-to-end distance of a chain of size N scaling $\propto \sqrt{N}$, for which the historical precedence was mentioned. Should this screening have not been applicable to polymer melts as suggested by Flory, an exponent other than 0.5 would have been the outcome for this end-to-end distance, which is not the case that is observed. Another is the applicability and accuracy of the mean-field theory for the study of the system. As we shall show, this theory replaces the interchain interactions with an external field. Furthermore, despite an absence of a rigorous treatment of the hardcore interactions among chains in this theory, it is seen to correctly describe polymer melt behavior, such as the $\sqrt{N}$ scaling in the bulk. The reason for this accurate outcome lies in the fact that these hardcore interactions are screened which in turn allows us to utilize a mean-field approximation in our study. In the following section, this scaling is shown theoretically and the role of the screening effect is made evident.

1.1.1 Average size of a polymer chain

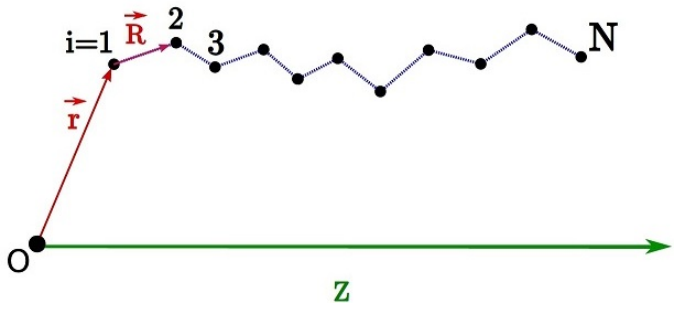

Figure 1.2: Polymer chain with N beads and N-1 bonds

As outlined in the previous section, in polymer melts it is known that the excluded-volume interactions, which could potentially be a source of complicated behavior, are screened to a good approximation. Consequently, chains in melts exhibit random walk statistics in the bulk, which gives the average end-to-end distance to be related to the square root of the chain length as will be shown here. In figure 1.2, a schematic of one representative chain is shown which contains N monomers and hence $N-1$ bonds. With the subscript i allocated to each monomer ranging from 1 to N, the position vector is shown with $\mathbf{r}_i$ while bond vectors are given by $\mathbf{R}_i = \mathbf{r}_i - \mathbf{r}_{i-1}$. The end-to-end vector of this polymer, denoted by $\mathbf{R}_e$, is clearly the sum of all bond vectors,

$$\mathbf{R}_e = \mathbf{r}_N - \mathbf{r}_1 = \sum_{i=1}^{N-1} (\mathbf{r}_{i+1} - \mathbf{r}_i) = \sum_{i=1}^{N-1} \mathbf{R}_i \ . \tag{1.1}$$

If we were to take an ensemble average of this quantity $\langle \mathbf{R}_e \rangle$, which would mean the average of this quantity for one chain over all possible conformations, it would not grant us any useful information. Considering the fact that each conformation would correspond to a random walk as mentioned before, allowing for no correlations between various forms of the chain, this average would evaluate to zero [5]. In this light, another form of averaging needs to be taken into consideration. The simplest non-zero average to evaluate is the mean square end-to-end distance, the root of which could provide us with a useful length scale of these polymer chains. With $\mathbf{R}_e$ obtained from equation 1.1, we see that the square of this quantity is

$$R_e^2 = \sum_{i=1}^{N-1} \sum_{j=1}^{N-1} \mathbf{R}_i \cdot \mathbf{R}_j \ . \tag{1.2}$$

This gives the ensemble average

$$\begin{aligned}\langle R_e^2 \rangle &= \sum_{i=1}^{N-1} \sum_{j=1}^{N-1} \langle \mathbf{R}_i \cdot \mathbf{R}_j \rangle \ , \\ &= \sum_{i=1}^{N-1} \left(\sum_{j=1}^{i-1} \langle \mathbf{R}_i \cdot \mathbf{R}_j \rangle + \langle R_i^2 \rangle + \sum_{j=i+1}^{N-1} \langle \mathbf{R}_i \cdot \mathbf{R}_j \rangle \right) \ , \xrightarrow[i \neq j]{\langle \mathbf{R}_i \cdot \mathbf{R}_j \rangle = 0} \\ &= \sum_{i=1}^{N-1} \langle R_i^2 \rangle \ , \end{aligned} \tag{1.3}$$

where again we have noted the absence of correlations among chains in the melt. In other words, the bond vector of monomer j is not related to the one for monomer i which results in only the term with $i = j$ surviving ($\langle \mathbf{R}_i \cdot \mathbf{R}_j \rangle = 0$). To see how this quantity is related to the bond lengths, we must define the bond potential, $u_b(\mathbf{R}_i)$. This allows us to define the square of the statistical segment length of a bond as

$$a^2 \equiv \langle R_i^2 \rangle = \frac{\int R_i^2 \ \exp\left(-u_b(\mathbf{R}_i)/k_B T\right) \ \mathrm{d}\mathbf{R}_i}{\int \exp\left(-u_b(\mathbf{R}_i)/k_B T\right) \ \mathrm{d}\mathbf{R}_i} \ , \tag{1.4}$$

where k_B is the Boltzmann constant and T is the absolute temperature. The bond potential can easily be scaled such that the denominator in equation 1.4 is one, which shall prove to be useful later on. By taking the definition of the statistical segment length into account, equation 1.3 gives

$$\langle R_e^2 \rangle = \sum_{i=1}^{N-1} \langle {R^2}_i \rangle = \sum_{i=1}^{N-1} a^2 = (N-1)a^2 \ .$$

Finally we can obtain the rms end-to-end distance of the chain denoted by R_0 as

$$R_0 = \sqrt{\langle R_e^2 \rangle} = a\sqrt{N-1} \approx a\sqrt{N} \ ,$$

which is the same scaling that was mentioned in the prior section and now has been proven for melts. That is to say, we can see with the absence of correlations among chains, as Flory had hypothesized to be the case in melts of polymer chains, the $\sqrt{N}$ proportionality is recovered. R_0 shall be used as a characteristic length scale of polymer chains, and the statistical segments length, a, will be used as a characteristic size of a monomer. These will both provide us with appropriate length scales by which we can compare and explain the phenomena shown in the systems considered.

1.2 Polymer surface behavior

As evident from the previous discussions, polymer chains have various inherent lengths in their structure such as the monomer as well as the molecular length scales. In order to accurately characterize the behavior of the chain, the details of the system need to be determined on all relevant lengths. This multi-scale nature of polymer chains has indeed presented some challenges for their experimental study, whereas it is more readily dealt with by theoretical studies which sheds light on the advantages of this method compared to experiments. In this section, there will not be a focused discussion on the different theoretical treatments of these polymers, as it will be thoroughly considered later on. However, it is beneficial to point out that the ability to utilize polymer theories followed by computer simulations to confirm and later predict the properties of polymers has progressed greatly from its onset, mainly due to the increase in computational power and the development of improved theories. Furthermore, the insight granted by these methods has complemented and extended the results obtained from experiments, specially at the molecular scale.

From the development of polymer theory, there has been a keen interest in observing the effect of a surface on the conformations of chains [17]. As theoretical as this may seem, applications such as extrusion and polymer welding as well as their interactions with fillers [18] could benefit from this detailed knowledge as they involve polymers near surfaces. The reason for this focused interest is that interfacial thermodynamic properties such as surface tension, can be modified to ensure the successful design of a polymer material towards specific goals in applications such as the ones noted above [19]. We shall point out the difficulties involved with the experimental study of these systems when going through the literature, but as mentioned before, this is more successfully considered theoretically. The study of polymer melts at surfaces has long been a fundamental problem of interest which intrinsically involves knowledge of how chains behave at very minute scales. To a first approximation, the surface acts as a reflecting boundary hence leaving the chain statistics unchanged as first postulated by Silberberg [20]. Before commenting on the hypothesis, it would be beneficial to state the original argument as well as its assumptions.

1.2.1 Silberberg Hypothesis

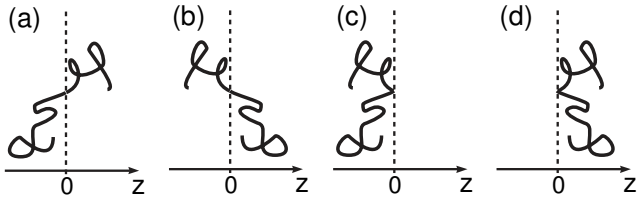

Figure 1.3: Illustration of the Silberberg argument [2]. (a) shows a polymer taken from the bulk, while (b)-(d) show configurations of equivalent energy (and thus probability) obtained by reflections about the plane $z = 0$. The surface is created by removing (a)-(c) and doubling the probability of (d).

In order to look at chain conformations near a surface, we require statistical mechanics from which we know the probability of a given configuration with an energy E, to be proportional to the Boltzmann weight of this energy, $\exp(-E/k_BT)$. Accordingly, as long as the energy of the configuration remains the same, so will its probability of occurring. This is integral to the original argument made by Silberberg, which looked at the behavior of polymer surfaces. The discussion begins by considering an infinite polymer melt for which a surface is created at $z = 0$ by removing any material crossing that point and going to $z < 0$. One such polymer configuration is shown in figure 1.3a from which the subsequent configurations b, c and d, are determined from reflecting either one or both parts of the initial configuration about $z = 0$. For a flexible molecule, all of the arrangements shown in the figure will have equal energies and hence will occur with equal probability.

To place a surface at $z = 0$, the first three configurations in 1.3 must be removed. Removing the first two will reduce the concentration at $z > 0$ but it can be compensated for by doubling the concentration of configuration each time. To generalize, if we denote the number of times the polymer crosses the surface by m, the occurrence of the allowed configuration will be needed to be increased by a factor of 2^m. This will result in a uniform concentration for the total as well as the individual monomer concentration, which will include the ends. Furthermore, the free energy cost required for the creation of the surface would be proportional to the number of polymer bonds that initially crossed $z = 0$, which is not dependent on the number of monomers in a chain. These outcomes have been since disputed, owing to the assumptions discernible from this argument which are a total concentration with the shape of a step profile, as well as no bending penalty for the bonds. When these features are not applicable, which will be the case for more realistic representations of polymer melt surfaces, results will disagree with this hypothesis.

The Silberberg argument is true up to the edge of the surface, where the reduction in the conformational entropy of chains results in the polymers adopting the form that grants them the highest freedom of movement which will manifest differently depending on the system. For example, in polymer solutions, the freedom of movement that the solvent provides, allows the polymer molecules to move away from the hard surface so as to increase configurational entropy. This results in a depletion profile for the polymer close to the surface [21, 22]. However, if there is no solvent present, as in melts of polymeric materials, the situation will be somewhat altered. The surface reduction in entropy favors a chain depletion there but is inhibited by the space filling requirement for the melt, hence a competition exists. Moreover, in addition to the aforementioned entropic effect, it is not uncommon for the ends of polymer chains to chemically vary from the middle monomers, which could cause attractive or repulsive enthalpic potentials for ends to be at the surface [23]. That is to say, the segments with the lowest surface energy are enriched at the surface which has been observed both in theory and experiments conducted [5, 24, 25]. However, in the case of the polymer chains not varying chemically with ends being identical to middle segments, there is an entropic effect present that will manifest differently in monodisperse and polydisperse melts.

In the case of a monodisperse melt, which is a melt of polymer chains of the same length, this entropic effect is exhibited in the excess concentration of end monomers at the surface. The underlying reason being in the additional configurations that are made available to the polymer chain by having the end monomer segregate to the surface instead of a middle segment. On the other hand, for polydisperse melts, which are constituted of polymer chains of various lengths, this excess of ends results in the shorter components segregating to the surface, since they have a higher number of ends per unit volume. Both of these effects violate the hypothesis made by Silberberg, which would suggest a uniform end monomer concentration, and have been observed in previous literature as will be presented and discussed in sections 1.4.1 and 1.4.2, respectively. The overall goal in this work will be to conduct a thorough investigation into this entropic segregation of ends for monodisperse melts as well as the consequent segregation of shorter components to the surfaces of polydisperse melts. There are a variety of methods that can be successfully applied towards the theoretical study of polymer melts, each offering their own advantages and disadvantages. In this light, the following section will review different methods for studying polymers theoretically.

1.3 Methods used in theoretical studies

As mentioned previously, the theoretical developments on polymeric systems as well as the subsequent computer simulations that complemented these theories vastly broadened the understanding of polymeric materials. The wide range of structural variety [7] added to the multi-scale nature of polymeric systems [38, 39] motivated the use of several simulation techniques. At the smallest scale are atomistic models, which attempt to capture polymer properties at the atomic scale [40]. Typically, in these procedures, potential functions are used to describe the bond and molecular interactions involved. Equilibrium and non-equilibrium properties are thus obtained through the use of Monte Carlo (MC) or Molecular Dynamic (MD) methods [8]. The use of these techniques, whilst providing us with invaluable insight, is limited in the number of particles it can simulate due to the extensive computational requirements. Hence, any study involving a large number of molecules, multi-phase systems or other such complexities is a challenging task using these methods.

One attempt at solving this particular difficulty is through coarse grain models [41], where groups of atoms are regarded as larger particles. Interactions are replaced with an effective term and properties of systems obtained by MD/MC simulation methods once again [42]. One example is the bead-spring model in which each bead represents a number of polymer backbone atoms [40]. Even with these simplifications, the calculations prove to be still far too expensive to be carried out for intricate systems of interest. Another somewhat distinct but noteworthy method of applicable interest is the use of lattice models to specify the conformations of polymer molecules. Lattice models have contributed greatly to the simulation of polymeric systems [35, 36] as well as theoretical work but are prone to some shortcomings [16, 43], with the artificial nature of the lattice presence being the main concern.

These lattice models were first rigorously developed in a series of papers by Helfand *et al.* [44, 45, 46] whereby they considered many systems such as polymer melts, solutions and interfaces thereof. In 1980, Scheutjens and Fleer [47] developed a lattice model which gives the probabilities of chain conformations as a function of chain concentrations in each configuration. This is unlike the one by Helfand, for which chain conformations depend on segment concentrations. These two distinct methods were both based on the mean-field approximation and were given the respective names of site and bond lattice models in a paper by Theodorou in 1988 [48]. In site models, the chance of a conformation occurring is related to a product of the site probabilities as segments occupy positions on the lattice, whereas in bond models the conformation probability for a segment of a chain depends on preceding segments. The paper then provided a detailed description

of both methods for hompolymers at interfaces, and the results for the site model were presented in their following work [49]. In all the aforementioned literature, it is evident that lattice models grant a simple picture of these systems and therefore are well-suited for cases where conformational properties vary rapidly within a narrow region, as is true for polymer surfaces.

Having outlined these early developments of lattice models, for which the essence still remains unchanged, albeit with newer and more powerful computational methods being applied for their calculations, they do involve some inaccuracies as mentioned before. Whilst the presence of lattices in the system is undoubtedly artificial, it makes computationally intensive calculations such as MC lattice simulations, thoroughly investigated in [50], feasible. As evident from the work of Kumar *et al.* [43, 51] as well as many other attempts that shall be outlined later in detail, off-lattice simulations can be implemented in order to improve upon some of the aforementioned inaccuracies of lattice models but they become much more computationally intensive. This causes off-lattice simulations to be limited in the system and chain sizes that can be considered. A useful outline of off-lattice MC simulations is provided in the work of Binder and coworkers [52]. As things remain, when good statistics are needed, the preferred method remains to be simulations using lattice models since the simplicity of the model allows one to gather more statistics, hence resulting in a higher accuracy in the results. However, if off-lattice models are preferred, one can apply a mean-field treatment in order to simplify the calculation.

For the study of the polymer systems here, both a mean-field approach as well as Monte-Carlo simulations will be implemented, for which an in-depth description of each method is given in their respective chapters. In brief, the first method involves a field representing the non-bonded interactions between monomers and will be implemented for both an off-lattice and lattice model while the second method is exclusively applied to a lattice model. As mentioned previously, there are some downsides to including an artificial lattice for the monomers to be placed on, some of which will be outlined in a section to follow. We could have implemented an off-lattice MC simulation but that would have introduced an extra layer of complexity not necessary for the comparison in mind here. Additionally, we would have been more limited in terms of the systems we could effectively study while still maintaining a high level of statistical accuracy, that is readily obtained by having the simpler lattice model.

1.4 Literature review

As previously pointed out, the increasing industrial applications of polymeric materials throughout recent years has made an in-depth characterization of their surfaces a top priority for experimentalists and theorists alike. These surface effects manifest as the entropic excess of end monomers in monodisperse melts, which had been observed through simulations and theory but not directly by experiments until fairly recently. Nonetheless, what had been observed by experiments was the dependence of surface tension on chain length which is a direct consequence of the aforementioned entropic excess of ends as will be outlined here. For polydisperse melts, this entropic effect causes the surface segregation of shorter components, which consequently results in a modification of the surface tension that is seen and validated by experiments also. The timeline of previous efforts looking at these systems will be outlined so that the contributions of the current work as well as its advantages can become evident.

1.4.1 Monodisperse melts

As noted in section 1.2.1, Silberberg [53] had argued that the surfaces of polymer melts act as reflecting boundaries for polymer chains, which is a good approximation for the most part as investigated in previous works [54, 55]. Nonetheless, it would suggest a uniform end monomer concentration throughout polymer melts as well as no chain length dependence for the surface tension, whereas both have been refuted. Initially motivated by the idea of experimentally tracking down the position of chain ends, in order to confirm or dispute their enhanced presence near surfaces, attempts were made to replace the hydrogen at polymer chain ends. Due to the closeness of deuterium and hydrogen, it was believed that switching them at the end of polymer chains would have no adverse effect on the entropic behavior of the polymers being considered. The relative ease of tracking the position of deuterium particles gave rise to the belief of this being a good technique to observe the concentration of ends at surfaces of these systems of interest. The experiments were conducted and results obtained [56, 57]. However, as is seen in the aforementioned experiments, the surface energy of the polymer samples with deuterium changes [58], which proves the need for improvement on the quantitative accuracy of the experimental methods.

With the experimental difficulties in tracking the polymer chain ends becoming evident, the next focus was on observing the dependence of surface tension on chain length [19, 59], which is the more readily observed experimental indicator of an excess of ends at surfaces of polymer melts. Many authors contributed to these studies [19, 59], and experiments were able to verify this phenomenon [24, 31, 32] thus presenting a counterargument for the Silberberg hypothesis. The reason for the dependence could be enthalpic due to a difference in the interaction of the end monomers versus the middle monomers, which is not uncommon for polymers [23], in light of chemical processes used in their manufacturing. On the other hand, it could be purely entropic and seen to exist when there is no difference in the interactions, which is the case we are looking to consider in this work. For polymer chains, the number of ends is inversely proportional to the chain length, N, therefore we expect the aforementioned end segregation to cause an N^{-1} correction to the surface tension.

Having outlined these experimental efforts, as well as the challenges they face, it is evident why a large portion of our current understanding on the topic stems from theoretical work in addition to computer simulations. These methods have ways of dealing with the systems that are exempt from the experimental difficulties but nevertheless face problems of their own. In computer simulations, the simplicity offered by having a lattice that chains could be placed on, motivated many to utilize this approach. On the other hand, theoretical studies such as mean-field theories have underlying assumptions that in turn allow them to simplify the study of the polymers. These simplifications provided opportunities for the consideration of more challenging problems, with the use of off-lattice models, and posed less of an issue when being carried out computationally. We shall begin with the historical precedence of lattice models before focusing on off-lattice simulations that looked at monodisperse polymer melts.

In 1975, Helfand *et al.* [46] utilized a lattice model for the study of a polymer melt near a surface to consider its loss of conformational entropy as well as how the addition of solvent to the melt will make it adsorb near the surface to relieve this configurational loss for the polymer chains. They analyzed this behavior in terms of the surface tension, where they observed the quantity to decrease as the concentration of the solvent was increased, since the polymer melts were relieved from their constrained forms. Theodorou looked at this system in 1988 using both a bond model [48] as well as a site model [49], where these terms were mentioned in the prior section. They applied their generalized site model for hompolymers at interfaces, from which they confirm the Flory hypothesis that conformations in the bulk of polymer melts are unperturbed by the presence of other chains. They comment on restrictions imposed by the interface on polymer chains in addition to confirming the molecular weight dependence of the surface tension. When comparing to surface

tension values obtained from experiments, they mentioned factors such as simplifications of the lattice model, ignoring chain stiffness as well as long range interactions, responsible for the observed disagreement between experimental and theoretical values. Others have also obtained results confirming this excess of ends by using lattice simulations [60, 61].

One argument that had been made early on by others against lattice calculations, was their inability to perform simulations at full occupancy. This was disproved in the work of Pai-Panandiker [62] in 1997 where they succeeded in observing the entropic excess of ends in an incompressible melt, *i.e.* a completely filled lattice, by lattice MC simulations. Another concern was how the placement of an artificial lattice might affect results, hence prompting many to use off-lattice computer simulations. A notable early attempt is the work of Kumar *et al.* in 1988 where their MC simulations aimed to consider the effect of surfaces on polymers without the use of lattice sites to construct them [43]. In this work, an excess of ends is observed close to the surface in the equilibrium configuration and the dependence of surface tension on chain length is readily seen [51]. They later on confirmed the same phenomenon for the free surface of a polymer melt [63]. Yethiraj *et al.* [64] used a continuous MC simulation to look at entropic effects which was successful in discerning this excess end concentration at surfaces of polymer melts. It is evident from their study that the intensity of their computational work resulted in them choosing the lowest number of possible monomers such that the chain could still exhibit polymeric behavior, which is indeed a difficulty with off-lattice simulations. Another interesting observation is disclosed through the first notable atomistic MC simulation done by Vacatello *et al.* in 1990 [65] where they observe this excess of ends also. Other than MC methods, MD simulations such as the work of Bitsanis *et al.* [16] have considered these systems and confirmed the excess end concentration near neutral walls due to entropic effects as early as 1990.

Mean-field calculations looking at the excess of ends at surfaces of polymer melts, have a great number of benefits to offer compared to simulations. The lower computational requirement of these calculations allows one to consider the underlying phenomena that could be at play, as well as more complex arrangements, which might be unfeasible using the prior methods mentioned. For instance, off-lattice calculations are more readily implemented using this technique and for longer chains at not such great costs. Some attempts such as the work of Muller *et al.* [42] have looked at both methods in order to compare their results. Historically, two of the most notable early attempts that had observed the segregation of ends to surfaces of monodisperse melts were the mean-field consideration of Wu *et al.* [33] as well as the simulations of Kumar *et al.*[43, 51]. In order to understand their findings, it is beneficial to consider them with respect to the aforementioned hypothesis by Silberberg.

In the work of Wu *et al.* [33] they observed violations to this hypothesis due to their concentration profile, being that of a compressible melt, not conforming to the step profile considered by Silberberg. Since they utilized the continuous Gaussian chain model, there was no penalty for chain bending and the only source for not conforming to this argument was the compressibility of the melt. Unsurprisingly, in the incompressible limit, they observed the excess of ends to vanish and recovered the uniform end monomer concentration that the Silberberg argument would suggest. They made the conclusion that this excess of ends was solely dependent on compressibility, but that was true only due to the model they had used. In the simulations of Kumar *et al.* [43, 51], where they had a discrete chain representation, there is a penalty for bending the chains. Thus, reflections will affect the energy [67] and in turn the probability of configurations occurring. This shows discreteness of the chains to be another factor of importance [42], which is seen to be influential even for an incompressible melt [66]. In this work, while studying the excess of ends at surfaces of monodisperse melts, we will be looking at various sources that cause deviations to the Silberberg hypothesis. By combining the effects of compressibility as well as chain discreteness for the monodisperse melt, we can ascertain the relative importance of each. Our mean-field calculations, unlike the ones by Wu *et al.* [33], still recover the excess of ends even as we go to the incompressible limit, the reasons of which will be thoroughly discussed in chapter 3.

Moreover, based the assumptions of the aforementioned hypothesis, we can anticipate additional influential factors that could affect the segregation of ends to surfaces of monodisperse melts. Excluded volume effects are an obvious choice, which can be considered by having hard-core interactions among monomers [68, 69]. These types of interactions would forbid chain overlaps, which could certainly occur as a result of chain reflections, thus altering the probability of certain configurations. We will consider this by having lattice model simulations that incorporate excluded volume interactions by rigorously enforcing only one monomer per lattice site. Another factor is chain stiffness, which can be taken into account by having a chain with a specified flexibility using a model such as the worm-like chain model [70]. In this case, a reflection would result in a kink in the chain that is disallowed, hence affecting the probabilities once more. Our plans for future work include consideration of the worm-like chain model in order to clarify the relative effect of chain rigidity, as noted in appendix B.

1.4.2 Polydisperse melts

The aforementioned entropic phenomenon of the segregation of ends to surfaces of monodisperse melts results in a similar occurrence for the surfaces of polydisperse melts. When there is a disparity in the chain lengths of the melt, the shorter chains have a higher number of ends per unit volume and as such tend to segregate to the surfaces of these melts. There are many implications arising from this excess of shorter components at surfaces such as the modification of surface tension [71, 72, 73], wall slip [74, 75, 76], entanglement of chains [77, 78], glass transition in thin films [79, 80, 81] and effective forces between polymer surfaces [82]. The same effect can also be seen in melts of polymers with a variety of architectural forms when they are chemically identical [37, 83, 84, 85, 86, 87]. Generally, as the number of ends in the structures is increased, such as stars versus linear chains, they tend to have a lower surface energy and as such migrate towards surfaces. The three most notable works that have theoretically studied the entropic segregation of shorter components to surfaces of polymer melts shall be summarized here.

Hariharan *et al.* [35] were among the first to theoretically demonstrate the entropic segregation of short chains to the surface of a bidisperse polymer melt, which contains polymer chains of two different lengths. Utilizing a mean-field lattice model for their calculations, polydispersity was noted to be a key property of polymer melts that needs to be taken into account. They stated the loss of configurational entropy to be greater for the longer chains at the vicinity of the surface hence resulting in an excess of short chains in that region, which was said to affect physical properties such as the surface tension of the melt. In their lattice model, chain back-folding was not prohibited, hence, excluded volume interactions were not directly taken into account. They went on to consider the absolute excess of short chains at the surface, as a measure of the net entropic loss in the system. In this light, influential parameters on the excess were determined to be factors such as the composition of the melt as well as the lengths of the chains. The integrated excess of short chains was also calculated and the surface tension seen to be related to the reciprocal of the number average degree of polymerization, given by N_n.

The aforementioned work was extended to a fully polydisperse melt by Van der Gucht *et al.* [36] using a lattice mean-field model. For their incompressible mixture of polymers of various lengths, they presented a simple expression that determined the surface excess of a component with a given length N, which was denoted by θ_N. This empirically predicted form showed the amount of excess to be related to the weight average degree of polymerization, N_w, and was tested out against numerical results for a melt of chains with three different lengths. The strikingly good agreement observed between the numerical results and the given formulation provided tangible evidence towards its validity. They

went on to use the expression for the excess to find one for the surface tension, once more confirming its relation to N_n. Moreover, this proposed form agreed fairly well with its counterpart previously determined by Hariharan *et al.*. These formulas postulated by the two previous studies mentioned, were later on derived for the first time by Minnikanti *et al.* [88]. In this work they considered Gaussian chains for which an enthalpic potential was chosen to represent the preference of the ends to be closer to the surface. By applying the mean-field approximation, they were able to obtain expressions that agreed nicely with the prior attempts mentioned, thus providing a collective argument in favor of the formulation proposed. Nevertheless, it should be taken into consideration that these relations were either empirical or derived using the wrong treatments of ends which shall be remedied in the work shown here.

Other than the mentioned theoretical attempts, simulations have yet to quantify this entropic short chain segregation in these melts, but have confirmed their existence in terms of the dynamics of the migrations [78] and the entanglement effects [77]. As for experimental evidence of the occurrence, many attempts have looked at studying similar setups [29, 80, 81, 82], the result of which confirm the segregation of short chains toward the surface in a blend of chemically identical polymers. Nevertheless, due to the difficulties present in these tests, they are usually qualitative in nature. For methods that have performed a quantitative study [80, 88], the comparison between experiment and theory elaborates great necessity for improvement. In account of these difficulties, theoretical attempts will be the main strategy for studying entropic effects at surfaces of polydisperse melts, which do not have the same difficulty as experiments in isolating these phenomena. Unlike the aforementioned theoretical attempts, we shall implement an off-lattice mean-field calculation for a polydisperse system, for which no potential will be considered for the ends. In this light the excess of short chains at the surface is seen to be due to purely entropic effects and the previously mentioned formulas for the excess as well as the surface tension will be derived using these assumptions. Moreover, we will conduct the first simulations considering only entropic effects for this surface segregation of shorter components.

1.5 Outline of thesis

Having outlined the previous literature regarding the polymer melts being considered here, the need for improvement in certain aspects of the work conducted thus far is clearly recognizable. By pointing out the experimental difficulties inherently intertwined in these studies, the advantages of theoretical methods motivated us to utilize them in the work at hand. The general outline of the document to be presented, is as follows. Prior to the detailed assessment of the systems of interest, a few key concepts require an in-depth introduction. In this light, theoretical topics central to the study shall be presented in chapter 2. Here, the main features of both the off-lattice mean-field study as well as the lattice mean-field and simulation methods are outlined and a semi-analytical calculation is introduced. The motivation for having a semi-analytical prediction is providing valuable insight in addition to means of testing numerical results, in order to judge their validity. Once the introductory topics are presented, the following two chapters are devoted to the study of each of the systems of interest, *i.e.* monodisperse as well as polydisperse melts, respectively. Hence, the segregation of ends to surfaces of monodisperse melts and the enrichment of shorter components at the surfaces of polydisperse melts will be the focus of chapters 3 and 4. Comparison of the results from different methods as well as discussions relevant to each system will be given in each respective chapter and the document will be concluded by a summary and outline of future work.

Chapter 2

Theory and simulation

2.1 Off-lattice model

In the model we are considering here, as the name suggests, the monomers are not constrained to be on lattice sites and can move freely in space. Since the systems we study are polymer melts, the chain conformations are ideal as the interactions among them are screened [5, 89], the reasons for which were outlined in the previous chapter. In this light, all non-bonded interactions amongst the polymers are represented with an effective field, $w(\mathbf{r})$ and the bonded interactions are given as suitable potentials, $u_b(\mathbf{R})$ as functions of position and bond vectors, $\mathbf{r}$ and $\mathbf{R}$, respectively. The field will be adjusted to ensure that the total polymer concentration conforms to a specific shape, which will create the surface that we are interested in exploring. The reasoning and motivation behind this methodology versus the one used by others such as the theoretical treatment of Wu *et al.* [33] of the surface is worth noting. In their work, they utilized a potential to penalize deviations from bulk density whereas in our study, by simplifying the calculation in this way, the focus can be on the phenomena involved.

One aspect of the theory that requires definition is the choice of the model for representing each individual polymer chain. In the previous chapter, a brief description of a number of possible models were given and the differences between them noted. For reasons that shall become evident, as we focus on each system to study the quantities of interest, the freely jointed model shall be utilized throughout the following chapters. For this model, no correlation is present for the direction of different bonds [5] and the bond length, b, remains constant. In the application of the aforementioned model to our off-lattice calculations, the statistical segment length, a, is equivalent to the bond length, which will not be the

case for the lattice model that shall be presented later on. The nature of these differences as well as their cause shall be pointed out as in the section involving lattice models.

In the off-lattice model, we shall consider the mean-field limit whereby the many body interacting system is replaced with a one body system with a suitable external field to represent the aforementioned interactions. The statistical mechanics of a chain placed in one such field will be presented in the following section as well as the steps required to determine its concentration. This will provide the theoretical background for the systems that are going to be studied. Once the general steps are outlined, their application to the polydisperse melt as well as the monodisperse melt, which are the systems of interest, will be given in complete detail. An additional quantity of interest is the surface tension of melts, for which the knowledge of the free energy is required, owing to its definition as the excess free energy at the surface. For each of the aforementioned systems, the free energy and the surface tension calculations will be provided in the current chapter.

2.1.1 Chain in an external field

In the current section, we are interested in using statistical mechanics to find the concentration of a polymer in a monodisperse melt acted on by an external field. The extension of these basic principles to the polydisperse melts are straightforward and will be given in detail later on. In subsequent sections, this external field will be determined self-consistently resulting from a suitably chosen pairwise interaction potential between the molecules [90] and satisfying a predefined criterion. That is to say, we shall have a desired form for the total concentration profile for which the field will be adjusted until its acquirement.

For the monodisperse melt, each polymer is of the same length and has N monomers (beads) and subsequently $N-1$ bonds. The schematic that was shown in the introduction, figure 1.2, depicts the beads starting from $i = 1$ and going up to N. The position and bond vectors are indicated in the figure for additional clarity, whereby for each monomer the corresponding subscript i will be used. For all of the individual beads, we define a position vector pointing from the origin to its location and denote it by $\mathbf{r}_i$ while bond vectors are given by $\mathbf{R}_i = \mathbf{r}_i - \mathbf{r}_{i-1}$.

In the manner of mean-field calculations, the focus will be on one chain owing to the fact that the steps will not differ depending on the chain that is chosen, since any of them will be representative of the system. The energy of this chain will have two separate contributing factors. One will be the bonds connecting each individual monomer to the next in the chain, which will be dependent on the bond vector. The other being the field required to represent the interactions among different chains. The bond potential can be chosen suitably in order to represent a chain of desired properties whereas the field, as previously mentioned, will have to be determined self-consistently. The details of the latter will be given later on based on the specific requirements from the model utilized. Based on the aforementioned concepts, we have

$$H[\{\mathbf{r}_i\}] = \sum_{i=1}^{N-1} u_b(\mathbf{r}_{i+1} - \mathbf{r}_i) + \sum_{i=1}^{N} w(\mathbf{r}_i) \ , \tag{2.1}$$

which gives the single chain Hamiltonian as a function of the set of position vectors denoting where each monomer is situated in the chain. Having specified the energy of a chain, we can consider the probability of a state with that energy occurring. This should be scaled by the partition function, Q, such that the sum of the probabilities can accumulate to one [91]. As mentioned in the introduction, statistical mechanics will give the probability of a particular configuration of the chain by

$$P(\{\mathbf{r}_i\}) = \frac{1}{Q} \exp\left(-\frac{H}{k_B T}\right) \ , \tag{2.2}$$

with the partition function determined from

$$Q = \int \exp\left(-\frac{H}{k_B T}\right) \prod_{i=1}^{N} \mathrm{d}\mathbf{r}_i \ . \tag{2.3}$$

Now if we hold $\mathbf{r}_i$ at a constant position and let all the other position vectors vary, the probability for this case is expressed by

$$P_i(\mathbf{r}_i) = \int P(\{\mathbf{r}_j\}) \mathrm{d}\mathbf{r}_1 \mathrm{d}\mathbf{r}_2 \ldots \mathrm{d}\mathbf{r}_{i-1} \mathrm{d}\mathbf{r}_{i+1} \ldots \mathrm{d}\mathbf{r}_N = \int P(\{\mathbf{r}_j\}) \prod_{\substack{j=1 \\ j \neq i}}^{N} \mathrm{d}\mathbf{r}_j \ . \tag{2.4}$$

If we substitute the expression for the energy from 2.1 inside the exponential we get

$$\exp\left(-\frac{H}{k_BT}\right) = \exp\left(\sum_{i=1}^{N-1}\left(-\frac{u_b(\mathbf{r}_{i+1}-\mathbf{r}_i)}{k_BT}\right)+\sum_{i=1}^{N}\left(-\frac{w(\mathbf{r}_i)}{k_BT}\right)\right) , \tag{2.5}$$

where it is seen that this expression is just the multiplication of two exponentials for which each is a multiplication of a number of terms. Hence, we simply have

$$\exp\left(-\frac{H}{k_BT}\right) = \prod_{j=1}^{N-1}\exp\left(-\frac{u_b(\mathbf{r}_{j+1}-\mathbf{r}_j)}{k_BT}\right)\prod_{j=1}^{N}\exp\left(-\frac{w(\mathbf{r}_j)}{k_BT}\right) = \prod_{j=1}^{N-1} g(\mathbf{r}_{j+1}-\mathbf{r}_j)\prod_{j=1}^{N} h(\mathbf{r}_j) , \tag{2.6}$$

where we have defined two new functions $g(\mathbf{R}) \equiv \exp\left(-u_b(\mathbf{R})/k_BT\right)$ and $h(\mathbf{r}) \equiv \exp\left(-w(\mathbf{r})/k_BT\right)$. It is useful to note that the bond potential is chosen suitably such that it is normalized to satisfy

$$\int g(\mathbf{R})\mathrm{d}\mathbf{R} = 1 , \tag{2.7}$$

as was noted in the definition of the statistical segment length in equation 1.4 as part of the introduction. Taking all previous steps into consideration, the probability becomes

$$P_i(\mathbf{r}_i) = \frac{1}{Q}\int \prod_{j=1}^{N-1} g(\mathbf{r}_{j+1}-\mathbf{r}_j)\prod_{j=1}^{N} h(\mathbf{r}_j)\prod_{\substack{j=1\\ j\neq i}}^{N}\mathrm{d}\mathbf{r}_j . \tag{2.8}$$

In order to calculate these probabilities, we define two new functions labeled the forward and backward propagators, $G_i(\mathbf{r}_i)$ and $G_i^\dagger(\mathbf{r}_i)$, as follows :

$$G_i(\mathbf{r}_i) = \int \prod_{j=1}^{i-1} g(\mathbf{r}_{j+1}-\mathbf{r}_j)\prod_{j=1}^{i} h(\mathbf{r}_j)\prod_{j=1}^{i-1}\mathrm{d}\mathbf{r}_j , \tag{2.9}$$

$$G_i^\dagger(\mathbf{r}_i) = \int \prod_{j=i}^{N-1} g(\mathbf{r}_{j+1}-\mathbf{r}_j)\prod_{j=i}^{N} h(\mathbf{r}_j)\prod_{j=i+1}^{N}\mathrm{d}\mathbf{r}_j . \tag{2.10}$$

When inserting the last two equations in the formulation of $P_i(\mathbf{r}_i)$ in equation 2.8, by taking into account that $h(\mathbf{r}_i)$ has been counted twice, the probability is simply of the form

$$P_i(\mathbf{r}) = \frac{1}{Q}\frac{G_i(\mathbf{r})G_i^\dagger(\mathbf{r})}{h(\mathbf{r})} . \tag{2.11}$$

All that remains to obtain this probability, is the evaluation of the propagators.

Evaluating Propagators

To specify the propagators, we begin from $i = 1$ for G in equation 2.9 and $i = N$ for $G^\dagger$ in equation 2.10 for the definition of initial conditions. The remaining points can then be evaluated using a convolution integral which is subsequently presented for each. If we let $i = 1$ for G inside integral 2.9 it becomes evident that g and $\mathrm{d}\mathbf{r}$ have no components, which gives

$$\begin{aligned} i = 1 : \qquad & G_1(\mathbf{r}_1) = h(\mathbf{r}_1) \ , \\ i = 2 : \qquad & G_2(\mathbf{r}_2) = \int g(\mathbf{r}_2 - \mathbf{r}_1) h(\mathbf{r}_2) h(\mathbf{r}_1) \mathrm{d}\mathbf{r}_1 \ , \\ i = 3 : \qquad & G_3(\mathbf{r}_3) = \int g(\mathbf{r}_3 - \mathbf{r}_2) g(\mathbf{r}_2 - \mathbf{r}_1) h(\mathbf{r}_3) h(\mathbf{r}_2) h(\mathbf{r}_1) \mathrm{d}\mathbf{r}_2 \mathrm{d}\mathbf{r}_1 \ , \end{aligned}$$

and in general

$$G_{i+1}(\mathbf{r}_{i+1}) = \int G_i(\mathbf{r}_i) g(\mathbf{r}_{i+1} - \mathbf{r}_i) h(\mathbf{r}_{i+1}) \mathrm{d}\mathbf{r}_i \ . \tag{2.12}$$

By looking at the last integral, it is observed that $h(\mathbf{r}_{i+1})$ is not a function of $\mathbf{r}_i$ and hence can come out of the integration to give

$$G_{i+1}(\mathbf{r}_{i+1}) = h(\mathbf{r}_{i+1}) \int G_i(\mathbf{r}_i) g(\mathbf{r}_{i+1} - \mathbf{r}_i) \mathrm{d}\mathbf{r}_i \ . \tag{2.13}$$

If we let $\mathbf{r}_{i+1} = \mathbf{r}$ and $\mathbf{r}_i = \mathbf{R}$, the initial condition and equation 2.13 become

$$\begin{aligned} i = 1 : \qquad & G_1(\mathbf{r}) = h(\mathbf{r}) \ , \\ G_{i+1}(\mathbf{r}) = h(\mathbf{r}) & \int G_i(\mathbf{R}) g(\mathbf{r} - \mathbf{R}) \mathrm{d}\mathbf{R} \ , \end{aligned} \tag{2.14}$$

in which equation 2.14 is seen to be a convolution integral. Following the same procedure for $G^\dagger$ we will obtain

$$\begin{aligned} i = N : \qquad & G_N^\dagger(\mathbf{r}) = h(\mathbf{r}) \ , \\ G_{i-1}^\dagger(\mathbf{r}) = h(\mathbf{r}) & \int G_i^\dagger(\mathbf{R}) g(\mathbf{r} - \mathbf{R}) \mathrm{d}\mathbf{R} \ . \end{aligned} \tag{2.15}$$

A note should be mentioned here that in the case of identical ends for both sides of polymer, *e.g.* homopolymers which are chemically identical from both ends, we have

$$G_i^\dagger(\mathbf{r}) = G_{N+1-i}(\mathbf{r}) \ . \tag{2.16}$$

The partition function

From equation 2.11, we have an expression for the probability of a certain arrangement. As mentioned before, we know that the sum of all probabilities for all formations must equal one. Here, the sum takes the form of an integral

$$1 = \int \frac{1}{Q} \frac{G_i(\mathbf{r}) G_i^\dagger(\mathbf{r})}{h(\mathbf{r})} \, \mathrm{d}\mathbf{r} \ . \tag{2.17}$$

It is clear that the total partition function Q is thus evaluated from

$$Q = \int \frac{G_i(\mathbf{r}) G_i^\dagger(\mathbf{r})}{h(\mathbf{r})} \, \mathrm{d}\mathbf{r} \ . \tag{2.18}$$

Total concentration

In a system comprised of n polymers each of length N with all monomers having an equal volume, ρ_0^{-1}, the total volume would be $V = nN/\rho_0$. Based on the probability of monomer i being in position $\mathbf{r}$, we can find the concentration of the material at a certain position by summing the probabilities for any of the monomers being there. By inserting the form found for the probability in terms of the propagators, seen in equation 2.11, as well as noting that the system consists of homopolymers, allowing us to apply the simplification of equation 2.16, we have

$$\phi(\mathbf{r}) = \frac{V}{N} \sum_{i=1}^{N} P_i(\mathbf{r}) \xrightarrow{\text{equations 2.11, 2.16}} \phi(\mathbf{r}) = \frac{V}{NQh(\mathbf{r})} \sum_{i=1}^{N} G_i(\mathbf{r}) G_{N+1-i}(\mathbf{r}) \tag{2.19}$$

where the concentration has been normalized so as to be one in the bulk. This will give the total concentration of the polymer chain at a given point in space in terms of the propagators. It can be shown that additive constants to the field do not affect the calculation, hence for simplicity we can set the field to be zero in the bulk. This would make $h(\mathbf{r}) = 1$ in that region which based on equation 2.14, and by taking equation 2.7 into account would give $G_i(\mathbf{r}) = 1$ for all monomers. Now, for the total concentration being scaled to be one in the bulk, equation 2.18 gives $Q = V$ and the concentration is given by

$$\phi(\mathbf{r}) = \frac{1}{Nh(\mathbf{r})} \sum_{i=1}^{N} G_i(\mathbf{r}) G_{N+1-i}(\mathbf{r}) \ . \tag{2.20}$$

With the general quantities and concepts thus defined, the details of the self-consistent field calculations for the more general case of polydisperse melts as well as the monodisperse ones will follow.

2.1.2 Self-consistent field theory for polydisperse melts

Having demonstrated the basic concepts of self-consistent field theory (SCFT) for a chain in an external field in the previous section, the specifics of the theory will be given for the two systems of interest in this section and the next. Here, the outline of SCFT will be presented for a polydisperse melt of polymers each comprised of N monomers with a concentration of ρ_0, where N is no longer a constant value among the components. As before, the bonds have an energy $u_b(\mathbf{R})$, with $\mathbf{R}$ being the bond vector and an effective field, $w(\mathbf{r})$, represents the interactions among the monomers which gives the energy of a single chain by equation 2.1. Since the amount of each component in the melt is not known beforehand, we solve the system in the grand-canonical ensemble where the number of chains are controlled by the chemical potential, μ_N [12, 90]. The concentration of a chain with length N is calculated as before and is seen to differ by the coefficient

$$\phi_N(\mathbf{r}) = \frac{z_N}{h(\mathbf{r})} \sum_{i=1}^{N} G_i(\mathbf{r}) G_{N+1-i}(\mathbf{r}) \ , \tag{2.21}$$

where z_N is the fugacity of the polymer chain given by $z_N = \exp(\mu_N/k_BT)$, $G_i(\mathbf{r})$ is the propagator of monomer i at position $\mathbf{r}$, $h(\mathbf{r}) \equiv \exp(-w(\mathbf{r})/k_BT)$ is the Boltzmann weight for the field acting on a monomer. Once more, by noting that additive constants to the field do not affect the calculations, the field is set to be zero in the bulk. Following the same logic as before, by defining the bulk volume fractions of each of the components to be given by $\bar{\phi}_N \equiv \lim_{z\to\infty} \phi_N(\mathbf{r})$, the fugacity will have to be $z_N = \bar{\phi}_N/N$ so that the concentration is given by the correct value in the bulk. All the previous considerations determine its form as

$$\phi_N(\mathbf{r}) = \frac{\bar{\phi}_N}{N h(\mathbf{r})} \sum_{i=1}^{N} G_i(\mathbf{r}) G_{N+1-i}(\mathbf{r}) \ . \tag{2.22}$$

As previously seen, the propagators are determined from the recursion relation given by equation 2.14 that starts from $G_1(\mathbf{r}) = h(\mathbf{r})$. From before, we know that the bond potential is $g(\mathbf{R}) \propto \exp(-u_b(\mathbf{R})/k_BT)$ which is normalized so as to satisfy equation 2.7. As previously shown in 1.1.1, the rms end-to-end length of the chains with the statistical segment length a, defined in equation 1.4, is $R_0 = a\sqrt{N-1} \approx a\sqrt{N}$ for large N, which is a good measure of the size of the polymer molecules. This value, in conjunction with the statistical segment length shall provide appropriate length scales for the characterization and specification of the phenomena being observed later on. By imposing the surface of the melt to be at $z = 0$, quantities such as $w(z)$, $h(z)$, $G_N(z)$ and $\phi(z)$ would all have translational invariance in the other two directions (x and y). This, in turn, will provide

further simplifications for other expressions involved in the calculations. For example, by implementing the integration over the X and Y coordinates for the bond potential we get

$$g(Z) \equiv \int g(\mathbf{R}) \mathrm{d}X \mathrm{d}Y \ , \tag{2.23}$$

hence the dimensionality of the problem is reduced from 3d to 1d. The concentration of the chain is now

$$\phi_N(z) = \frac{\bar{\phi}_N}{N h(z)} \sum_{i=1}^{N} G_i(z) G_{N+1-i}(z) \ , \tag{2.24}$$

and the propagators are evaluated from

$$G_{i+1}(z) = h(z) \int G_i(z - Z) g(Z) \mathrm{d}Z \ , \tag{2.25}$$

in which the bonds are taken to be Hookean springs with the potential

$$g(Z) = \left(\frac{3}{2\pi a^2} \right)^{1/2} \exp\left(-\frac{3Z^2}{2a^2} \right) \ , \tag{2.26}$$

that already has the scaling requirement of equation 2.7. The SCFT study is implemented such that the field is adjusted to have the total concentration, $\phi(z) = \sum_N \phi_N(z)$, conform to a specific profile shape . The sigmoidal profile will be given focused attention as it is the shape that has been observed for the surface of melts in detailed atomistic simulations [8]. As for the implementation of the method, the field is initialized with some given value and the resultant concentration profile is determined through the equations shown thus far. If this calculated profile does not match the required one within a desired error tolerance, adjustments should be made to the field which can be implemented in many ways. A straightforward approach would be to use the simple mixing method whereby the next iteration of the field is related to the previous one by

$$\frac{w^{(m+1)}(z)}{k_B T} = \frac{w^{(m)}(z)}{k_B T} + \lambda(\phi(z) - \phi_{\text{target}}(z)) \ , \tag{2.27}$$

and $0.01 < \lambda < 0.1$ is a mixing parameter. However, this method is not greatly efficient, therefore, the Anderson mixing scheme is utilized [92] which takes previous iterations of the calculation into account [93]. Having this history often leads to faster convergence when its parameters, such as the mixing parameter as well as the number of histories, are suitably chosen.

Free energy for polydisperse melts

As mentioned previously, the variation of the composition at the surface compared to the bulk, alters various properties of melts such as the surface tension. In order to quantify the change in the aforementioned quantity, it requires knowledge of the system's free energy. That is to say, by having the expression for the free energy of the system, the surface tension can be determined by the calculation of the excess free energy at the surface. Having already gone through the steps of the mean-field theory method, the goal was to find the field, $w(z)$, such as to provide the target surface profile, $\phi(z)$, for the total concentration. Once that is done, the free energy of a polydisperse melt, considered in the grand-canonical ensemble, is determined by [12]

$$F = -k_B T \rho_0 \sum_N z_N Q_N - \rho_0 \mathcal{A} \int w(z)\phi(z)\mathrm{d}z \ , \tag{2.28}$$

where $\mathcal{A}$ is the surface area and Q_N is the single-chain partition function for a polymer of length N given by

$$Q_N = \mathcal{A} \int \frac{G_i(z) G_{N+1-i}(z)}{h(z)} \mathrm{d}z \ . \tag{2.29}$$

By noting equations 2.24 and 2.29 it is seen

$$z_N Q_N = \frac{\mathcal{A}}{N} \int \phi_N(z)\mathrm{d}z \ , \tag{2.30}$$

which inserted into equation 2.28 gives

$$F = -k_B T \rho_0 \mathcal{A} \sum_N \frac{1}{N} \int \phi_N(z)\mathrm{d}z - \rho_0 \mathcal{A} \int w(z)\phi(z)\mathrm{d}z \ . \tag{2.31}$$

By remembering the field adjustment, which sets it to be zero in the bulk, the free energy far away from the surface would be

$$F_{\text{bulk}} = -k_B T \rho_0 \mathcal{A} \sum_N \frac{1}{N} \int \bar{\phi}_N \phi(z)\mathrm{d}z \ . \tag{2.32}$$

Subtracting equation 2.32 from equation 2.31, diving by $\mathcal{A}$ and introducing the notation $\delta\phi_N(z) = \phi_N(z) - \bar{\phi}_N \phi(z)$ to give the concentration difference of a component from its bulk value at each position, the entropic contribution to the surface tension of a polydisperse melt is given by

$$\gamma_{\text{en}} = -k_B T \rho_0 \sum_N \frac{1}{N} \int \delta\phi_N(z)\mathrm{d}z - \rho_0 \int w(z)\phi(z)\mathrm{d}z \ . \tag{2.33}$$

Self-consistent field theory for monodisperse melts

Having outlined this theory for the polydisperse melt, the differences of SCFT applied for the monodisperse melt will be presented here. The theory for the polydisperse melt is more general and can readily be altered to correspond to monodisperse melts, which is the reason for its presentation preceding the other system in all of the sections that follow. The system now consists of n polymer chains each of the same length, N, where once more the non-bonded interactions are given by a field, $w(z)$. Since the amount of material is fixed, we solve the system in the canonical ensemble. The field is adjusted using one of the methods previously described, such that the concentration profile calculated from

$$\phi(z) = \frac{1}{Nh(z)} \sum_{i=1}^{N} G_i(z) G_{N+1-i}(z) \ , \tag{2.34}$$

conforms to the desired surface profile shape. Here, the expression in the sum is the monomer concentration determined from

$$\phi_i(z) = \frac{G_i(z) G_{N+1-i}(z)}{h(z)} \ , \tag{2.35}$$

where for $i = 1$ we have the end monomer concentration. This is the quantity we are interested in looking at for the monodisperse melts, which is given by

$$\phi_e(z) \equiv \phi_1(z) = G_N(z) \ . \tag{2.36}$$

Free energy for monodisperse melts

The entropic segregation of polymer chain ends to surfaces of polymer melts, as will be shown in the following chapters, alters the surface composition therefore changing the surface tension of the melt. As was observed for the polydisperse melt, a knowledge of free energy is required for the determination of surface tension. The free energy expression for monodisperse melts differs from the one for polydisperse melts presented in equation 2.31. That is to say, its general form in the canonical ensemble is given in previous literature as [66]

$$\frac{F}{nk_BT} = -\ln\left(\frac{Q}{V}\right) - \frac{N}{k_BTL} \int w(z)\phi(z) \mathrm{d}z \ , \tag{2.37}$$

where L is the length of the system in the z direction. If the field is set to be zero in the bulk, this requires $Q = V$ as was noted in the section describing the behavior of a chain in an external field. This will allow the specification of the free energy in the

bulk, F_{bulk}, for which the first term in equation 2.37 will be zero. Additionally, by noting $V = \mathcal{A}L = nN/\rho_0$, we can determine the entropic contribution to the surface tension as

$$\gamma_{\text{en}} = -\rho_0 \int w(z)\phi(z)\mathrm{d}z \ . \tag{2.38}$$

2.1.3 Semi-analytical calculation for polydisperse melts

In order to have a deeper understanding of our SCFT results, we shall compare them to a semi-analytical calculation that is described in the current section. This methodology will require the determination of the field and propagators for infinitely long chains, the placement of finite chains in these fields followed by correcting the field to account for the chains being finite (and not infinite) using linear-response theory [94]. The details for each of the three aforementioned steps will be duly explained. Linear-response (LR) theory has been developed for Gaussian chains, [33] which are chains that behave as flexible strings [12] and would be the large N limit of our model. We shall introduce the steps to the semi-analytical approach for the general case of the polydisperse as well as the monodisperse melt, while providing insight towards the LR theory in this section. The details of the theory presented here will closely follow previously utilized approaches [3, 66].

Step 1 : Infinite molecular weight limit

The first step will be to extend the calculations shown for mean-field theory to the $N \to \infty$ limit. In order to help distinguish these quantities from the previous ones, a subscript of infinity will be used for variables corresponding to this limit. The field now accordingly becomes $w_\infty(z)$ which gives $h_\infty(z) \equiv \exp(-w_\infty(z)/k_BT)$. Once more, the field will have to be adjusted such that the total concentration, previously given by equation 2.34 and now determined from

$$\phi(z) = \frac{G^2_\infty(z)}{h_\infty(z)} \ , \tag{2.39}$$

conforms to the chosen surface profile. This propagator will satisfy

$$G_\infty(z) = h_\infty(z) \int G_\infty(z - Z)g(Z)\mathrm{d}Z \ , \tag{2.40}$$

and is either found through iterating equation 2.40 multiple times or, as shown in previous work [2], through a more efficient method that involves solving the integral equation

$$G_\infty(z) = \int h_\infty(z)G_\infty(z')g(z - z')\mathrm{d}z' = \int I(z, z')G_\infty(z')\mathrm{d}z' \ , \tag{2.41}$$

where $I(z,z') = h_\infty(z)g(z-z')$. In the form given by equation 2.41, discretizing the z coordinate makes this into a matrix equation for which it becomes an eigenvalue problem as seen in Appendix A. In other words, $G_\infty(z)$ is the eigenvector of the matrix $I(z,z')$ corresponding to an eigenvalue of one. The aforementioned problem can be solved using a standard linear algebra subroutine. This method is evidently much more efficient at determining the propagator for infinitely long chains compared to the multi-iteration method mentioned prior. In this light, the matrix method is notably the preferred one used for calculations.

Step 2 : Finite chains in $w_\infty(z)$

After determining the field for infinitely long chains, finite chains are placed in $w_\infty(z)$ and their concentrations are determined as before. From previous work [3, 2] there is an expression to predict the concentration form for a chain of length N, when placed in $w_\infty(z)$. That is to say, the form of the propagators in $w_\infty(z)$ are known [67, 66] from which the concentration can be evaluated. This quantity is denoted by $\phi_N^0(z)$ where the superscript denotes the chains being in the field of infinitely long ones and is given by

$$\phi_N^0(z) \approx \bar{\phi}_N\phi(z) + 4A\bar{\phi}_N\sqrt{\frac{6}{\pi N}}\frac{\phi(z)}{G_\infty(z)}\left\{\left[f(z/aN^{1/2})-1\right]H(z)+G_\infty(z)\right\}\ , \tag{2.42}$$

where $H(z)$ is the Heaviside step function that switches from zero to one at $z=0$,

$$f(\zeta) \equiv \int_0^1 \frac{1}{2\sqrt{s}}\exp\left(-\frac{3}{2s}\zeta^2\right)\mathrm{d}s\ , \tag{2.43}$$

and

$$A = \frac{1}{a}\int[G_\infty(z)-\phi(z)]\mathrm{d}z\ . \tag{2.44}$$

The significance and meaning of this coefficient, A, will be explained further in the following chapters and its dependence on model details will be discussed. Due to the chains being finite in length, they will not have the correct concentration in $w_\infty(z)$ and will subsequently require corrections. The excess of concentration due to the field not being correct is denoted by $\delta\phi_N^0(z) = \phi_N^0(z) - \bar{\phi}_N\phi(z)$ for which the sum over all the components will not give zero *i.e.* $\sum_N \delta\phi_N^0(z) \neq 0$. The adjustment needed for the field so as to correct these concentration profiles will be the last step of the semi-analytical calculation.

Step 3 : Correction to $w_\infty(z)$

As previously pointed out, the concentrations determined in the last step require corrections for which adjustments must be made to the field. In other words, we need to make a change to the field, $\delta w(z)$ to make the total excess zero and restore the target surface profile shape. Therefore, the final form of the field will be $w(z) = w_\infty(z) + \delta w(z)$. If the molecular weight is high, this field alteration will be small and its relation to the change in concentration for a component of length N, denoted by $\delta\phi_N^1(z)$, can be given in Fourier space by linear-response theory [12, 33]. With the Fourier transform given by

$$\widehat{g}(k_z) \equiv \int_{-\infty}^{\infty} g(z) e^{-ik_z z} \mathrm{d}z \ , \tag{2.45}$$

linear-response states

$$\widehat{\delta\phi_N^1}(k_z) = -N\bar{\phi}_N s_\phi(x_N) \frac{\widehat{\delta w}(k_z)}{k_B T} \ , \tag{2.46}$$

where $s_\phi(x) = 2(e^{-x} + x - 1)/x^2$ is the Debye function and $x_N \equiv k_z^2 a^2 N/6$. By applying these corrections we expect the total excess to be zero or

$$\sum_N [\widehat{\delta\phi_N^0}(k_z) + \widehat{\delta\phi_N^1}(k_z)] = 0 \ . \tag{2.47}$$

The first term in this equation is given by taking the Fourier transform of 2.42 which gives

$$\widehat{\delta\phi_N^0}(k_z) = 4Aa\bar{\phi}_N s_e(x_N) \ , \tag{2.48}$$

where $s_e(x) = (1 - e^{-x})/x$ is a Debye-like function. Substituting equations 2.48 and 2.46 into equation 2.47 and noting that the change in the field can come out of the sum, gives

$$\sum_N 4Aa\bar{\phi}_N s_e(x_N) - \frac{\widehat{\delta w}(k_z)}{k_B T} \sum_N N\bar{\phi}_N s_\phi(x_N) = 0 \ , \tag{2.49}$$

or

$$\frac{\widehat{\delta w}(k_z)}{k_B T} = 4Aa \frac{\sum_N \bar{\phi}_N s_e(x_N)}{\sum_N N\bar{\phi}_N s_\phi(x_N)} \ . \tag{2.50}$$

By knowing the required modification to the field through equation 2.50, we can determine the correction to the concentration from equation 2.46. As this is determined in Fourier space, we can obtain the quantity in real space by performing an inverse Fourier transform

$$g(z) \equiv \frac{1}{2\pi} \int_{-\infty}^{\infty} \widehat{g}(k_z) e^{ik_z z} \mathrm{d}k_z \ . \tag{2.51}$$

Now we can adjust the excess concentration that was determined in the field of infinitely long chains (equation 2.42) by adding the correction to it , *i.e.* $\delta\phi_N(z) = \delta\phi_N^0(z) + \delta\phi_N^1(z)$, where $\delta\phi_N(z)$ is the corrected excess concentration. For example, for the bidisperse melt which we will consider in detail later on, the final form for the excess of short chains at the surface, denoted by $\delta\phi_s(z)$, after adding this correction is

$$\delta\phi_s(z) \approx \begin{cases} AN_s^{-1/2}C(0)\phi(z) \ , & \text{for } z < 0 \ , \\ AN_s^{-1/2}C(z/aN_s^{1/2}) \ , & \text{for } z > 0 \ , \end{cases} \tag{2.52}$$

where

$$C(\zeta) = 4\bar{\phi}_s \left(\sqrt{\frac{6}{\pi}} f(\zeta) - c(\zeta) \right) \ . \tag{2.53}$$

The first term in equation 2.53 comes from the long range limit of equation 2.42 written for the short chains in a bidisperse melt and the function $c(\zeta)$ is obtained from an inverse Fourier transform of

$$\hat{c}(k_\zeta) = \frac{s_\phi(x)[s_e(x) + \eta s_e(\alpha x)]}{s_\phi(x) + \alpha\eta s_\phi(\alpha x)} \ , \tag{2.54}$$

where $x = k_\zeta^2/6$, $\alpha = N_l/N_s$ and $\eta = \bar{\phi}_l/\bar{\phi}_s$ and the subscripts s and l denote each quantity specific to short and long chains of lengths N_s and N_l respectively. This is found from noting that equation 2.46 written for the short chains is

$$\widehat{\delta\phi_s^1}(k_z) = -N_s\bar{\phi}_s s_\phi(x)\frac{\widehat{\delta w}(k_z)}{k_BT} \ , \tag{2.55}$$

where

$$\frac{\widehat{\delta w}(k_z)}{k_BT} = 4Aa\frac{\bar{\phi}_s s_e(x) + \bar{\phi}_l s_e(\alpha x)}{N_s\bar{\phi}_s s_\phi(x) + N_l\bar{\phi}_l s_\phi(\alpha x)} \ . \tag{2.56}$$

The accuracy of these predictions as well as the model dependent aspects of the universal function $C(\zeta)$ given by equation 2.53, which describes the general form of the excess of short chains in a bidisperse melt, will be one of the main topics addressed in chapter 4.

Semi-analytical calculation for monodisperse melts

As noted before, another system of interest that will be thoroughly investigated is the monodisperse melt so that the excess concentration of ends can be determined at the surface. Once more, by going through the semi-analytical calculation, a deeper understanding of the underlying phenomena will be obtained. The main steps of the method will be as before with the difference here being that we are interested in the concentration of ends, for which the formulas are presented. Determination of $w_\infty(z)$ will not change and we shall focus on the things that are altered. The expected form that the propagators will have in the field of infinite chains is given by [66]

$$G_N^0(z) \approx G_\infty(z) + A\sqrt{\frac{6}{\pi N}} \times \left\{ \left[\exp\left(-\frac{3z^2}{2a^2 N} \right) - 1 \right] H(z) + G_\infty(z) \right\} \ , \tag{2.57}$$

where all quantities have been introduced before. Based on equation 2.36, we can see equation 2.57 is the estimation for the concentration of ends in infinite fields. We can once again determine a form for the concentration in $w_\infty(z)$ by substitution of these propagators into equation 2.35

$$\phi^0(z) \approx \phi(z) + 4A\sqrt{\frac{6}{\pi N}} \frac{\phi(z)}{G_\infty(z)} \times \left\{ \left[f\left(\frac{z}{aN^{1/2}} \right) - 1 \right] H(z) + G_\infty(z) \right\} \ , \tag{2.58}$$

where $f(\zeta)$ is as before (equation 2.43) and terms have been kept up to order $N^{-1/2}$. Similar to equation 2.46, with $\delta\phi^0(z) = \phi(z) - \phi^0(z)$, from linear-response, we have

$$\widehat{\delta\phi^0}(k_z) = -N s_\phi(x) \frac{\widehat{\delta w}(k_z)}{k_B T} \ , \tag{2.59}$$

and the Fourier transform of the correction to the concentration of ends, $\widehat{\delta\phi_e^1}(k_z)$, is given by LR to be related to the change in the field by [66]

$$\widehat{\delta\phi_e^1}(k_z) = -N s_e(x) \frac{\widehat{\delta w}(k_z)}{k_B T} \ , \tag{2.60}$$

where all quantities have already been introduced. Combining 2.60 and 2.59 and by knowing

$$\widehat{\delta\phi^0}(k_z) = -4Aa s_e(x) \ , \tag{2.61}$$

from the Fourier transform of equation 2.58, we obtain

$$\widehat{\delta\phi_e^1}(k_z) = -4Aa \frac{s_e^2(x)}{s_\phi(x)} \ . \tag{2.62}$$

Equation 2.62 will be converted back to real space to be added to the approximate form for the concentration of ends, equation 2.57, to correct for the chains being finite, *i.e.* $\delta\phi_e(z) = \delta\phi_e^0(z) + \delta\phi_e^1(z)$. By going through these steps, we are able to obtain the final expression for the concentration of end monomers from the semi-analytical calculation which is

$$\phi_e(z) \approx G_\infty(z) + \frac{A}{N^{1/2}} \times \left\{ \left[B\left(\frac{z}{aN^{1/2}}\right) - B(0) \right] H(z) + B(0) G_\infty(z) \right\} \ , \tag{2.63}$$

where

$$B(\zeta) = \sqrt{\frac{6}{\pi}} \exp(-\frac{3}{2}\zeta^2) - b(\zeta) \ , \tag{2.64}$$

is a universal function. In this form, $b(\zeta)$ is obtained by performing a numerical inverse Fourier transform of

$$\hat{b}(k_\zeta) = \frac{2\,[\exp(-\frac{1}{6}k_\zeta^2) - 1]^2}{\exp(-\frac{1}{6}k_\zeta^2) + \frac{1}{6}k_\zeta^2 - 1} \ , \tag{2.65}$$

which is obtained from equation 2.62. Equation 2.64 will give the universal shape of the depletion of ends in the long range limit which is a result of the excess amount present at the surface. The in-depth discussion of these phenomenon shall be deterred until chapter 3 where the model dependent and universal features are described.

To summarize this section, there are some key features to be pointed out about the predicted forms presented here for both the excess of short chains for bidisperse melts as well as the depletion of chain ends for monodisperse melts. The steps involved in obtaining these predictions, other than the initial evaluation of the field for infinitely long chains, have been analytical and hence provide a good measure for testing the accuracy of the other methods used to look at these systems later on. If the forms presented by the semi-analytical calculation are truly universal, we should observe agreement among the results regardless of the model utilized. As a test, we will perform simulations to study the same systems, for which the simplest model is chosen in order to ensure high statistical accuracy in the calculations. In this light, lattice models need to be introduced which have the simplicity we require. Moreover, we perform mean-field calculations using the same lattice model so that comparisons between the results can successfully be carried out. The next section shall provide the details for the lattice mean-field model as well as the simulation method, to complete the theoretical considerations of this work before results can be presented for each of the systems mentioned up to this point.

2.2 Lattice model

The universal forms predicted for the aforementioned systems thus far, *i.e.* $\delta\phi_e(z) \propto B\left(z/a\sqrt{N}\right)$ and $\delta\phi_s(z) \propto C\left(z/a\sqrt{N_s}\right)$, are very powerful. If the concentrations found in this manner are truly universal, other methods of calculating the behavior, such as simulations and experiments should give the same results as mean-field theory. One aspect that is not fully considered in the mean-field theory is excluded-volume interactions which could result in inaccuracies for results obtained this way. The reason for this being that excluded volume interactions, which are not explicitly taken into account by SCFT, cause violations to the Silberberg argument and as such could be a major contributing source to the entropic segregation. One simple method of assessing this inaccuracy will be to compare mean-field results to those of simulations but only when they are applied to the same identical model, such that comparisons are justified. In this section, the lattice models utilized for both the mean-field theory and the simulations are introduced so that later on they can be applied to both systems of interest and their results compared.

2.2.1 Self-consistent field theory for polydisperse melts

Firstly, we will describe the lattice model for mean-field theory as well as giving the details of its application for each of the systems considered, before introducing the simulations implemented. As noted in the introductory chapter, the use of mean-field theory for lattice models has been developed for some time [45, 47, 48]. The basics of the SCFT remains similar to what was presented previously in 2.1.1 such as the non-bonded interaction given by an external field, $w(z)$, as well as its adjustment such that the resultant concentration profile is of a desired shape. Hence, only the main differences will be outlined and explained here. Since the polymer chains are placed on discrete lattice sites, the previous recursion relation given by equation 2.25 for the evaluation of the propagators is now a sum

$$G_{i+1}(z) = h(z) \sum_{Z} g(Z) G_i(z - Z) \ , \tag{2.66}$$

starting from $G_1(z) = h(z)$, where $h(z) \equiv \exp(-w(z)/k_BT)$ as before. The bonds are between nearest neighbor sites and the coordination number is twelve, since an fcc lattice is considered, which is created by deleting every second site from a simple-cubic lattice [95]. In order to determine $g(Z)$ for the plane at the position z, we need the fraction of nearest neighbors at $z + Z$ with Z being the bond length. If we are looking at bonds on the same plane as the monomer, $Z = 0$ and $g(0) = 4/12 = 1/3$ since four of the twelve

nearest neighbors are on the same plane. For the two adjacent planes, $|Z| = 1$ and we have four nearest neighbors on each which gives $g(\pm 1) = 4/12 = 1/3$ [95, 96]. The value of this quantity will be zero elsewhere.

The recursion relation, eq 2.66 is evaluated as before starting from $G_1(z) = h(z)$ where $h(z) = 0$ for $z < 0$. The size of the system is chosen such that bulk behavior is obtained at far away distances and a reflecting boundary is placed at the ends of the system. The field is adjusted using the simple mixing method that was described by equation 2.27 in 2.1.2, such that the total concentration is uniformly one throughout the domain. This can also be explained in terms of the target surface profile described before, now being enforced to be a step profile, which is chosen for its simplicity that will prove beneficial once we are looking to implement simulations. Additive constants to the field do not make a difference in the calculation and as such it is adjusted to be zero in the bulk for convenience. For polydisperse melts, the total concentration is $\phi(z) = \sum_N \phi_N(z)$, where the concentration of a polymer with the polymerization N is exactly the same as equation 2.24. Once this quantity conforms to the step profile, comparisons between the concentration of the shorter components at the surface and bulk can be made.

Self-consistent field theory for monodisperse melts

For the lattice model applied to the monodisperse melt, everything will be implemented as was just described for the polydisperse melt, with the difference that now the system is only comprised of polymers of constant chain length N for which the total concentration is determined from equation 2.34. The field, $w(z)$, is adjusted through simple mixing once more such that the total concentration is uniformly one throughout the system. As was the case in the off-lattice calculations, for this system we are interested in determining the average end-monomer concentration which is given by $\phi_e(z) = G_N(z)$. The excess of this quantity at the surface compared to unity, which should be the total concentration throughout the system and therefore at the surface, will give the excess end monomer value we are seeking. Having outlined the differences between the previous off-lattice SCFT and the current lattice model, we shall do the same to highlight the changes in the semi-analytical calculation for this new method in the next section.

2.2.2 Semi-analytical calculation for polydisperse melts

As mentioned before, for the semi-analytical results to be truly universal, they should also be able to describe the results from the lattice model calculations, whether implemented in the mean-field approximation or by simulations. With this goal in mind, the results from the mean-field lattice model will be compared to the semi-analytical predictions later on. The application of this theory to the lattice model is just as was mentioned in 2.1.3 with minor alterations, and the differences noted here will be exactly the same for both the polydisperse and monodisperse melts. Here, with the points being placed on lattice sites, the integrals mentioned before for the calculations become sums. For example, to determine $G_\infty(z)$ which was previously given by equation 2.40, the following sum needs to be evaluated [95]

$$G_\infty(z) = h_\infty(z) \sum_Z g(Z) G_\infty(z - Z) \ , \tag{2.67}$$

where $h_\infty(z)$ is adjusted for the total concentration to be uniformly one, *i.e.* $G_\infty^2(z)/h_\infty(z) = 1$. Once this quantity is determined, the magnitude of A is found by

$$A = \frac{1}{\sqrt{2}} \sum_z [G_\infty(z) - 1] \ , \tag{2.68}$$

which completes the quantities required for the semi-analytical calculation. In this manner, we observe that the details of the model affect the constant A, which appears as a coefficient in the semi-analytical predictions for both the monodisperse and polydisperse systems. Nonetheless, the main features of the results, such as the shape of the observed excess or depletion given by this theory, should not change. The aforementioned behavior shall be one of the main points of interest in our comparisons to be conducted using the result from simulations. The outcome of these will be deferred for the detailed discussions of results in each respective chapter. For the last section of the theoretical topics introduced here, we shall go over the main concepts of the Monte Carlo simulations.

2.2.3 Monte Carlo simulations

For the lattice model simulations, the Monte Carlo method will be implemented for which the basics are introduced in this chapter. There are prerequisite concepts which will need to be mentioned prior to the details of the MC simulations. Firstly, this method involves statistics since different states of the system are sampled for which, based on the energy of the new state, a transition will occur with some probability [5]. Therefore, the understanding of the statistical mechanics involved here requires knowledge of Boltzmann weights and how they are used to obtain averages. Additionally, these weights will be related to the probability of transitions between states as shall be shown.

The simulation results that will be presented in the following chapters will be for polymer melts (both monodisperse and polydisperse) and as such will encapsulate a large number of interacting molecules. As shown previously, the interactions between the aforementioned system constituents are given by a suitable Hamiltonian. By determining the Boltzmann weights of the various states they can be in, we can attain thermodynamic averages for desirable quantities such as the energy of the system. This, in turn, will allow us to find the most stable arrangement with the highest probability of occurring by using the MC method [39]. A brief introduction on the aforementioned concepts interwoven in the study will follow shortly and the steps to the metropolis algorithm used for the MC method will be outlined. The specific details of the implementation of this method for studying the polymer melts will conclude the section.

Boltzmann weights

It is clear that information about the state of the system is required to determine its energy as well as the probability of that state occurring. When talking of a many particle system, the specification of the state of all these particles is denoted as a *microstate*. Whereas the general state of the whole system is given by a *macrostate* which could correspond to a multitude of microstates [91]. The probability of a system being in a given microstate denoted by m, with the energy H, is proportional to the Boltzmann factor $P_{\mathrm{m}} \propto \exp\left(-H_{\mathrm{m}}/k_B T\right)$, where the proportionality constant is the partition function, $Z = \sum_{\mathrm{m}} \exp\left(-H_{\mathrm{m}}/k_B T\right)$ which also ensures that the probabilities add up to one [97]. In other words

$$P_{\mathrm{m}} = \frac{1}{Z} \exp\left(-\frac{H_{\mathrm{m}}}{k_B T}\right) = \frac{1}{Z} \exp\left(-\beta H_{\mathrm{m}}\right) \ , \tag{2.69}$$

with $\beta = 1/k_B T$ defined for convenience. This equation will be greatly utilized in simulations as it can help us determine thermodynamic quantities as well as averages that are required for the problem at hand [97] .

Average values

With simulations, we can look at variables at each step, or consider the more relevant quantity of their average over a certain number of simulation steps, chosen to be large enough for the system to reach a desired state. In order to determine the average of any quantity, we need to determine its value in the current state of the system and take into account the probability of that state occurring. In other words, having obtained knowledge of the Boltzmann weights of each state, we can find the average value of a quantity, *e.g.* the energy, by multiplying it by the chance that the system is currently in that state. For the energy of the system mentioned as an example here, we can obtain its average for a given microstate, denoted by $\bar{H}_{\mathrm{m}}$, by [97]

$$\bar{H}_{\mathrm{m}} \equiv \sum_{\mathrm{m}} P_{\mathrm{m}} H_m \xrightarrow{\text{equation } 2.69} \bar{H}_{\mathrm{m}} = \frac{\sum_{\mathrm{m}} H_m \exp\left(-\beta H_{\mathrm{m}}\right)}{\sum_{\mathrm{m}} \exp\left(-\beta H_{\mathrm{m}}\right)} \ . \tag{2.70}$$

Monte Carlo

In the study of physical systems, one of the main simulation methods is Monte Carlo which involves random sampling of the possible states [5]. In this method, the initial state is chosen arbitrarily following which a set of transition rules are implemented to attempt it going into a different state. The probability of these transitions occurring depends on the differences in their respective energies. This is due to the fact that the ratio of probabilities for going from state m to n based on equation 2.69 is

$$\frac{P_{\mathrm{m}}}{P_{\mathrm{n}}} = \frac{\exp\left(-\beta H_{\mathrm{m}}\right)}{\exp\left(-\beta H_{\mathrm{n}}\right)} = \exp\left(-\beta(H_{\mathrm{m}} - H_{\mathrm{n}})\right) = \exp\left(-\beta \Delta H_{\mathrm{m}\to\mathrm{n}}\right) \ , \tag{2.71}$$

where the partition function cancels out and only the difference in the energies of these respective states is seen to affect the likelihood of the occurrence. This is a key concept in the Metropolis algorithm that will be introduced next.

Metropolis MC algorithm

One of the simplest implementations for MC methods is the Metropolis algorithm [98, 99]. Here, going to a state with a lower energy than the initial one is always accepted. However, going to a higher energy state is accepted with the Boltzmann weight of the difference of their energies [5]. In other words

$$\begin{aligned} P_{\mathrm{m}\to\mathrm{n}} &= 1 && \text{if} && H_{\mathrm{n}} < H_{\mathrm{m}} \ , \\ P_{\mathrm{m}\to\mathrm{n}} &= \exp\left(-\beta(H_{\mathrm{n}} - H_{\mathrm{m}})\right) && \text{if} && H_{\mathrm{n}} > H_{\mathrm{m}} \ . \end{aligned}$$

The computational implementation of the method differs somewhat in that if the energy of the state is increased from the transition, a random number is generated and compared to the Boltzmann weight of the difference in energies. If the random number is smaller, the transition is accepted else the system will stay in the initial state [97]. Another important aspect of the algorithm is the moves that are utilized for these transitions, which greatly affect its efficiency. A description of the moves that will be used later on for the study of the polymer melt systems should be provided, to conclude all the required introductory concepts involved.

Monte Carlo moves

As mentioned previously, the Monte Carlo method samples different states of the system from an initial starting point. The energy of the system is changed through the use of suitable moves applied to the particles in the system, here the polymer chains, in order to see whether they would result in an energy reduction or increase. In the cases studied here, two moves are utilized with equal probability of occurrence which are the slithering snake and the crankshaft moves as introduced in [96]. We shall describe them briefly here.

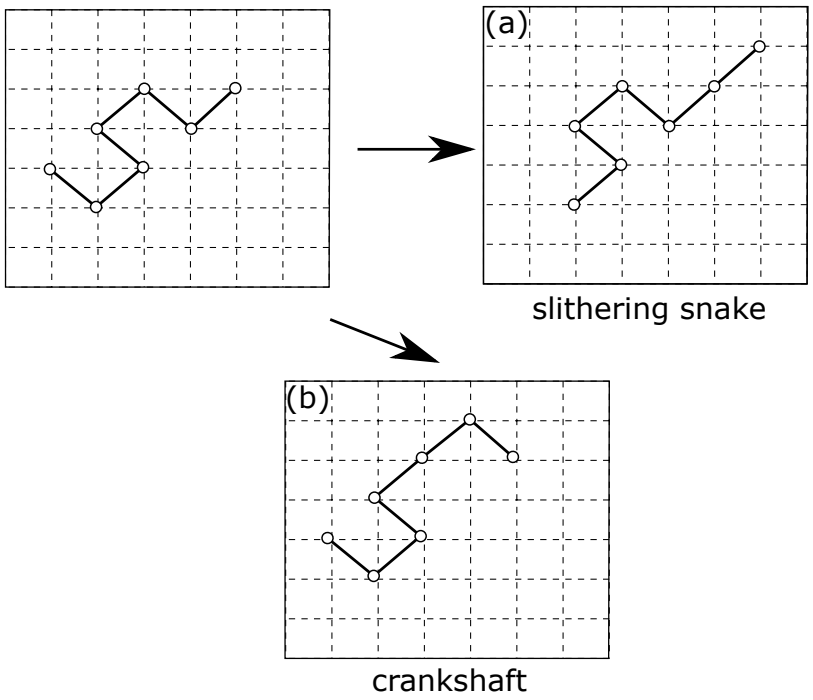

Figure 2.1: Illustration of the (a) slithering snake move and the (b) crankshaft move.

For the slithering snake move shown in figure 2.1a, a chain end is chosen randomly with one of its nearest neighbor sites. It then involves moving the chain end to that site which means all the other monomers are shifted by one site along the chain. The transition will occur if the site chosen is vacant, or if full, it contains the other end of the same chain. This is because the excluded volume interactions included in these lattice model simulations, strictly prohibit double occupancy in any of the sites. The other move attempted is the crankshaft move, as shown in figure 2.1b, which involves choosing one of the non-end monomers and moving it while its two bonded neighbors are fixed. Based on the angle of the chosen bonds, the move will either have different possible choices or none at all. In the case of multiple possibilities, one is selected at random and the move is implemented.

MC simulations for polymer melts

Having covered the basic concepts of MC simulations, its application to our polymer melt systems can be presented [95]. As was previously mentioned, with the aim of comparing the results to those of the SCFT lattice model, the polymers are constrained to be on an fcc lattice in this case as well. Bonds of length b between monomers are on nearest neighboring sites and each lattice site will be occupied by a maximum of one monomer. To constitute the lattice, a simple cubic $L \times L \times L$ lattice is created and every other site is deleted to create a total of $L^3/2$ sites. The average monomer density is set to be $\rho_0 \approx 0.8\sqrt{2}/b^3$ to allow the polymers room to move around. From previous studies [100] we know the segment length a to be related to the bond length b by $a = 1.233b$, where the bond length is equal to the lattice spacing.

Similar to what was outlined in 2.2.1 for the mean-field lattice model, the surface is created by applying a field to ensure the total concentration is of a specific shape. That is to say, the average polymer concentration is constrained to be $\phi(z) \equiv \left\langle \hat{\phi}(z) \right\rangle = 1$ by applying a field $w(z)$ to polymers confined in the z direction. For this to occur, periodic boundary conditions are applied in the x and y directions while the material is set to be between $z = 0$ and $(L-1)\Delta z$, where $\Delta z = b/\sqrt{2}$ is the distance between lattice planes. Needless to say, the magnitude of L is chosen such that bulk properties are exhibited in the middle of the box.

With the monomers placed on lattice sites and the bonds being between nearest neighbor sites, we ensure that the bond length is constant and the energy of the system results from the field interacting with the monomers. The total number of monomers in a lattice layer are given by the quantity $\hat{m}(z)$, which will give the energy as

$$E = \sum_z \hat{m}(z) w(z) \ , \tag{2.72}$$

and the dimensionless concentration by

$$\hat{\phi}(z) \equiv \frac{2\sqrt{2}\hat{m}(z)}{\rho_0 b^3 L^2} \ . \tag{2.73}$$

In order to allow the system to adopt its correct form, we start from an initial state where the polymers are placed on the lattice sites in an extended configuration from which moves are attempted to allow the system to evolve. With each Monte Carlo step (MCS), a polymer chain is chosen randomly and one of the two moves presented previously, *i.e.* a slithering snake or crankshaft move is attempted, with equal probability allocated to both [96]. The acceptance rate of the moves is determined by the Metropolis criterion as mentioned before. The start of the simulation usually involves a large number of MCS (typically 10^6 per monomer) such that the polymers attain realistic configurations. Then, as before, the field is adjusted by simple mixing

$$w^{(k+1)}(z) = w^{(k)}(z) + \lambda(\hat{\phi}(z) - 1) \ , \tag{2.74}$$

with a mixing parameter of $\lambda = 0.01$ for about 10^5 MCS per monomer. This is followed by fixing the field and collecting statistics for about 10^7 MCS per monomer. Once every 40 MCS per monomer, thermodynamic averages of interest are calculated.

It has already been noted that the size of the box, L, should be big enough to allow bulk behavior to be achieved in the middle of the system. However, having a larger box will be more computationally extensive, hence the trade-off should be considered carefully. In this light, mean-field calculations will guide the value chosen for the length, which will be used to run the simulations and tweaked if the concentrations in the bulk are not within a desired tolerance (usually one percent) of the target value. This will all be done while ensuring that the overall monomer concentration is kept to be $\rho_0 = 0.8\sqrt{2}/b^3$. With the considerations mentioned thus far, we can conclude the theoretical concepts that are prerequisites to presenting the results, and begin our presentation of the findings for each of the systems described to this point.

Chapter 3

Monodisperse melts

As noted in the introduction, the presence of a surface hinders and constrains the configurational space of polymer chains, thus resulting in a decrease in entropy. The end monomers suffer less of an entropy loss when placed near the surface compared to the middle monomers. This becomes evident when we consider the greater freedom of movement the chain has with an end close to the surface, as compared to having the middle monomers there. The resulting entropic end-monomer segregation to melt surfaces, as observed in simulations [8, 16, 43, 51, 64] as well as theory [2, 66], is in disagreement with the Silberberg argument which stated the surface to act as a reflecting boundary. As previously noted in section 1.4.1, there should be an N^{-1} dependence for the surface tension. This relation stems from the ends of chains of length N being proportional to its reciprocal, thus signifying alterations in surface tension with changes in molecular weight, which is observed and confirmed in many experiments [24, 31, 32].

We have already mentioned a number of reasons for these violations of Silberberg's theory in the introduction. One being the finite width, ξ, over which the surface concentration goes to zero. This was shown by Wu *et al.* [33], where they had also observed the N^{-1} dependence in the surface tension. Another is chain discreteness as seen from both simulation [42] as well as theory [66]. We begin by implementing an SCFT calculation in order to combine the effects of both chain discreteness as well as the surface width to compare and gauge the influence of each. Moreover, the results will be compared to the semi-analytical calculations introduced in the previous chapter, in order to attain which aspects of the results are universal and which depend on microscopic details. Simulations will also be done in order to test the universality of the behavior observed. In keeping with the order of presentation in the previous chapter, the results for the off-lattice model precede the ones for the lattice model, each of which shall be followed by a detailed discussion of the observed phenomena.

3.1 Off-lattice model

Having presented the theory for this model for a monodisperse melt in the previous chapter, we shall briefly summarize the main equations to be followed by the results for our SCFT calculations. Both the end monomer concentrations as well as the surface tension, which will be affected by the segregation of ends, will be investigated. Instead of utilizing an equation of state to provide the relationship between the field and the concentration, which would give the shape of the surface as a result, we will simply assume a reasonable functional form for the surface profile. The logic of this choice will be explained in detail in the discussion following the results. Two distinct surface profiles, sigmoidal and linear shapes, will be considered to surmise the dependence of results on the chosen forms. The surface width of the aforementioned profiles, ξ, is simply an input in our study. In this light, we will be able to investigate how the excess of ends depends on the interfacial width in addition to other parameters. The semi-analytical prediction and its comparison to our numerical findings from SCFT will grant us a deeper insight into the behavior of the system.

3.1.1 Theory

Here we have n polymer chains each containing N monomers connected with bonds of a Hookean spring nature, whereby the effect of this chosen bond potential has been tested and characterized previously [66]. The total volume of the system is $V = nN/\rho_0$ with the denominator being the segment concentration. The surface of the melt is placed at $z = 0$ and extends in the x-y plane with an area of $\mathcal{A}$. With the non-bonded interactions given by a field, $w(z)$, the propagators required for the determination of the concentration are evaluated by the recursion relation

$$G_{i+1}(z) = h(z) \int g(Z) G_i(z - Z) \mathrm{d}Z \ , \tag{3.1}$$

where $G_1(z) = h(z) \equiv \exp(-w(z)/k_B T)$ and for Hookean springs

$$g(Z) = \left(\frac{3}{2\pi a^2} \right)^{1/2} \exp\left(-\frac{3Z^2}{2a^2} \right) \ . \tag{3.2}$$

Having obtained the propagators, if the field is set to be zero in the bulk, the concentration of monomer i is given by

$$\phi_i(z) = \frac{G_i(z) G_{N+1-i}(z)}{h(z)} \ , \tag{3.3}$$

which gives the total concentration as

$$\phi(z) = \sum_{i=1}^{N} \phi_i(z)/N \ , \tag{3.4}$$

where the concentration has been scaled to be one in the bulk. The SCFT calculation is carried out by adjusting the field such that $\phi(z)$ conforms to the chosen surface profile. The field is initialized with a given value and the total concentration is attained through the use of the aforementioned equations. Should the resultant total concentration not agree with the target surface profile, the field will be altered and the steps implemented once more until the field and the concentration satisfy the self-consistent set of equations above. The field adjustment is done through the Anderson mixing algorithm [92, 101] as it is more efficient than the simple mixing method for the systems studied here, specially as the profile width increases. We consider two surface profile shapes to test the sensitivity of the results to the chosen form, one being the sigmoidal profile

$$\phi(z) = \frac{1}{2}\left[1 + \tanh\left(\frac{2z}{\xi}\right)\right] \ , \tag{3.5}$$

and the other a simple linear shape

$$\phi(z) = \begin{cases} 0 \ , & \text{if} \ \ z < -\frac{\xi}{2} \ , \\ \frac{1}{2} + \frac{z}{\xi} \ , & \text{if} \ \ -\frac{\xi}{2} < z < \frac{\xi}{2} \ , \\ 1 \ , & \text{if} \ \ \frac{\xi}{2} < z \ . \end{cases} \tag{3.6}$$

The case of the sigmoidal profile is given special attention, as it is seen to occur in polymeric melt surfaces in simulations [8, 63]. With the previous definitions, which resulted in the simplified form of the monomer concentration in equation 3.3, we can see that the concentration of ends, which we are looking at determining, are given by

$$\phi_e(z) \equiv \phi_1(z) = G_N(z) \ . \tag{3.7}$$

Lastly, the steps to calculating the surface tension have been previously shown, where its form was given by equation 2.38. This shall give us the numerical results for the surface tension, which can then be compared to values obtained from the semi-analytical prediction. With the theoretical considerations developed in this manner, we proceed to present the results for the mean-field calculation of the monodisperse melt using the off-lattice model, in the section that follows.

3.1.2 Results

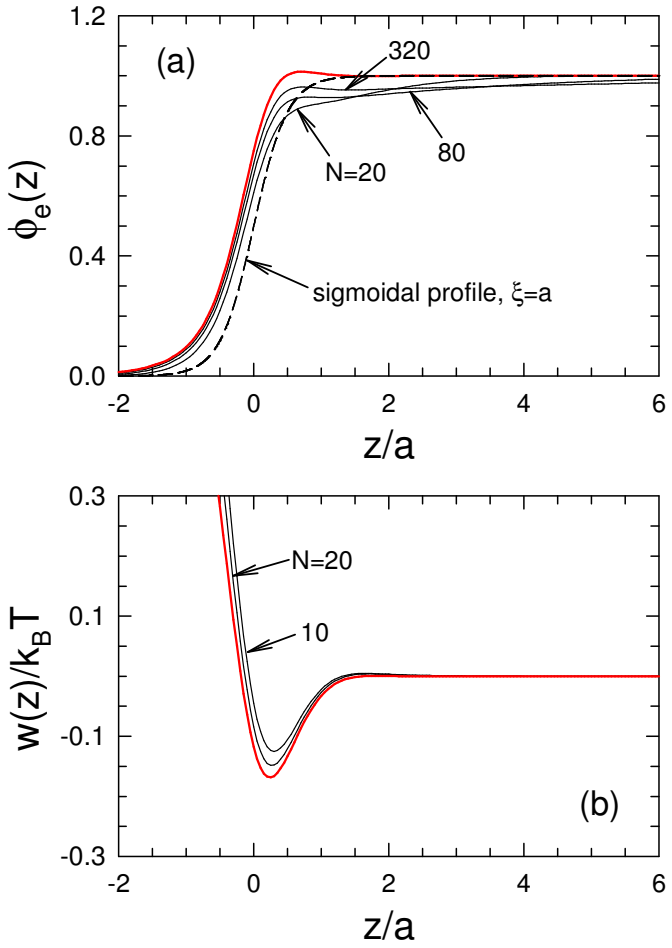

Figure 3.1: (a) Concentration of ends, $\phi_e(z)$, and (b) self-consistent field, $w(z)$, for the sigmoidal polymer profile, eq. (3.5), of width $\xi = a$, as shown by the dashed curve in plot (a). The red curves denote the infinite molecular weight limit while the finite length results are shown by the black curves.

As the width of the polymer surface is generally seen to be similar to the size of the monomers [8, 43, 68], here being a, we focus on a sigmoidal profile of the width $\xi = a$ for the total concentration. In figure 3.1 the end monomer concentration, $\phi_e(z)$, is given for chains with N being finite (black curves) as well as the infinite limit (red curve) where they are compared to the total concentration, $\phi(z)$ (dashed curve). There is a clear excess of ends

($i.e.$, $\phi_e(z) > \phi(z)$ for $z \lesssim a$) near the surface which is followed by a depletion. The self-consistent field required to produce this sigmoidal profile for the total concentration of each individual case is shown in figure 3.1b. Here it is clear that the effect of chain length is very small since the field, $w(z)$, for finite chains of length $N \gtrsim 100$ is almost indistinguishable from $w_\infty(z)$ (red curve). Similar to figure 3.1, the end monomer concentrations as well as the self-consistent fields used to obtain them are shown for the linear profile, eq. 3.6, in figure 3.2. Once more the surface width is set to be $\xi = a$, and the behavior is observed to be qualitatively the same.

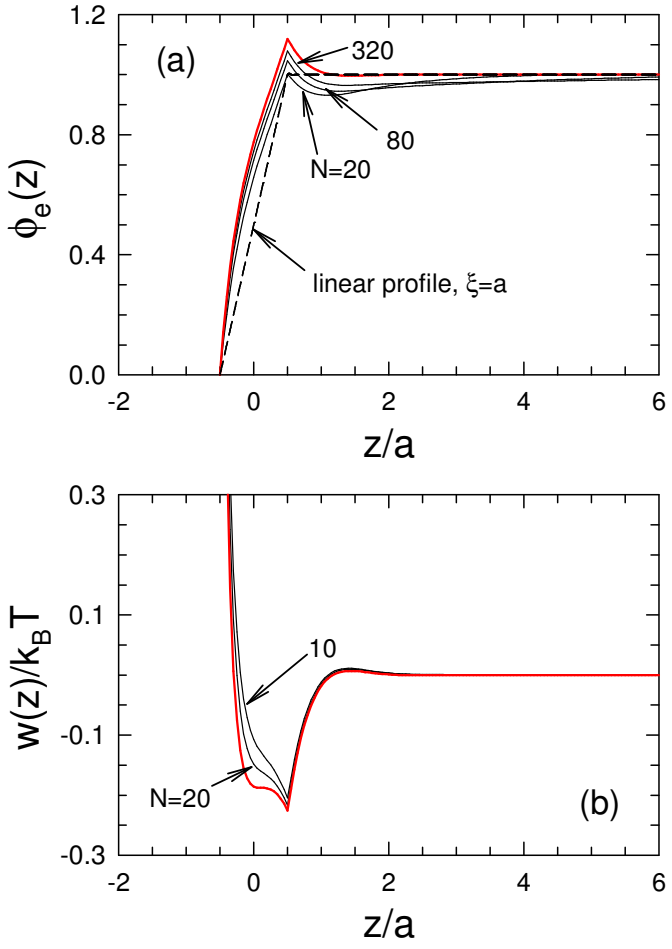

Figure 3.2: Analogous plots to those of fig. 3.1, but calculated for a linear polymer profile, eq. (3.6), of width $\xi = a$.

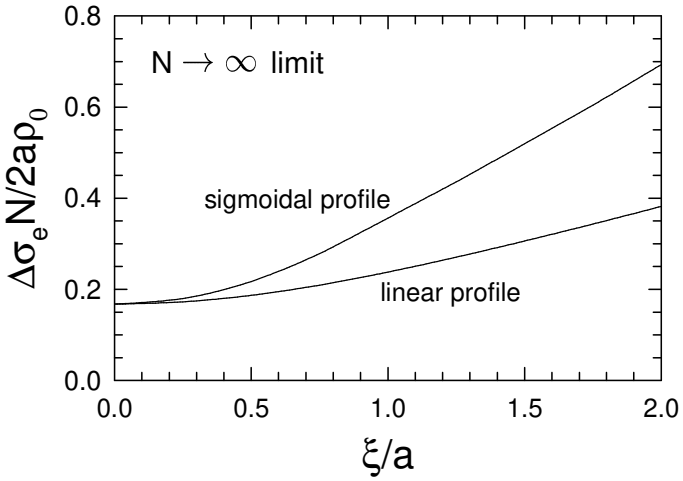

Figure 3.3: The surface excess of ends per unit area, $\Delta\sigma_e$, plotted in terms of the width, ξ, of the concentration profile in the infinite molecular-weight limit. The ratio appearing in the vertical axis is precisely the A appearing in eqs. (3.10), (3.11), (3.13) and (3.20).

Now that we have shown the existence of an excess of ends at the surface, we can find the total excess of ends by

$$\Delta\sigma_e = \frac{2\rho_0}{N}\int_{-\infty}^{z_0}[\phi_e(z)-\phi(z)]\mathrm{d}z\ , \tag{3.8}$$

where z_0 is the point at which $\phi_e(z_0)=\phi(z_0)$. With an excess of ends observed at the surface, there must be a depletion of them in the bulk since this is where they must segregate from. The range of this phenomenon is seen to be proportional to $N^{1/2}$, which makes the depth of the depletion scale as $N^{-1/2}$. Hence, in the infinitely long chain limit, the distribution of ends given by $G_\infty(z)$, has only an excess and no depletion (as evident from the red curves in figures 3.1a and 3.2a). This gives the approximation for the large N to be

$$\lim_{N\to\infty}\frac{\Delta\sigma_e N}{2a\rho_0} = \frac{1}{a}\int_{-\infty}^{\infty}[G_\infty(z)-\phi(z)]\mathrm{d}z\ , \tag{3.9}$$

as shown in figure 3.3. This figure provides evidence that the surface width plays a comparable role to chain discreteness (the value at $\xi=0$) in terms of the entropic excess of ends. That is to say, the intercept at $\xi=0$ gives the end excess for a sharp step profile for which the cause of the segregation would solely be the discreteness of the chains [66]. As the width is increased however, its influence becomes evident and presents itself to result in an effect of approximately equal magnitude for the excess, *e.g.* at $\xi=a$.

From our semi-analytical calculation, for which the details were presented in the previous chapter, we can see how $\phi_e(z)$ relates to $G_\infty(z)$ (*e.g.*, the red curves in figures 3.1a and 3.2a). Having previously gone through the steps of this calculation, they will be omitted here for brevity, hence only the final forms of interest are mentioned. A reminder is given that the superscript of zero denotes the quantities when the chains are placed in the field of infinitely long ones. The propagator in $w_\infty(z)$ assumed the form given by equation 2.57

$$G_N^0(z) \approx G_\infty(z) + A\sqrt{\frac{6}{\pi N}} \times \left\{ \left[\exp\left(-\frac{3z^2}{2a^2 N} \right) - 1 \right] H(z) + G_\infty(z) \right\} \ , \tag{3.10}$$

which gave the total concentration in this field by equation 2.58

$$\phi^0(z) \approx \phi(z) + 4A\sqrt{\frac{6}{\pi N}} \frac{\phi(z)}{G_\infty(z)} \times \left\{ \left[f\left(\frac{z}{aN^{1/2}} \right) - 1 \right] H(z) + G_\infty(z) \right\} \ . \tag{3.11}$$

The coefficient A appearing in these equations needs to be determined from [66]

$$A = \frac{1}{a} \int_{-\infty}^{\infty} [G_\infty(z) - \phi(z)] \mathrm{d}z \ . \tag{3.12}$$

To show the validity of the aforementioned formulations from the semi-analytical calculation, we compare the value given by these expressions to numerical results obtained by placing finite chains in $w_\infty(z)$. That is to say, we compare values from the SCFT calculation to those obtained from the aforementioned expressions, *i.e.* equations 3.10 and 3.11. In this light, we begin by considering the propagator in $w_\infty(z)$. Parts a and b of figure 3.4 show the short and long range corrections to $G_N^0(z) - G_\infty(z)$ as given by equation 3.10, for the sigmoidal profile of width $\xi = a$. We see that the numerical results (black curves) converge to both limits as the length of the chain increases which shows the validity of the predicted forms. As mentioned in the previous chapter, the next step of the semi-analytical calculation requires the field to be corrected by linear-response theory to remove the excess polymer concentration $\phi^0(z) - \phi(z)$ as seen in figure 3.5. Both parts of this figure serve to validate the form given by equation 3.11 for each length scale. Following the logic of the steps formerly shown for this calculation, the change in the end monomer concentration due to the change in the field can be determined. The addition of the correction to the predicted form from equation (3.10) gives the final result presented in equation 2.63, which was

$$\phi_e(z) \approx G_\infty(z) + \frac{A}{N^{1/2}} \times \left\{ \left[B\left(\frac{z}{aN^{1/2}} \right) - B(0) \right] H(z) + B(0) G_\infty(z) \right\} \ , \tag{3.13}$$

with the universal function $B(\zeta)$ defined in equation 2.64.

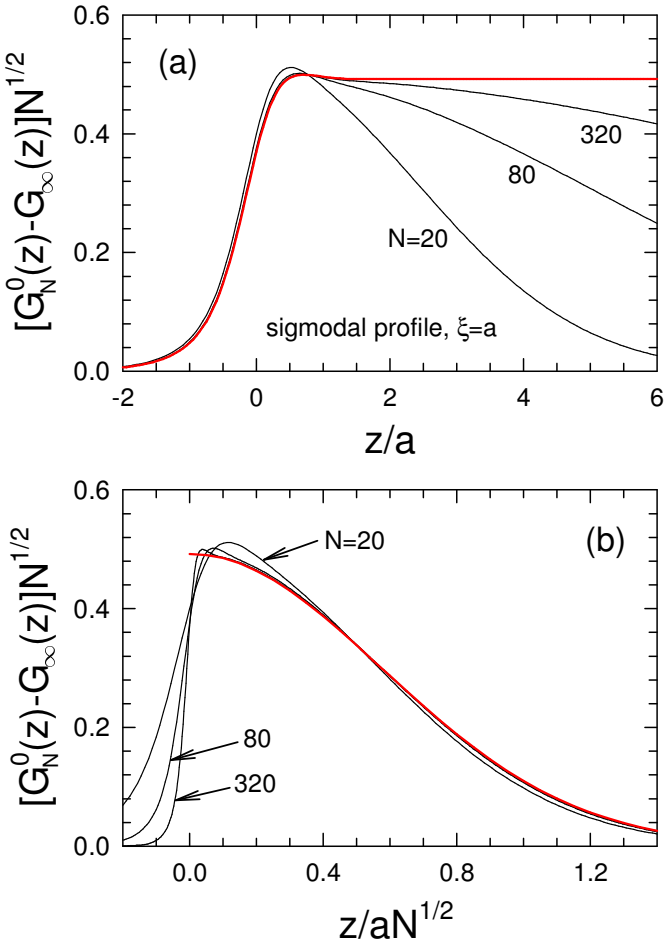

Figure 3.4: Correction to $G_N^0(z) \approx G_\infty(z)$ plotted on the (a) monomer and (b) molecular length scales for different values of N. The red curves show $A\sqrt{6/\pi}G_\infty(z)$ and $A\sqrt{6/\pi}\exp(-3z^2/2a^2N)$, depicting the short and long range parts of equation 3.10, respectively.

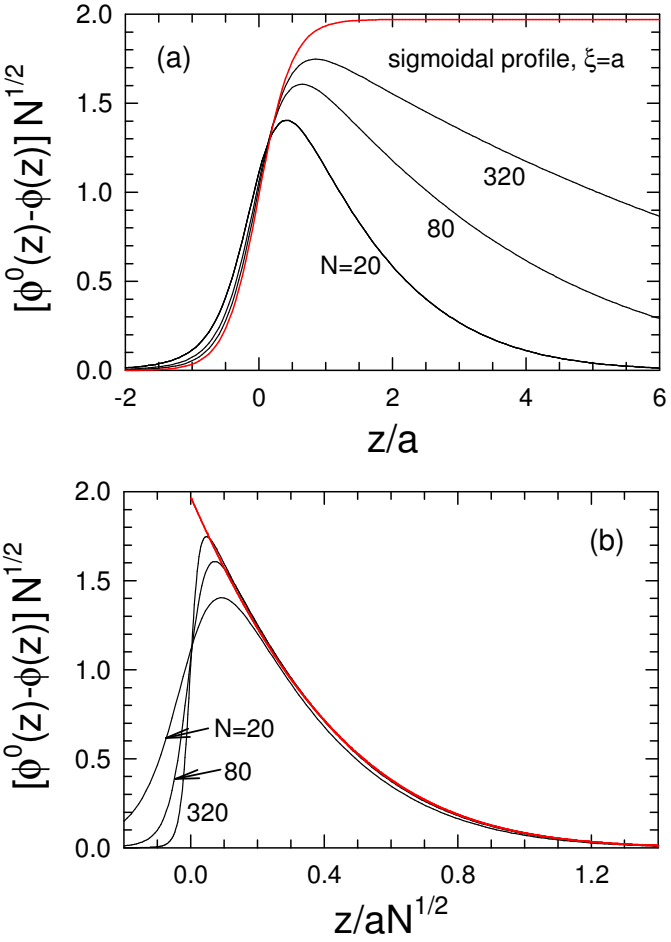

Figure 3.5: Correction to $\phi^0(z) \approx \phi(z)$ plotted on the (a) monomer and (b) molecular length scales for different polymerizations, N. The red curves denote $4A\sqrt{6/\pi}\phi(z)$ and $4A\sqrt{6/\pi}f(z/aN^{1/2})$, depicting the short and long range parts of equation 3.11, respectively.

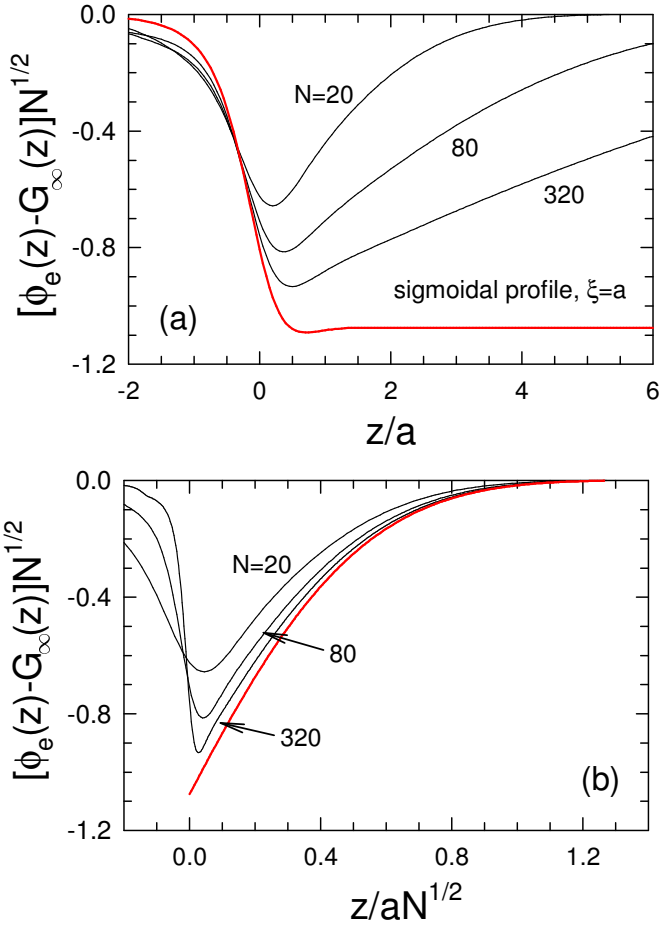

Figure 3.6: Correction to $\phi_e(z) \approx G_\infty(z)$ plotted on the (a) monomer and (b) molecular length scales for polymers of various lengths N, calculated for a sigmoidal surface profile of width $\xi = a$. The red curves denote $AB(0)G_\infty(z)$ and $AB(z/aN^{1/2})$, verifying both length scales of the semi-analytical formulation as proposed by equation 3.13, respectively.

Figure 3.6 confirms the short and long range corrections from equation 3.13 in parts a and b respectively. That is to say, the assumption that the field of infinitely long chains would not be the correct self-consistent field required for chains of finite length has been applied and the correction from linear-response theory included. Once more, the black curves show the results from mean-field theory and are seen to approach the red curves (corresponding to the predictions) as the chain lengths increase, which is in agreement with our expectations. This figure is for the sigmoidal profile of width $\xi = a$ and a similar one is presented for the linear profile of the same width in figure 3.7.

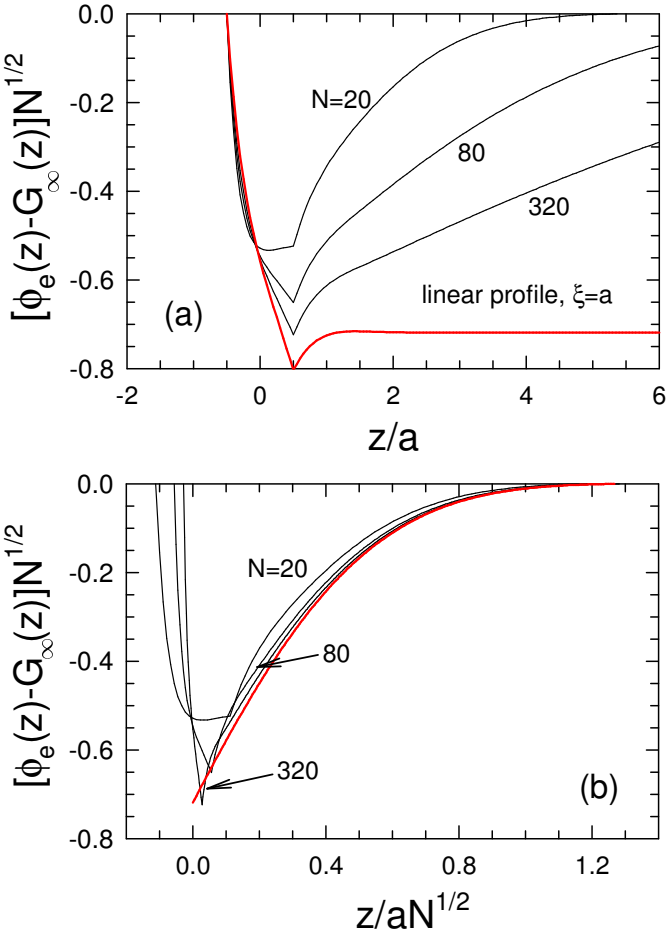

Figure 3.7: Analogous plots to those in figure 3.6, but calculated for a linear surface profile of width $\xi = a$.

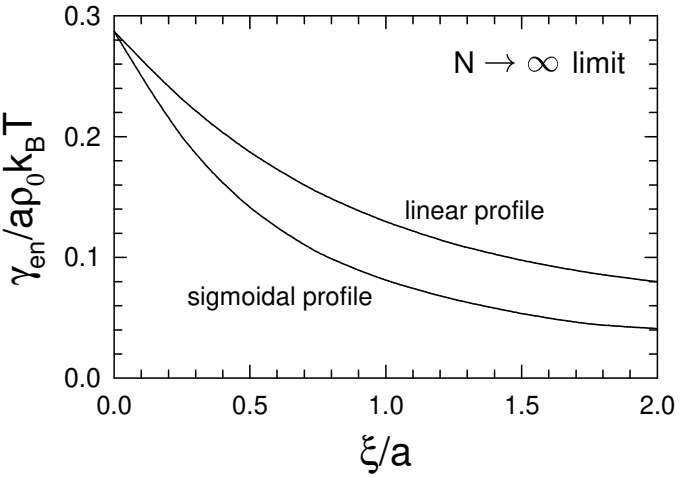

Figure 3.8: Entropic contribution to the surface tension, γ_{en}, as a function of the width, ξ, of the concentration profile in the infinite molecular-weight limit. The dimensionless ratio plotted on the vertical axis equates to the Γ_∞ appearing in equation 3.20.

The last remaining quantity to be considered is the entropic contribution to the surface tension, γ_{en}, given by the expression in equation 2.38. In the manner of the previous predicted forms we obtained for the propagator as well as the concentration of ends, a corresponding equation for the surface tension would help us test the accuracy of the mean-field results through comparison. To obtain such a prediction for the surface tension, the same steps must be followed as before. In this light, we must first calculate its large N limit to then correct it from LR theory. This gives the surface tension as

$$\gamma_{\text{en}} = -\rho_0 \int w(z)\phi(z)\mathrm{d}z \approx -\rho_0 \int \left[w_\infty(z) + \delta w(z)\right]\phi(z)\mathrm{d}z \tag{3.14}$$

or in dimensionless form

$$\frac{\gamma_{\text{en}}}{a\rho_0 k_B T} \approx -\frac{1}{ak_BT}\int w_\infty(z)\phi(z)\mathrm{d}z - \frac{1}{ak_BT}\int \delta w(z)\phi(z)\mathrm{d}z \tag{3.15}$$

$$= \Gamma_\infty - \frac{1}{ak_BT}\int \delta w(z)\phi(z)\mathrm{d}z\ . \tag{3.16}$$

Both parts of equation 3.16 require further explanation and will be outlined here. For a more detailed clarification of the steps involved, the reader is referred to previous work by Matsen *et al.* [66]. The first term is the dimensionless surface tension of an infinitely long chain

$$\begin{aligned}\Gamma_\infty &\equiv \lim_{N\to\infty} \frac{\gamma_{\text{en}}}{a\rho_0 k_B T} \,, \\ &= -\frac{1}{ak_BT}\int w_\infty(z)\phi(z)\mathrm{d}z \,, \xrightarrow{\text{equation 2.39}} \\ &= \frac{1}{a}\int \phi(z)\ln\left[\frac{G_\infty^2(z)}{\phi(z)}\right]\mathrm{d}z \,, \end{aligned} \tag{3.17}$$

where the values for Γ_∞ are presented in figure 3.8 as a function of the width ξ of the surface profile. For the second term, from linear-response theory for hompolymer melts, equations 2.59 and 2.61 give

$$\widehat{\delta w}(k_z) = \frac{4Aas_e(x)k_BT}{Ns_\phi(x)} \,. \tag{3.18}$$

By noting the Fourier transform definition given in equation 2.45, we see

$$\int_0^\infty \delta w(z)\mathrm{d}z = \frac{1}{2}\widehat{\delta w}(0) \,, \tag{3.19}$$

where we have made use of the reflecting BC placed at $z = 0$ which makes this an even function. From the definitions of the Debye function and the Debye-like function, $s_\phi(x) = 2(e^{-x}+x-1)/x^2$ and $s_e(x) = (1-e^{-x})/x$, it is evident that $s_e(0) = s_\phi(0) = 1$. Considering all of the above, we obtain $\widehat{\delta w}(0) = 4Aak_BT/N$. The inclusion of this expression, which by considering equation 3.19 will give the second part of equation 3.16, allows us to obtain the predicted form for the surface tension as

$$\frac{\gamma_{\text{en}}}{a\rho_0 k_B T} \approx \Gamma_\infty - \frac{2A}{N} \,. \tag{3.20}$$

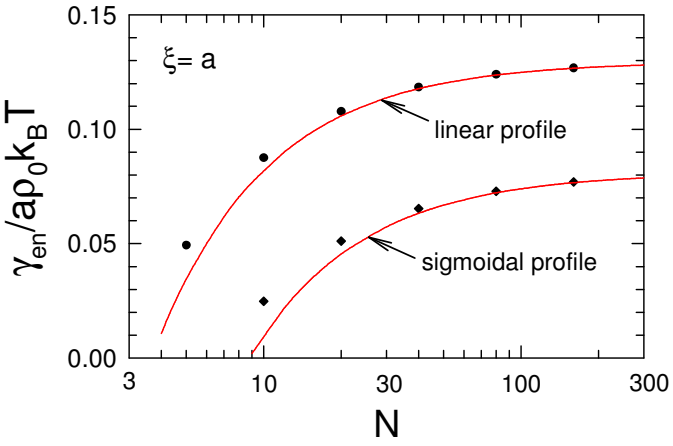

Figure 3.9: Entropic contribution to the surface tension, γ_{en}, as a function of polymerization, N. The symbols denote the full SCFT calculation while the red curves denote the approximation from equation 3.20.

All quantities in equation 3.20 have already been fully introduced, hence all that remains is the comparison of mean-field numerical results to values obtained from this expression. It is worth mentioning that the two quantities A and Γ_∞ are seen to be dependent on model details such as the interfacial width, as is evident from figures 3.3 and 3.8, respectively. The accuracy of this approximate form is illustrated in figure 3.9 (red curves) through its comparison to the full SCFT calculation (symbols) from which it is seen to perform adequately. Once more, we observe better agreement at the higher chain lengths between the two methods. The aforementioned behavior is in line with our expectations, since this is where the discrete chain model approaches the Gaussian chain limit, for which linear-response theory is developed.

3.1.3 Discussion

In our presentation of the original argument made by Silberberg in section 1.2.1, it became evident that factors such as the discreteness of the chains as well as the total concentration not conforming to a step profile would be influential in observing the excess of end monomers. Here we have considered the combined effects of chain discreteness as well as compressibility by imposing a specific shape with a given width for the surface profile. Nonetheless, we have yet to fully motivate our method of choice for approaching the calculations which, in turn, should highlight the significance of the results obtained and emphasize the importance of their universality. We had initially thought to utilize the

equation of state used by Wu *et al.* [33], which relates the field to the concentration of the melt by $w(z) = \phi(z)/\kappa$, where κ is the compressibility of the melt. Although this treatment would give the shape of the surface profile with a width, ξ, that depends on κ, the results would be unphysical due to the unrealistic nature of this equation of state.

Firstly, as is evident from their energy functional, $U[\phi]$, given by

$$\frac{U[\phi]}{\mathcal{A}} = -\frac{\rho_0^2}{2\kappa}\int \phi^2(z)\mathrm{d}z \ , \tag{3.21}$$

this treatment would allow the melt to fill all the space in the system, similar to how a gas would behave. Their solution for this is setting the concentration to be zero at the wall, which is key to the results they obtained. In addition, it was their use of a Gaussian chain model that resulted in a continuous profile, which would not be the case for the discrete chain model we had sought to use. That is to say, by setting the constraint of zero concentration at the wall we would observe a discontinuous profile. Lastly, their method is not tractable, as is evident in them resorting to solving the last steps of their calculation numerically. In considering all of the above, we decided to separate the issue of having a realistic equation of state and looking at the surface behavior of a polymer melt. We could have used a more intricate equation of state, thus allowing us to obtain the actual shape of the surface profile instead of assuming one for the melt. However, as the work of Wu *et al.* [33] would suggest, even with a simple albeit unrealistic equation of state, one would get lost in the numerical calculations. This does not bode well for the tractability of the method in terms of using a more elaborate equation of state. In addition, we had wanted to obtain analytical results to enhance our understanding, which is what they were unsuccessful in completing.

In our implementation, instead of obtaining a profile shape, we chose to assume one for the total concentration with a width, ξ, that is simply an input parameter in our study. This simplification enabled us to look at realistic surface shapes, such as a sigmoidal profile, that were not as sharp as the ones obtained in the results of Wu *et al.* [33] and hence were more representative of polymer air surfaces. In addition, we were able to complete our analytical calculation for the long range depletion of the ends given by $B(z/aN^{1/2})$. Our calculation involved only one step that required numerical evaluation, that being the simple evaluation of $G_\infty(z)$. As a result of our method, the coefficients A and Γ_∞ from the semi-analytical results will depend on model details such as the value of ξ, as seen in figures 3.3 and 3.8, respectively. This would suggest the need for an atomically realistic model to obtain the quantitative amount of the surface end excess, that is not within the scope of a coarse-grain model. Nonetheless, the general trends observed here such as the increase in $\phi_e(z)$ at the surface as $N \to \infty$, can be trusted since they are also observed by simulations

[16, 51, 62]. Moreover, once N is large enough, the universal predictions such as the shape of the long range depletion in equation 2.64, should be quantitatively accurate.

It should be noted that although our semi-analytical method involved one numerical step, its extension to the continuous Gaussian chains can be made fully analytical. In this case, with the field spread evenly along the chain contour, $G_\infty(z) = \sqrt{\phi(z)}$ instead of $G_\infty(z) = \sqrt{h_\infty(z)\phi(z)}$. Insertion of this into equation 3.12 gives the value of the coefficient A as

$$A \approx \frac{1}{a}\int \left(\sqrt{\phi(z)} - \phi(z)\right) \mathrm{d}z \ , \tag{3.22}$$

and further simplification using approximations for the Gaussian chains [12] gives

$$\Gamma_\infty \approx \frac{a}{24}\int \frac{[\nabla\phi(z)]^2}{\phi(z)}\mathrm{d}z \ . \tag{3.23}$$

By using equations 3.22 and 3.23 in conjunction with equation 3.20, we should be able to analytically determine the entropic contribution to the surface tension in terms of a given surface profile shape. This, in turn, should allow us to obtain the equilibrium surface profile since we can find the total surface tension by having a realistic functional, $U[\phi]$. We would have to minimize the total surface tension, $\gamma = U[\phi]/\mathcal{A} + \gamma_{\text{en}}$ under the constraint $\int \phi(z)\mathrm{d}z = \text{constant}$, since the total amount of material is fixed. In lieu of the unrealistic energy functional mentioned in equation 3.21 that does not produce two-phase coexistence between melt and vapor states, we can use a more elaborate $U[\phi]$, *e.g.* from density functional theory [102, 103]. This would allow us to obtain fully analytical results, which Wu *et al.* [33] were not able to do. The aforementioned arguments highlight the benefits of our method of choice, in terms of its simplicity as well as its capability in allowing us to obtain semi-analytical, or in terms of Gaussian chains fully analytical, results.

To test the universality of the aforementioned predictions, a comparison to computer simulations will be presented in the following section. Segregation of end monomers to surfaces of monodisperse melts has been observed by numerous studies [8, 16, 43, 51, 62, 64] with Müller *et al.* [42] having even considered the effect of chain discreteness. The goal of performing these simulations will be observing the compensating depletion of ends as well as comparing the simulation outcome to both the numerical SCFT and semi-analytical results explained here. An issue with simulations is the difficulty of performing them at high molecular weights (*e.g.* $N \gtrsim 100$) due to the great demand of computational resources. This is resolved by performing the simplest simulation possible, which is done by placing the polymers on a lattice as well as choosing a step profile for the surface shape. As noted in the previous chapter, we shall also apply the mean-field calculation such that both are implemented for the same model.

3.2 Lattice model

As previously mentioned, excluded volume interactions are one of the ways the Silberberg argument is violated. We shall focus on this effect by implementing our calculations for a lattice model with MC simulations as well as the mean-field method [95]. In order for comparisons between the two methods to be justified, the same model will have to be applied for both. Thus, in contrast with the previous section, a lattice model will be utilized for the SCFT method, for which the principle definitions have been introduced in the preceding chapter. The changes implemented to the previous theory are seen in full in 2.2.1 and will be outlined here. Once the necessary descriptions have been presented, the combined results which compare both methods are given and tested against the semi-analytical predictions to gauge the universality of the predictions.

3.2.1 Theory and simulation

Mean-field Theory

The mean-field theory for lattice models was given in the previous chapter in section 2.2.1 hence the equations that were previously introduced are utilized here. We have the non-bonded interactions among the monomers expressed by the field, $w(z)$, determined self-consistently such that the total concentration conforms to a step profile . In the monodisperse melt, where all chains are of the same length N, we are interested in determining the end-monomer concentration, $\phi_e(z) = G_N(z)$, where the propagator is determined by the recursion relation, as given by equation 2.66.

Simulation

The general implementation of the MC simulation was given in 2.2.3 which is what shall be applied here. As previously described, the non-bonded interactions are represented by a field that is adjusted to provide the desired step profile for the total concentration. The lattice model considered here is equivalent to the model being implemented for the mean-field theory so that comparisons can readily be made. With ρ_0 giving the average monomer density and L being the size of the box, from equation 2.73 we can determine the end-monomer concentration by

$$\hat{\phi}_e(z) \equiv \frac{\sqrt{2}N\hat{m}_e(z)}{\rho_0 b^3 L^2} \ , \tag{3.24}$$

in which $\hat{m}_e(z)$ is the total number of end monomers at z. This is defined such that the average of the end concentration, *i.e.* $\phi_e(z) \equiv \left\langle \hat{\phi}_e(z) \right\rangle$, goes to one in the bulk so the excess of ends is given by

$$\delta\phi_e(z) \equiv \phi_e(z) - 1 \ , \tag{3.25}$$

which will be compared to the SCFT results.

Similar to the previous section, a comparison to the semi-analytical calculation will also be implemented, to grant us a deeper understanding. That is to say, the predictions have already been tested against the numerical mean-field results for the off-lattice model and in addition to doing the same for the lattice model at hand, we would like to extend this to include the simulation results. It was shown at the end of 2.1.3 that by evaluating the field for infinitely long chains, placing the finite chains in this field and correcting the field from linear-response theory, the end monomer concentration had the form shown in equation 2.63, which for the long range limit is

$$\delta\phi_e(z) \approx \frac{A}{N^{1/2}} B\left(\frac{z}{aN^{1/2}}\right) \ , \tag{3.26}$$

where $B(\zeta)$ was introduced in equation 2.64 as a universal function. This is the form that will be compared to both methods as we shall see in the results that follow.

3.2.2 Results

In figure 3.10a, the simulation result for the total concentration profile, $\phi(z)$ is shown for polymers of length $N = 80$. The blue curve shows the concentration without the field, which is clearly not the step profile we are seeking. However, once the correct field (shown in the inset) is applied, the profile conforms to the correct shape (black curve). The end-monomer concentration corresponding to this desired form of the total concentration, is shown for both the simulation (solid curve) as well as theory (dashed curve) in figure 3.10b where the agreement is observed to be reasonable. There is a clear excess of ends for both cases near the surface ($z = 0$) which is followed by a depletion. For the ends in the system to be conserved, this excess of ends at the surface should be balanced by the depletion in the bulk. As previously mentioned, this depletion is expected to have a universal shape, the investigation of which shall be one of the focal points of the study.

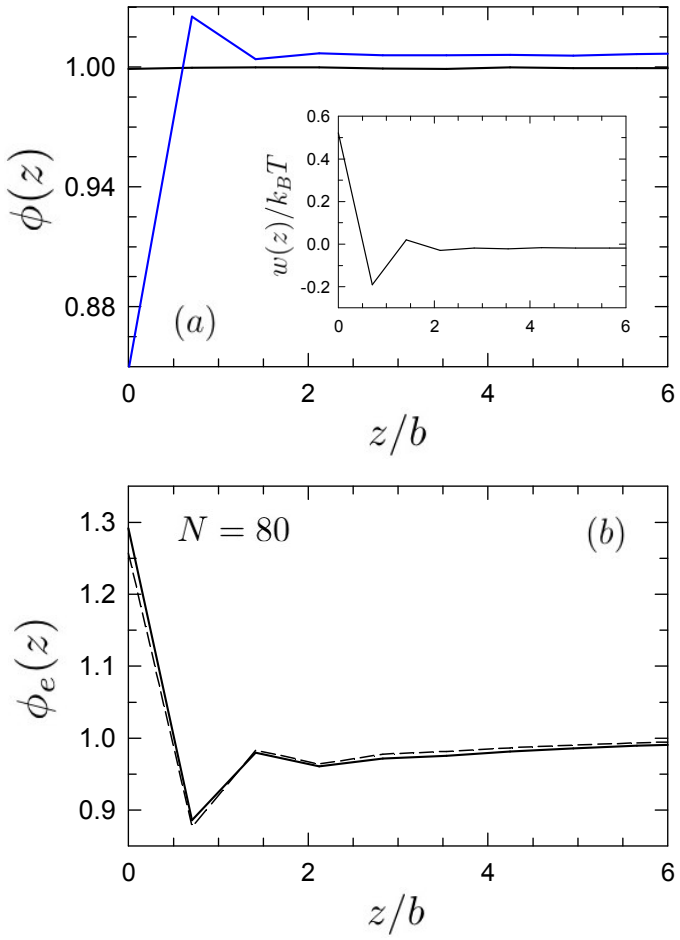

Figure 3.10: (a) Total concentration, $\phi(z)$, for a monodisperse melt of $N = 80$ polymers from simulation without (blue curve) and with (black curve) an external field, $w(z)$. The inset shows the field for the step profile. (b) distribution of end monomers, $\phi_e(z)$, from the simulation for the step profile (solid curve) compared to SCFT (dashed curve).

In this light, in figure 3.11a the depletion of ends for simulations (solid curves) is compared to SCFT results (dashed curves) for three values of the polymerization index, N. The range of depletion is seen to be greater for longer chains, as is expected. The agreement between the two methods is reasonable, with an evident overestimation in the depth from the simulations. It should be pointed out that this plot is scaled by the bond length, b. With the statistical segment length given by a, it is useful to note that for SCFT $a = b$ whereas for the simulation, $a = 1.233b$ [100]. Hence, once the data is scaled by $a\sqrt{N}$,

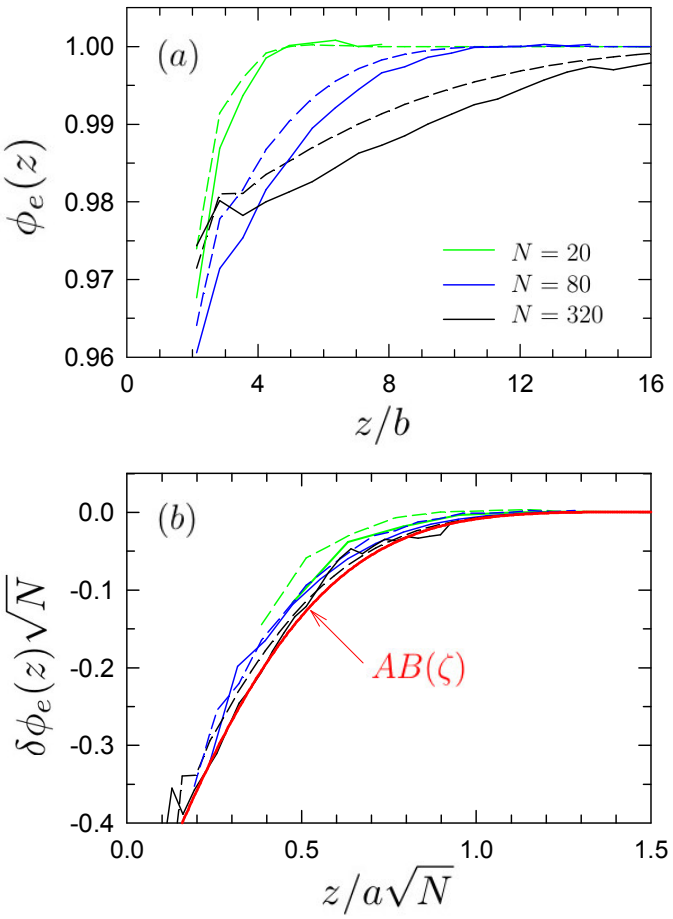

Figure 3.11: (a) Depletion of end monomers in monodisperse melts of various polymerizations, N, obtained from simulation (solid curves) and SCFT (dashed curves). (b) scaling plot comparing the results to the semi-analytical prediction in equation 3.13 (red curve).

there is excellent agreement between not only the two methods but also with the universal prediction from LR theory for the depletion (red curve), for which the formulation is given in equation 3.13. This further solidifies the idea that the prediction holds irrespective of the model utilized and is therefore universal.

3.2.3 Discussion

Universality is very powerful property that states the behavior of all systems, whether theoretical or experimental, to be quantitatively the same. The universal depletion of ends we previously obtained for the monodisperse melts, utilized linear-response theory which still relied on the mean-field approximation. So it remained to be seen whether the results were truly universal and if they would hold once excluded volume interactions, not strictly enforced in mean-field theory, were rigorously incorporated by preforming simulations. To attain higher statistical accuracy in these simulations, we simplified the study by placing the polymers on lattice sites as well as setting the total concentration to be a step profile. We applied the same model for mean-field theory so that the results could be compared and analyzed. Once more, in place of an equation of state, we have a field representing the non-bonded interactions so that we could focus on enhancing our understanding of violations to the Silberberg hypothesis, instead of dealing with the complexities the former method would entail. By having the same setup in both the simulation as well as the mean-field calculation, we ensured any variable affected by details, *e.g.* A, is changed by the same amount and no concern should arise from effects such as these.

As mentioned in the previous chapter, the excluded volume interactions considered here are screened in the bulk to a good approximation [50]. Hence mean-field theory, which in contrast to the simulations does not take excluded volume interactions into account explicitly, should be reasonably accurate. In this light, the predictions should hold for the lattice mean-field results, based on the previous argument as well as the proposed universality of the predictions, which is confirmed by the results. The excluded volume interactions are treated more rigorously by the MC simulations, since they strictly prohibit the placement of more than one monomer on each site, unlike mean-field theory which only restricts the average of this quantity and not its amount at each position. The screening is evidently still effective close to the surface since the results obtained from simulations, while treating the excluded volume interactions correctly, are seen to agree with the mean-field results. The aforementioned observance provides evidence towards the accuracy of the mean-field calculation, despite the lack of a precise treatment for excluded volume interactions. Lastly, the convergence of results from these two different methods to the prediction from linear-response theory, further solidifies the universality of these forms.

Chapter 4

Bidisperse Melts

The entropically driven end-monomer segregation observed in the previous chapter has a direction implication for polydisperse melts. When there are many chain lengths present in the system, the shorter components will be enriched near the surface due to having a higher number of ends per unit volume, and the longer constituents will be depleted in that region. The characterization of this phenomenon has been the focus of other previous works, in order to determine the integrated excess of a chain of length N at the surface, denoted by θ_N, as well as the entropic contribution to the surface tension, γ_{en}. This was first demonstrated by Hariharan *et al.* [35] for a bidisperse melt, using a mean field lattice calculation, where they looked at the amplitude as well as the range of this enrichment. They also considered the effect on the surface tension and found a simple expression for it

$$\frac{\gamma_{\text{en}}}{a\rho_0 k_B T} = 0.1842 - \frac{0.1934}{N_n} \ , \tag{4.1}$$

where

$$N_n = \left(\sum_N \frac{\bar{\phi}_N}{N} \right)^{-1} \ , \tag{4.2}$$

is the number average degree of polymerization and $\bar{\phi}_N$ is the volume fraction of chains of length N (here a is the lattice spacing and $\rho_0 = 1/a^3$).

The lattice SCFT calculations were extended to polydisperse melts by Van der Gucht *et al.* [36], whereby they determined a simple expression for the integrated excess

$$\frac{\theta_N}{a\rho_0} = 0.195\bar{\phi}_N \left(1 - \frac{N}{N_w}\right) \ , \tag{4.3}$$

where

$$N_w = \sum_N N\bar{\phi}_N \ , \tag{4.4}$$

is the weight-average degree of polymerization. Later on, the enthalpic attraction of chain ends to surfaces was considered by Minnikanti *et al.* [88]. The chains were taken to be Gaussian and the surface a reflecting boundary, in which a Dirac-delta potential attracted the ends to the surface. They applied a mean-field approximation and utilized linear-response theory. In brief, they were successful in obtaining the two aforementioned expressions with minor differences in the coefficients, which showed good agreement among the three studies.

Here we begin by extending the off-lattice SCFT considerations from the previous chapter towards the study of a polydisperse melt, in order to examine this entropic enrichment of shorter components at the surface. By preforming the semi-analytical calculation for the system at hand we derive expressions analogous to equations 4.1 and 4.3, that were postulated in the works of Hariharan *et al.* and Van der Gucht *et al.* respectively. To check the accuracy of the semi-analytical findings, they are fully tested against the numerical SCFT method for the special case of bidisperse melts. Moreover, in the concluding section of this chapter, we utilize our lattice model for this system to compare the aforementioned quantities of interest to results from MC simulations applied to the same model.

4.1 Off-lattice model

This model has been fully described in 2.1.2, hence only the main equations are outlined following which the results for the SCFT calculations will be given. The theory is presented for a polydisperse melt and the results consider the more specific case of the bidisperse melt. In accordance with the methodology of the previous chapter, the accuracy of the semi-analytical prediction is tested against the numerical SCFT results. Additionally, expressions for the integrated excess of short chains as well as the entropic contribution to the surface tension are derived and compared to numerical results. The agreement between the attained expressions and the results shown from previous literature, *i.e.* equations 4.3 and 4.1, are discussed and noted.

4.1.1 Theory

The necessary equations and definitions are presented here for the numerical self-consistent field theory (SCFT) of a polydisperse melt with a surface area $\mathcal{A}$ at $z = 0$. Each chain has N monomers with a concentration of ρ_0, connected with freely-jointed bonds that are taken to be springs, for which the bond potential was given in equation 3.2. The total concentration is obtained from the sum of the component concentrations of various lengths, $\phi(z) = \sum_N \phi_N(z)$, where the volume fraction of each component in the bulk is given by $\bar{\phi}_N \equiv \lim_{z\to\infty} \phi_N(z)$. A field, $w(z)$, represents the non-bonded interactions which, as seen in equation 2.22, gives the concentration for each component by

$$\phi_N(z) = \frac{\bar{\phi}_N}{N h(z)} \sum_{i=1}^{N} G_i(z) G_{N+1-i}(z) \ , \tag{4.5}$$

with $h(z) \equiv \exp(-w(z)/k_B T)$. Again, for convenience, we set the field to zero in the bulk. The evaluation of the propagators, $G_i(z)$, is exactly as before in section 3.1.1. The statistical segment length is a, which gives a rms end-to-end length of $R_0 \approx aN^{1/2}$ as seen in section 1.1.1.

Based on the argument mentioned in section 3.1.1, we enforce a specific surface profile with a width that is chosen as a parameter. Having already tested the effects of various profiles in the previous chapter, we focus on the more realistic sigmoidal shape here. This method is in place of handling the difficulties arising from an equation of state, relating the non-bonded interactions to the profile, which adds unnecessary complications without contributing to our understanding. As before, we start with an initial field, calculate the resultant concentration and adjust the field by the Anderson mixing algorithm [92] such that the profile conforms to the desired shape.

Once the correct field is determined and the concentration profiles for each of the components are known, we can look at the two quantities that were calculated in the previous studies. The first one being the integrated excess which requires evaluating the excess concentration for a chain of length N, found by $\delta\phi_N(z) = \phi_N(z) - \bar{\phi}_N\phi(z)$, to then give

$$\theta_N = \rho_0 \int \delta\phi_N(z)\mathrm{d}z \ . \tag{4.6}$$

The second quantity was the entropic contribution to the surface tension, which based on equation 2.33 and equation 4.6 is

$$\gamma_{\text{en}} = -k_B T \sum_N \frac{\theta_N}{N} - \rho_0 \int w(z)\phi(z)\mathrm{d}z \ . \tag{4.7}$$

Moreover, by utilizing the semi-analytical theory for polydisperse melts developed in 2.1.3, we can find predicted forms for the integrated excess as well as the surface tension for the system at hand, the details of which shall follow. The excess concentration defined in equation 4.6, can be described as the sum of the excess in the infinite field plus the correction as seen in equation 2.36. This gives

$$\theta_N \approx \rho_0 \int \delta\phi^0_N(z)\mathrm{d}z + \rho_0 \int \delta\phi^1_N(z)\mathrm{d}z = \frac{\rho_0}{2}\left[\widehat{\delta\phi^0_N}(0) + \widehat{\delta\phi^1_N}(0)\right] \ , \tag{4.8}$$

where based on the Fourier transform definition in equation 2.45, each integral is determined in the manner of equation 3.19. The first term is determined from equation 2.48 to be $4Aa\bar{\phi}_N$ where $s_e(0) = 1$ as noted before. The second term is evaluated from knowing equations 2.46 and 2.50 to amount to $-4Aa\bar{\phi}_N N/N_w$ where $s_\phi(0) = 1$. Substitution of both into equation 4.8 gives

$$\frac{\theta_N}{a\rho_0} \approx 2A\bar{\phi}_N\left(1 - \frac{N}{N_w}\right) \ . \tag{4.9}$$

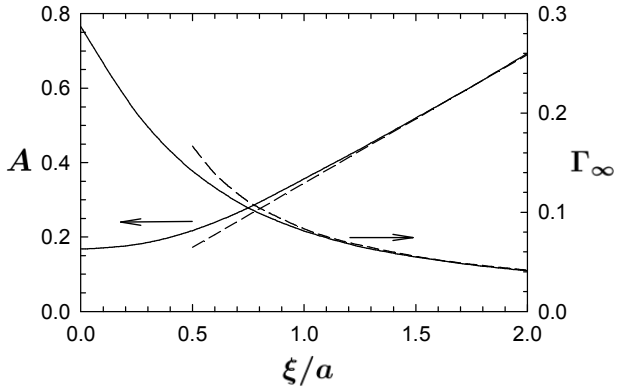

Figure 4.1: Numerical values of A and Γ_∞ evaluated using eqs. (3.9) and (3.17), respectively. The dashed curves give approximate values corresponding to the Gaussian chain model from [3].

Using equation 4.9 and $w(z) \approx w_\infty(z) + \delta w(z)$, the surface tension of equation 4.7 becomes

$$\gamma_{\text{en}} \approx -k_B T \sum_N 2Aa\rho_0 \bar{\phi}_N \left(\frac{1}{N} - \frac{1}{N_w} \right) + a\rho_0 k_B T \Gamma_\infty - \frac{\rho_0}{2} \widehat{\delta w}(0) \ , \tag{4.10}$$

where the definition of Γ_∞, the dimensionless surface tension of a chain with infinite molecular weight, was given in equation 3.17. Based on equation 2.50, the value of the last term in the equation above is seen to be $\widehat{\delta w}(0) = 4Aak_BT/N_w$. This gives the surface tension by

$$\frac{\gamma_{\text{en}}}{a\rho_0 k_B T} \approx \Gamma_\infty - \frac{2A}{N_n} \ . \tag{4.11}$$

As noted in the previous chapter, the values of A and Γ_∞ are dependent on the interfacial width, as shown in figure 4.1 which highlights the influence of model details. This concludes the theoretical considerations of the off-lattice mode, therefore we can proceed to present the obtained results followed by a detailed discussion of the phenomena observed.

4.1.2 Results

For these results, the focus will be on a bidisperse melt of short and long polymers. One being the shorter chain with the length N_s, the other a longer chain of length $N_l = \alpha N_s$ with bulk compositions of $\bar{\phi}_s$ and $\bar{\phi}_l$, respectively. By considering only two components, the quantities of interest are reduced to be three, *i.e.* the concentration of short chains, $\phi_s(z)$, their integrated excess, θ_s as well as the surface tension, γ_{en}. The number of independent system parameters are also seen to be only four, *i.e.* the ratio of lengths, $\alpha = N_l/N_s$, the surface width, ξ, composition of the bulk, $\bar{\phi}_s$ and the degree of polymerization for the shorter chains, N_s. The numerical SCFT results for each of the three aforementioned quantities will be given in terms of these four parameters. In addition, the accuracy of the semi-analytical results will be compared and tested for each.

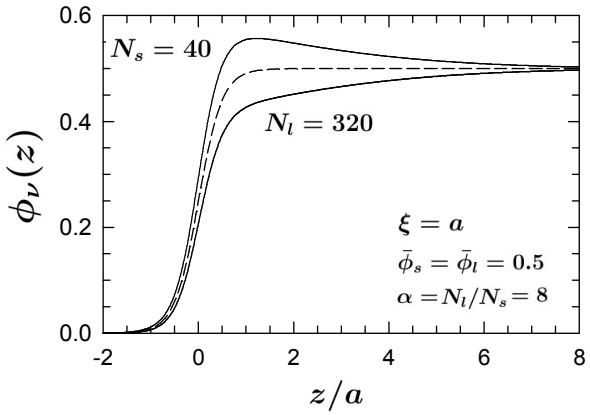

Figure 4.2: Polymer concentrations, $\phi_\nu(z)$ ($\nu = s$ or l), in a 50:50 mixture of $N_s = 40$ and $N_l = 320$ polymers, calculated for a surface profile, $\phi(z)$, of width $\xi = a$. The dashed curve denotes the reference concentration, $\phi(z)/2$, corresponding to zero surface segregation.

As was mentioned in 3.1.1, the surface width is predominantly seen to be similar to the size of the monomers [8, 43, 68], hence we focus on the $\xi = a$ case. The general behavior of the melt is seen in figure 4.2 for the parameters $\alpha = 8$ and $\bar{\phi}_s = 0.5$. There is a clear excess of short chains at the surface, as compared to the value in the bulk (dashed curve), in addition to an evident depletion of the long chains in that region. This is a direct result of the fact that the total concentration should amount to be the sigmoidal profile, as defined by equation 3.5. The area between the upper solid curve and the dashed line would give the integrated excess of short chains, θ_s.

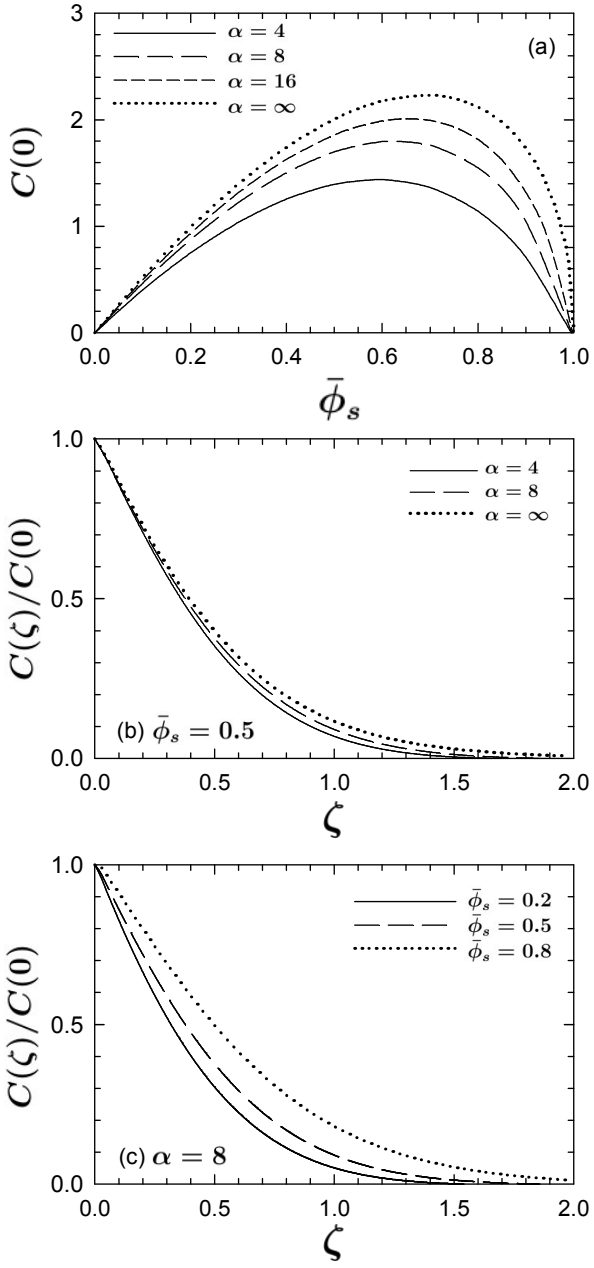

Figure 4.3: Dependence of $C(\zeta)$ on $\alpha \equiv N_l/N_s$ and $\bar{\phi}_s = 1 - \bar{\phi}_l$. Plot (a) demonstrates the dependence of its magnitude on the parameters, while plots (b) and (c) show how its shape changes with α and $\bar{\phi}_s$, respectively.

We have seen that the semi-analytical calculation predicts the excess of short chains in bidisperse melts to be given by equation 2.52 stating

$$\delta\phi_s(z) \approx \begin{cases} AN_s^{-1/2}C(0)\phi(z) \ , & \text{for } z < 0 \ , \\ AN_s^{-1/2}C(z/aN_s^{1/2}) \ , & \text{for } z > 0 \ , \end{cases} \tag{4.12}$$

where all the quantities have been introduced in section 2.1.3. The function $C(\zeta)$ seen in this equation, turns out to be a universal form that only depends on the system parameters α and $\bar{\phi}_s$. In figure 4.3a, the dependence of $C(0)$ on the molecular weight distribution is shown. In the limit of monodisperse melts, *e.g.* $\bar{\phi}_s = 0$, $\bar{\phi}_s = 1$, or $\alpha = 1$, this amplitude is seen to be zero as expected. Parts (b) and (c) of figure 4.3, depict an exponential decay for the function, in which the decay length is order one. This would imply that this excess scales with the size of the shorter component $\zeta = aN_s^{1/2}$ and not the larger polymer, $\zeta\alpha^{1/2} = aN_l^{1/2}$.

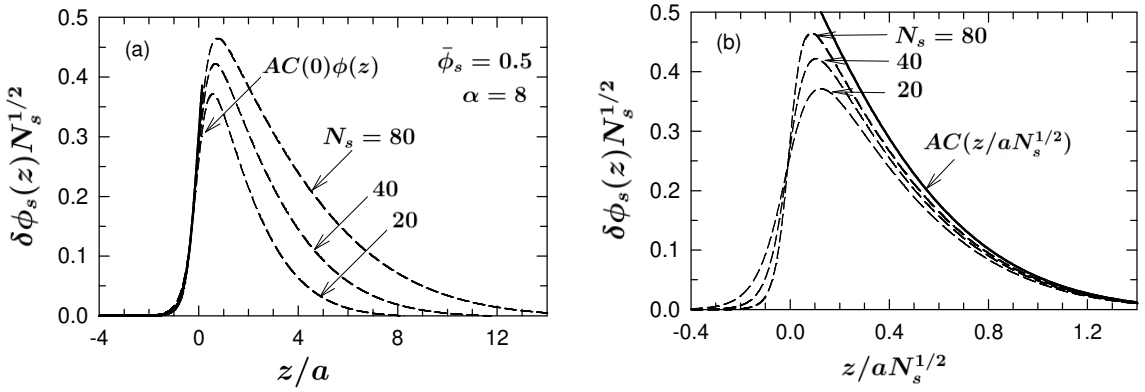

Figure 4.4: Excess concentration of short polymers, $\delta\phi_s(z) \equiv \phi_s(z) - \bar{\phi}_s\phi(z)$, plotted on the (a) monomer and (b) molecular length scales for $\alpha = 8$ and $\bar{\phi}_s = 0.5$. Dashed curves denote SCFT results and solid curves correspond to the approximation in equation (4.12).

In figure 4.4, the SCFT results for the excess concentration of short chains are plotted on the (a) monomer and (b) molecular length scales for the parameters being $\alpha = 8$ and $\bar{\phi}_s = 0.5$ with various values for N_s. While the dashed curves represent the SCFT results, the semi-analytical predictions are shown by solid lines for both length scales. The accuracy of the prediction is seen to increase as the length of the chain is increased which is as we expect. As previously mentioned, the underlying reason for this occurrence is that the linear-response theory is an approximation about the $N = \infty$ limit.

Having shown the concentration profiles of the short chains, the other two quantities of interest, *i.e.* the integrated excess, θ_s, and the entropic contribution to surface tension, γ_{en}, remain. These can be determined numerically by SCFT, from equations 4.6 and 4.7, which for a bidisperse melt would be

$$\frac{\theta_s}{a\rho_0} = \frac{1}{a}\int \delta\phi_s(z)\mathrm{d}z \ , \tag{4.13}$$

and

$$\frac{\gamma_{\text{en}}}{a\rho_0 k_B T} = -\frac{\theta_s(\alpha-1)}{a\rho_0\alpha N_s} - \frac{1}{ak_B T}\int w(z)\phi(z)\mathrm{d}z \ . \tag{4.14}$$

In addition to the previous numerical method, they can also be calculated from the semi-analytical predictions. The forms given by equations 4.9 and 4.11 for polydisperse melts will reduce to

$$\frac{\theta_s}{a\rho_0} \approx \frac{2A(\alpha-1)\bar{\phi}_s(1-\bar{\phi}_s)}{\alpha-(\alpha-1)\bar{\phi}_s} \ , \tag{4.15}$$

and

$$\frac{\gamma_{\text{en}}}{a\rho_0 k_B T} \approx \Gamma_\infty - \frac{2A[(\alpha-1)\bar{\phi}_s+1]}{\alpha N_s} \ , \tag{4.16}$$

for bidisperse melts. In the next three figures, the effect of each of the parameters will be presented for both θ_s and γ_{en} and the accuracy of the semi-analytical calculations will be tested against the numerical SCFT.

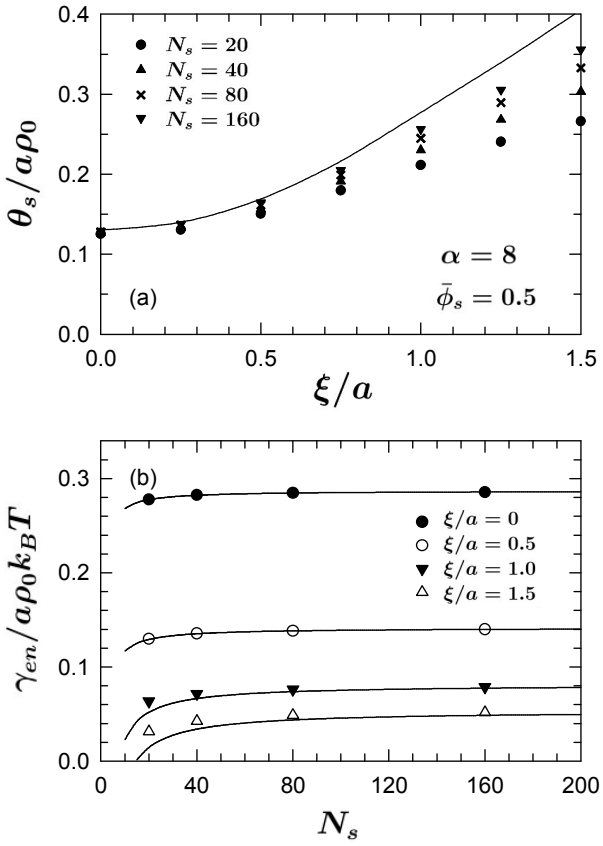

Figure 4.5: (a) Surface excess of short polymers, θ_s, as a function of the surface width, ξ, calculated for different chain lengths, N_s. (b) Entropic surface tension, γ_{en}, as a function of N_s calculated for different values of ξ. All results are for fixed values of $\alpha \equiv N_l/N_s = 8$ and $\bar{\phi}_s = \bar{\phi}_l = 0.5$. The SCFT calculations are denoted by symbols and the semi-analytical approximations, equations 4.15 and 4.16, are plotted with continuous curves.

Firstly, the effect of the surface width, ξ, is considered for $\alpha = 8$ and $\bar{\phi}_s = 0.5$ in figure 4.5. The solid curves are the predictions and the symbols give the SCFT results for various N_s values. The semi-analytical prediction varies with the width, since as seen in figure 4.1, both A and Γ_∞ are dependent on ξ. We see that as the interface broadens, the semi-analytical theory becomes less accurate. Also, as before, we observe an improvement in accuracy with the increase in N_s. The fact that figure 4.5a has a significant value at the step profile interface, *i.e.* at $\xi = 0$, suggests that the discreteness of the chain causes a significant fraction of the chain segregation at the interface. This would in turn imply that chain discreteness has a comparable effect to profile details [2] as suggested in the previous chapter also, which is not true in general. The dashed lines in figure 4.1 show the results corresponding to a continuous Gaussian chain, where it can be seen that the values for either set of plots converge after $\xi \gtrsim a$, suggesting that discreteness loses its effect in this region.

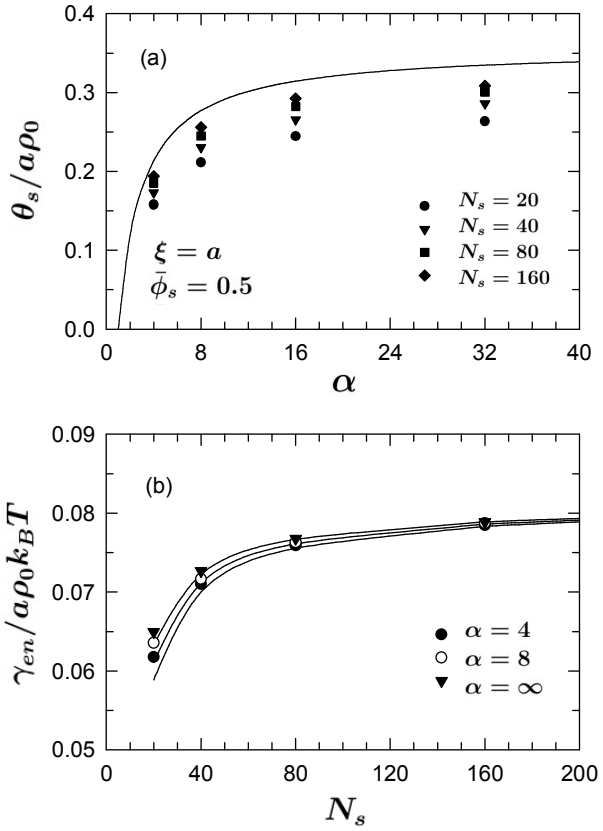

Figure 4.6: Analogous plots to those of figure 4.5 examining the dependence of θ_s and γ_{en} on α for fixed values of $\xi = a$ and $\bar{\phi}_s = \bar{\phi}_l = 0.5$.

Secondly, we focus on the effect of the ratio of the chain lengths $\alpha \equiv N_l/N_s$, on θ_s and γ_{en} in figures 4.6a and 4.6b respectively, for fixed $\xi = a$ and $\bar{\phi}_s = 0.5$. For θ_s, it is evident that the excess should be zero for $\alpha = 1$, since this would represent a monodisperse melt. There seems to be a rapid rise with the increase of α, which turns into a plateau that from the large limit case of equation 4.15 is given by $2Aa\rho_0\bar{\phi}_s$. The change in the surface tension as a function of N_s is shown for various α in figure 4.6b. This effect of changing α is seen to be relatively weak compared to changing N_s, since this is what controls the number of ends. As is also discernible from figure 4.5, the linear-response theory is seen to be more accurate for the surface tension than the integrated excess.

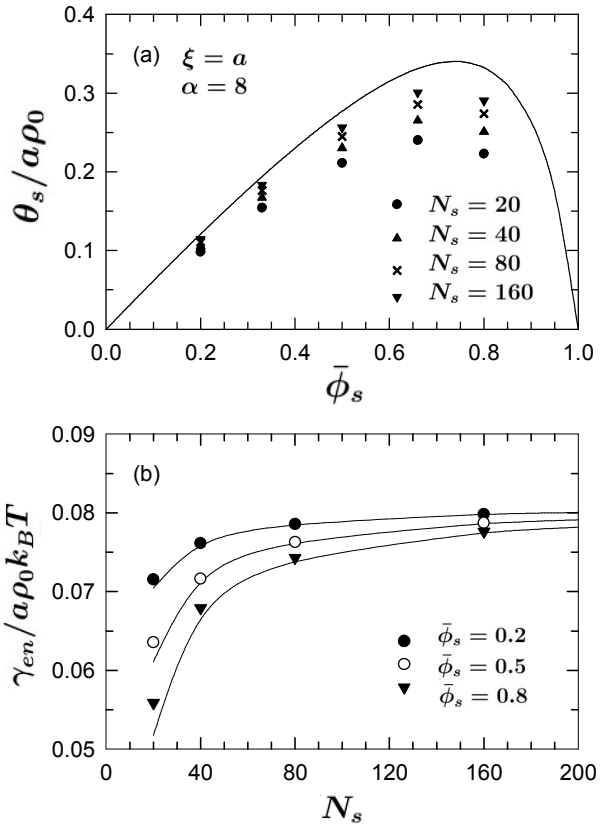

Figure 4.7: Analogous plots to those of figure 4.5 examining the dependence of θ_s and γ_{en} on $\bar{\phi}_s$, for fixed values of $\xi = a$ and $\alpha = 8$.

All that remains is to examine the effect of the composition of the blend, $\bar{\phi}_s$, for fixed $\alpha = 8$ and $\xi = a$. If the volume fraction of the short chain, $\bar{\phi}_s$, is zero or one, there should be no excess since this would correspond to a monodisperse melt. From the semi-analytical prediction given by equation 4.15, the peak would have to occur at $\phi_s^{\max} = 1/(1 + \alpha^{-1/2})$, which in this case corresponds to $\bar{\phi}_s^{\max} = 0.739$. This is reasonably accurate with what is observed from figure 4.7a. As for the dependence of γ_{en}, we observe noticeable reductions for higher volume fractions of short chains in figure 4.7b as well as a greater accuracy for the prediction compared to the θ_s results, as was noted for the two prior cases as well. With these comparisons carried out and the two methods tested for the system parameters, we move on to the discussion of the data presented thus far.

4.1.3 Discussion

As seen in figure 4.5, the predicted form for the excess $\delta\phi_N(z)$, and hence the integrated excess, θ_N, becomes inaccurate as the interface broadens. Nevertheless it does offer us a general understanding. For example, it shows universal behavior in the limit of $z \gg a$ as seen in figure 4.4b, which depends on the molecular weight distribution (*i.e.*, $\bar{\phi}_N$) and has a non-universal amplitude given by A. As seen in figure 4.1, the parameter A is affected by ξ, *i.e.* the compressibility of the melt. It has also been seen to depend on the type of interactions between monomers expressed as the bond potential [66], and will generally be affected by all microscopic details. It is interesting to note that the predictions are reasonably accurate for the entropic contribution to the surface tension even for broader surfaces seen in figure 4.5b. The formulation also shows the dependence on N_n^{-1} (equation 4.11) that has been previously observed by Hariharan *et al.* [35]. In the previous chapter, we observed the surface tension of monodisperse melts to be given by equation 3.20, which stated

$$\gamma = \gamma_\infty - k_B T \Delta\sigma_e \ , \tag{4.17}$$

with $\Delta\sigma_e = 2a\rho_0 A/N$ denoting the surface excess of chain ends. By noting that for polydisperse melts the excess would generalize to

$$\Delta\sigma_e = 2a\rho_0 A \sum_N \frac{\bar{\phi}_N}{N} = \frac{2a\rho_0 A}{N_n} \ , \tag{4.18}$$

this illustrates that the effect originates from the segregation of ends.

For the monodisperse melts, we have already looked at the effect of chain discreteness as well as the width of the surface profile in causing violations to the Silberberg hypothesis, which resulted in an excess of end monomers at the surfaces of these melts. In the bidisperse melt, due to the same argument, the ends will still want to go to the surface so the shorter chains which have a higher number of ends per unit volume will have an excess near the surface. Evidently, these are only two of the many possible influential factors, with examples of others being excluded volume interactions as well as the stiffness of the chains. Similar to previous chapters, the focus of the next section will be to study the former effect by performing simulations for this system. For the latter, more realistic models such as the worm-like chain [12, 104, 105] should be utilized. The additional stiffness parameter incorporated into the aforementioned model can be used to consider both limits of very rigid (rigid rods) to very flexible (Gaussian chain) chains, allowing for comparisons to be made to each of these cases [104]. To aid our goal of attaining a comprehensive understanding of these entropic effects, it becomes necessary to incorporate this model accounting for chain rigidity into our calculations which shall be the focus of the section pertaining to future work.

4.2 Lattice model

As noted in the previous chapter, other than chain discreteness and the surface width, excluded volume interactions will also violate the Silberberg argument [20]. In a manner similar to what was shown in section 3.2, the MC simulation method is applied to a bidisperse melt as described in section 2.2.1. By performing Monte Carlo simulations as well as the SCFT calculations on the same lattice model [95], we are able to compare their results. The theory has been outlined before in 2.2.1, hence only the key points will be mentioned here. Following a very brief description of each of the methods being carried out (*i.e.* SCFT, simulations), the results are presented and tested out against one another as well as the semi-analytical calculation. For simplicity, we will again restrict the study to a step profile *i.e.* $\xi = 0$. Thus, we only have three system parameters N_s, α and $\bar{\phi}_s$.

4.2.1 Theory and simulation

Mean-field Theory

For the mean-field theory being applied to the lattice model at hand, all variables and quantities have been introduced in 2.2.1, hence they will be omitted here. With the non-bonded interactions between the monomers given by $w(z)$, it is adjusted such that the total concentration conforms to the desired shape. The quantities and variables of the theory were introduced for the more general case of a polydisperse melt. However, in the manner of the previous section, the focus for the results will be a bidisperse melt composed of short and long chains of lengths N_s, $N_l = \alpha N_s$ and bulk volume fractions $\bar{\phi}_s$, $\bar{\phi}_l = 1 - \bar{\phi}_s$ respectively. The total concentration is $\phi(z) = \phi_s(z) + \phi_l(z)$, with the component concentrations being determined by equation 2.24 written for the bidisperse melt as

$$\phi_\nu(z) = \frac{\bar{\phi}_{N_\nu}}{N_\nu h(z)} \sum_{i=1}^{N_\nu} G_i(z) G_{N_\nu+1-i}(z) \ , \tag{4.19}$$

where $\nu = s$ or l.

Simulation

Details of the MC simulation method were presented in the previous chapter. In addition, the general application and formulation of the lattice model for polydisperse melts was given in 2.2.3. The same principles shall be applied here. Once more, the non-bonded interactions are given by a field determined such that the target surface profile is attained. Applying the same strategy as before, instead of the focus being on a truly polydisperse melt, a bidisperse melt is examined in the results that follow. With L being the size of the box and ρ_0 giving the average monomer density, the concentration of each component is obtained from equation 2.73 written as

$$\hat{\phi}_\nu(z) \equiv \frac{2\sqrt{2}\hat{m}_\nu(z)}{\rho_0 b^3 L^2} \ , \tag{4.20}$$

where $m_\nu(z)$ is the total number of monomers at z which belong to ν-type polymers. From this, the excess of short chains, $\delta\phi_s(z)$, can be evaluated with the bulk now being determined as the middle of the simulation box. For θ_s, equation 4.13 is altered by having the integral become a sum

$$\theta_s \equiv \rho_0 \sum_z \delta\phi_s(z)\Delta z \ , \tag{4.21}$$

where the summation is from $z = 0$ to the middle of the box (*i.e.*, to the point where $\delta\phi_s(z) = 0$).

Having already compared the SCFT as well as the simulation results to the semi-analytical prediction for the monodisperse melt in 3.2.2, the details of which were presented in 2.1.3, we would like to apply the same idea to bidisperse melts. That is to say, the aim will be to extend the previous comparison between the different methods to this system as well, which shall give us a greater understanding of the underlying phenomena. In the bidisperse case, we are interested in observing the excess of short chains at the surface and determining its integrated value, which can then be tested against the predicted values given by equation 4.15 as well as the mean-field result from equation 4.13. From the theory presented in the previous section, based on equation 2.52, the long range form of the excess of short chains should be

$$\delta\phi_s(z) \approx A N_s^{-1/2} C(z/aN_s^{1/2}) \ , \tag{4.22}$$

where the universal function $C(\zeta)$ is given by equation 2.53. By integrating this approximate form, we can obtain a prediction for the value of the integrated excess, to then be compared to the those obtained from fully numerical SCFT and simulation results.

4.2.2 Results

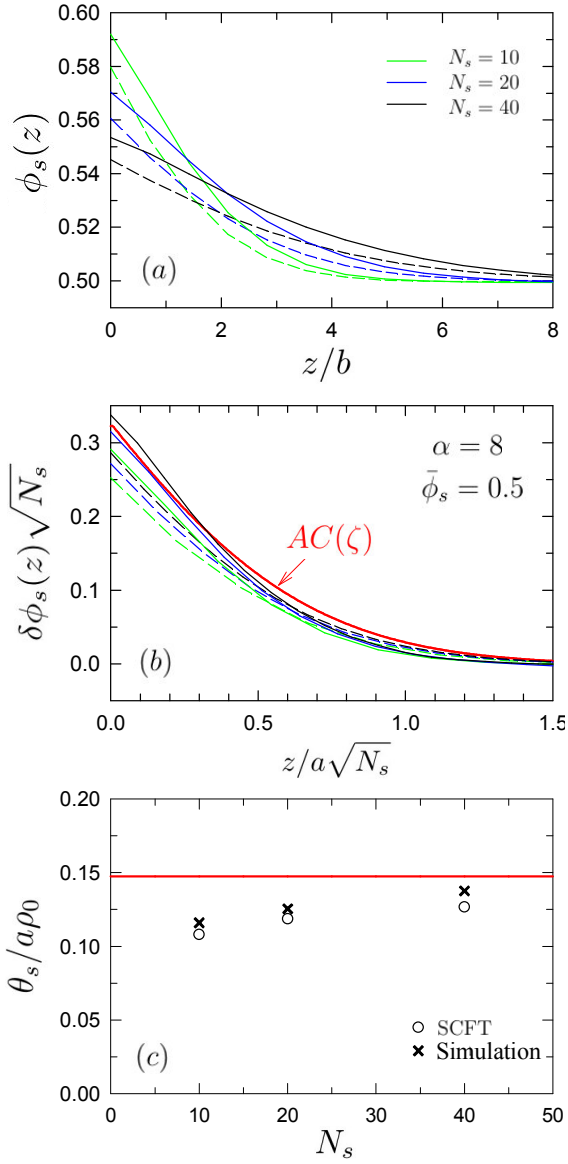

Figure 4.8: (a) Concentration of short chains, $\phi_s(z)$, for bidisperse melts of different polymerizations with fixed $\alpha \equiv N_l/N_s = 8$ and $\bar{\phi}_s = 0.5$, obtained from simulation (solid curves) and SCFT (dashed curves). (b) scaling plot comparing the results to the semi-analytical prediction in eq 4.22 (red curve). (c) integrated excess of short polymers, θ_s, from simulations (crosses) and SCFT (circles) compared to the semi-analytical prediction in equation 4.15 (red line).

We begin by presenting the concentration profiles for a 50:50 mixture of short and long chains (*i.e.*, $\bar{\phi}_s = 0.5$), with the ratio of lengths being $\alpha \equiv N_l/N_s = 8$. In figure 4.8a the concentration profiles of the short chains, $\phi_s(z)$, are presented from both simulations (solid curves) as well as SCFT (dashed curves) for various values of N_ν while the ratio of lengths is kept to be constant. A decrease in the amplitude followed by an increase in depth of the profile is observed as N_ν is increased. The comparison between the two results shows reasonable agreement, with a consistently larger amplitude and range for simulations. In light of the theory presented in the previous section, a scaling with respect to the length of the short chains should give us the universal behavior predicted by equation 4.22, if the two methods agree. This is plotted in 4.8b where the red line denotes the value given from the equation. The agreement seen in this graph suggests that the discrepancies in part a are due to the differences in the segment lengths between the two methods, as described in detail in 3.2.2.

The integrated excess, θ_s, given by equations 4.13 and 4.21 for SCFT and simulations respectively, is the focus of figure 4.8c . Here, the red line is the predicted value of θ_s as determined from the semi-analytical calculation, equation 4.15, which clarifies why it remains constant. That is to say, based on the aforementioned equation, the integrated excess is only seen to depend on model details (as represented by A) as well as molecular weight distributions (as given by $\bar{\phi}_s$ and α) all of which are constant here. By looking at the integrated excess as just the area underneath the curves in figure 4.8a, it is not surprising that this quantity is higher for the simulation results compared to SCFT. Nonetheless, it is worth noting that as described in previous chapters, the SCFT results are seen to approach the predicted value as the length of the chains are increased, due to linear-response theory being developed for the long chain limit of the model at hand. Having considered the effect of changing the lengths of the components here, whilst keeping α and $\bar{\phi}_s$ constant, next we shall alter each of these remaining parameters individually whilst the other two are kept constant.

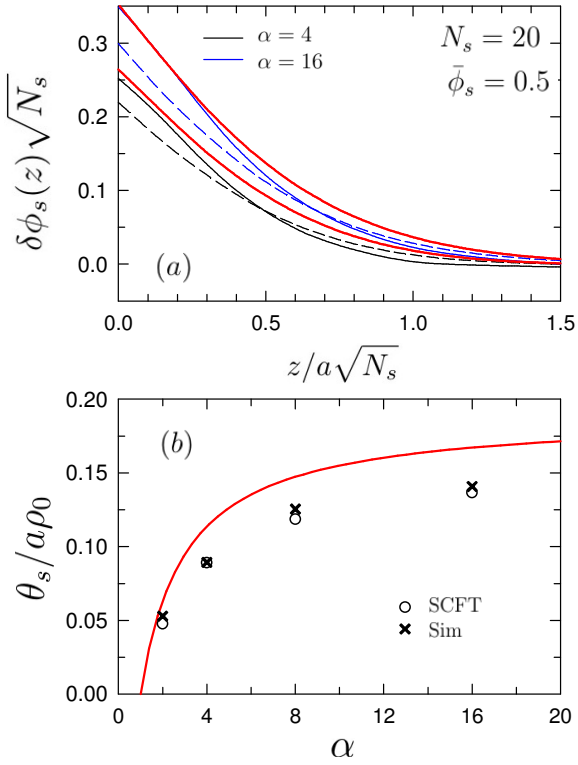

Figure 4.9: (a) Plot of the excess concentration of short chains in a bidisperse melt for $N_l = 80$ and 320 with fixed $N_s = 20$ and $\bar{\phi}_s = 0.5$, obtained from simulation (solid curves) and SCFT (dashed curves). (b) Integrated excess of short polymers from simulation (crosses) and SCFT (circles). The red curves denote the semi-analytical predictions.

In the next figure, for a fixed value of N_s and $\bar{\phi}_s$, we consider the effect of changing the ratio of lengths, α, on the excess profile as well as θ_s. Part (a) of figure 4.9 shows the profiles calculated from both simulation and SCFT for two values of α while the composition is kept to be 50:50. As seen in figure 4.3b, the universal function $C(\zeta)$ depends on α and hence the two red lines denote the values from the predicted form. Good agreement is observed between the different methods as well as the semi-analytical results. The changes in θ_s are shown in part (b) of figure 4.9, where both methods seem to give values that follow the trend predicted from theory (given by equation 4.15) as the ratio of length varies. The inaccuracy observed can clearly be attributed to the length of the short chains, $N_s = 20$. The small magnitude of this value is a certain cause of error in results derived using linear-response theory, as confirmed by comparisons we have seen in the previous sections.

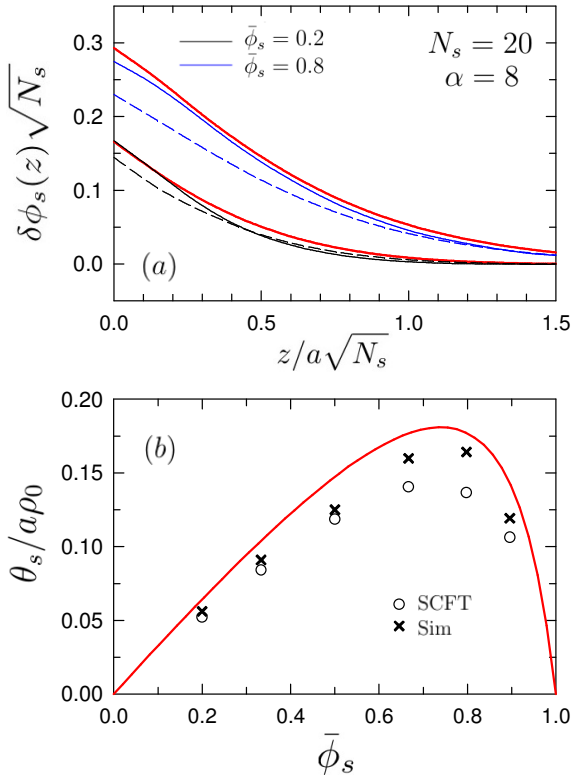

Figure 4.10: Analogous plots to those of figure 4.9 showing the dependence on $\bar{\phi}_s$ for $N_s = 20$ and $N_l = 160$.

Lastly the composition of the bidisperse melt is altered whilst the ratio of lengths is kept constant at $\alpha = 8$ and the short chain lengths held to be $N_s = 20$. Once more, referring to figure 4.3c, we see that the value of the universal function, $C(\zeta)$ depends on the composition. Hence in figure 4.10a, where the excess short chain profiles are given for both methods, two red lines are required to denote the values given from the prediction. As before, reasonable agreement is observed for both methods as well as the semi-analytical results. Focusing on figure 4.10b, we observe that the general trend foreseen from equation 4.15 with changing $\bar{\phi}_s$ is kept here. Additionally, θ_s is higher as calculated from simulations compared to SCFT results. Both are reasonably close in giving the point of maximum segregation, which from the previous section was calculated to be $\bar{\phi}_s^{\max} = 1/(1+\alpha^{-1/2}) = 0.739$. This figure concludes our exploration of the effects of changing each of the three influential parameters in the study, hence we can begin to discuss the observed effects.

4.2.3 Discussion

By considering a lattice model applied identically for both the simulation as well as the mean-field theory [95], comparisons were justified between their results. An important benefit of having a lattice model for the simulation was the ability to consider systems with relatively long polymers that would have been very computational otherwise. Since our aim was to look at the excluded volume effects in the simplest form possible, we created the surface by applying a field instead of having terms defining more realistic molecular interactions. The latter would have nevertheless created a surface, but at the expense of added complications. By creating the surface with the method utilized here, excluded volume interactions can be studied efficiently to see their effect on violations to the Silberberg theory. Furthermore, variables such as A which are affected by model details will be altered by the same amount for both methods since they have identical setups and hence will not cause any concerns.

In the first part of this chapter, the semi-analytical calculation had been shown to agree quite nicely with SCFT for an off-lattice model, specially in the large N limit. With the simulation results now at hand, comparisons were possible between not only the simulations and SCFT (both using the same lattice model) but to the predicted form of the quantities of interest also. In the previous chapter we saw good agreement between the excess of ends at the surface given by simulations and the form predicted by $B(\zeta)$. Here, this agreement seems to be also validated by the bidisperse melt results since the excess of short chains given by the simulations agrees to a good extent with $C(\zeta)$ determined from linear-response theory. An explanation for this is that the screening effect for the excluded volume interactions in the bulk, that would give accurate results for mean-field theory in that region, seems to extend to the surface as well. The fact that the amplitude of the excess agrees so well between the simulation and theory for this simple lattice model is quite fascinating and holds possible interest for further investigation, *e.g.* with a more realistic off-lattice model.

Another point of discussion is how our results compare to previous works that were mentioned in the initial section of this chapter. The lattice model utilized for our calculations, can be extended to the ones previously used by Hariharan *et al.* and Van der Gucht *et al.*. For this, the total concentration is set to be a step profile and the integrals implemented on Z, the bond coordinate, are replaced by sums over $Z = -a$, 0 and a for which $g(Z) = 1/6$, $2/3$, and $1/6$, respectively. The coefficients in equations (4.1) and (4.3) would turn out to be $2A = 0.1951$ and $\Gamma_\infty = 0.1842$ which are in agreement with the forms presented by Minnikanti *et al.* [88]. It should be mentioned that these values are specific to a simple cubic lattice with a surface normal to the (001) direction. If instead the focus was on the (001) surface of an fcc lattice, the values of $g(Z) = 1/3$ would hold at $Z = -a/\sqrt{2}$, 0, $a/\sqrt{2}$, for which the coefficients would become $2A = 0.3789$ and $\Gamma_\infty = 0.3088$. From the values above, it is evident that the choice of the artificial lattice plays a vital role in the magnitude of these quantities which would suggest that off-lattice models are better suited for more accurate predictions.

Chapter 5

Conclusions

The surface properties of polymer melts vary from their bulk behavior, due to the chain statistics being affected by the presence of a surface. This seemingly minute effect alters the physical properties of these materials, such as their surface tension, hence the study of polymer melt surfaces is a fundamental problem of interest. One phenomenon occurring at these scales is the entropic excess of end monomers towards polymer melts surfaces. As previously noted, most of the knowledge regarding this entropic effect has been obtained from theoretical studies as well as computer simulations, which were described in the introductory chapter. In this work, we have aimed to improve the previous works considering such behaviors whilst looking to obtain analytical results to gain valuable insight. By using both off-lattice as well as lattice models, which have many differences in their implementation as well as initial assumptions, we were able to exploit the advantages each had to offer whilst gaining the ability to compare results from both. In addition, we could test the universality of our semi-analytical predictions by comparing them to results from both models. For the entropic effects studied here, the concepts considered thus far represent a small portion of factors influencing the observed phenomena, thus elucidating a need for further investigation. A concise review is given to bring cohesion to the aforementioned concepts which presents an outlook for future work that could contribute immensely to our current understanding.

5.1 Summary

Polymer melt surfaces were initially postulated by Silberberg to simply behave as a reflecting boundary. While this is true to a first approximation, we were able to determine factors such as excluded volume interactions, the discreteness of chains, the profile shape as well as the width of the interface to be causes for disputing this hypothesis. The reasons for the disagreement with the Silberberg argument were discussed in detail in chapter 3 and were seen to stem from the assumptions utilized. By inclusion of the aforementioned factors, we were able to observe a surface excess of end monomers, which can be attributed to a lower loss of configurational entropy by having them segregate to the surface instead of middle segments. The segregation of shorter components to surfaces of polydisperse melts stems from the same entropic effect, since the shorter chains have a higher number of ends per unit volume. This phenomenon can also be seen for different architectural shapes of the same molecular weight, whereby the more ends the structure has, the higher chance of it migrating towards the surface.

The entropic enrichment of chain ends at surfaces of monodisperse polymer melts and the related segregation of shorter chains to surfaces of polydipserse melts constituted the main topic of the work at hand. With the difficulties in studying these systems experimentally outlined in our introductory chapter, the focus was on implementing both a mean-field theory approach as well as MC simulations for two different models (*i.e* off-lattice and lattice). Using mean-field theory in conjunction with the more realistic off-lattice model enabled us to gain a solid understanding of the underlying phenomena, as well as being able to perform a semi-analytical calculation to obtain universal predictions for the observed entropic effects. These universal forms still relied on the mean-field approximation and as such required simulations to test their accuracy, which were simplified by utilizing lattice models. In this sense, we could rigorously incorporate excluded volume effects to judge the applicability of our semi-analytical findings. In terms of creating the surface of the melt, as per our previous discussions, we chose to enforce a certain profile shape in lieu of using an equation of state. By steering clear of the latter, we were able to eliminate unnecessary complexities from the calculations, which resulted in our ability to obtain analytical forms for both systems of interest following a straightforward initial numerical step. We will summarize the main findings of both models for the monodisperse as well as the polydipserse melts before focusing on possible future considerations.

For the off-lattice calculations, certain profile shapes (sigmoidal as well as linear) were enforced with a width given by the parameter ξ. The polymers were represented by a discrete bead-spring model of length N and the statistical segment length a. In the case of the monodisperse melt, both ξ and the discreteness of the chain were seen to have a comparable effect on the entropic excess, which is necessarily followed by a complementing depletion of ends observed to extend a molecular distance of $a\sqrt{N}$ into the bulk. The effect of this excess of ends on surface tension was shown and results from the semi-analytical predictions provided us with equations for both the long-range depletion of ends as well as the modification to the surface tension, which were compared to the numerical results. The coefficients present in these formulas were noted to depend on model details such as the shape of the surface profile and its interfacial width, in addition to the bond type [66]. This observation indicated the need for more realistic models for the quantitative evaluation of the excess. Nevertheless, the semi-analytical calculation suggested the form for the bulk end depletion as well as the reduction in surface tension to be universal and hold irrespective of model details.

Using the off-lattice model, we also considered the specific case of bidisperse melts as a representative for including polydispersity in the system, since realistically polymer melts are rarely monodisperse. The melt contained only short and long chains of lengths N_s, N_l of volume fractions $\bar{\phi}_s$ and $\bar{\phi}_l$, respectively, and the total concentration was made to conform to a surface profile of width ξ once more. This allowed the system to be fully determined in terms of four parameters, ξ, $\alpha \equiv N_l/N_s$, $\bar{\phi}_s$ and N_s. Having already considered the effect of various surface profile shapes for the monodisperse melts, we focused on the more realistic sigmoidal profile for the total concentration. The excess of short chains was seen at the surface of the melt, for which both the monomer and molecular length scale behavior, *i.e.* at lengths a and $a\sqrt{N}$, were in good agreement with the form of the semi-analytical calculation extended to bidisperse melts. We went on to consider the outcome of changing each of the influential variables in the parameter space of the problem, to see the corresponding effects on the integrated surface excess of short chains as well as the surface tension. The expressions for the predictions were seen to be fairly accurate for both quantities but more so for the surface tension. Some inaccuracy was observed for the integrated excess as the interfacial width was increased, but was seen to improve as the chains were made to be longer.

As previously mentioned, the predictions for both the long range depletion of ends in a monodisperse melt as well the excess of short chains in bidisperse melts should be universal and independent of model details. Hence, by performing the previous studies using a different model, similar agreement should be observed. In this light, we performed simulations as well as mean-field calculations for the same lattice model. By utilizing this model, we ensured better statistics for the simulations, such that their results were more representative of equilibrium configurations. Moreover, by using the same model for the mean-field method, comparisons between the results are justified. One of the main differences between the two methods used, is the ability to accurately treat excluded volume effects. The simulations enforce these effects by strictly prohibiting the double occupancy of a site, whereas this is only true on average in mean-field theory, hence providing a less rigorous treatment. Despite this shortcoming of mean-field theories, results were seen to agree fairly well between the two methods, owing to the screening effect present in polymer melts. In addition, the long range depletion of the ends in monodisperse melts as well as the enrichment of short chains in bidisperse melts, were in good agreement with the predicted forms. This provided further tangible evidence not only towards the reliability and accuracy of the mean-field calculations, but also towards the universality of the predictions derived using the semi-analytical method.

Having observed good agreement between our semi-analytical results and the numerical findings, some further considerations should be noted. Undoubtedly, the most elaborate test for these calculations would be to gauge them against experimental results, for which the difficulties of solely focusing on entropic effects were previously pointed out. Very recently, Dr. Foster's group at the University of Akron were successful in conducting experiments looking at the entropic enrichment of shorter components at surfaces of polydisperse melts, using a novel approach [106]. In a collaborative effort, through our off-lattice SCFT calculations, we obtained results for the same system which showed qualitative agreement. Nonetheless, a quantitative comparison suggested a need for improvement, which could be stemming from a number of contributing factors. For instance, in reality, the end monomers may chemically vary from the middle segments and hence, there could be an enthalpic interaction that we have yet to incorporate in our study, which could be readily taken into account. In addition, real polymer chains have a degree of rigidity in their backbones, which has not been considered in our calculations thus far and could enhance this entropic effect. Flexibility of chains can be considered by utilizing a different model such as the wormlike chain model [12, 104, 105], which we will briefly introduce in Appendix B. This will give the outlook of the future work that could complement the studies implemented thus far and aid our understanding of prior results.

References

[1] David Chandler. Introduction to modern statistical mechanics. xi, 4

[2] P Mahmoudi and MW Matsen. Segregation of chain ends to the surface of a polymer melt: Effect of surface profile versus chain discreteness. *The European Physical Journal E*, 39(8):78, 2016. xi, 8, 29, 30, 44, 74

[3] P Mahmoudi and MW Matsen. Entropic segregation of short polymers to the surface of a polydisperse melt. *The European Physical Journal E*, 40(10):85, 2017. xii, 29, 30, 69

[4] Hermann Staudinger. Über polymerisation. *European Journal of Inorganic Chemistry*, 53(6):1073–1085, 1920. 1

[5] M. Rubinstein and R.H. Colby. *Polymer Physics*. OUP Oxford, 2003. 1, 5, 9, 19, 38, 39, 40, 106

[6] Paul J. Flory. *Principles of Polymer Chemistry*. George Fisher Baker Non-Resident Lec. Cornell University Press, 1953. 1, 3

[7] Sharon C. Glotzer and Wolfgang Paul. Molecular and mesoscale simulation methods for polymer materials. *Annual Review of Materials Research*, 32(1):401–436, 2002. 1, 10

[8] Kostas Ch Daoulas, Vagelis Harmandaris, and Vlasis Mavrantzas. Detailed Atomistic Simulation of a Polymer Melt / Solid Interface : Structure , Density , and Conformation of a Thin Film of Polyethylene Melt Adsorbed on Graphite. *Macromolecules*, (38):5780–5795, 2005. 1, 10, 26, 44, 46, 47, 59, 70

[9] T. Kawakatsu. *Statistical Physics of Polymers: An Introduction*. Advanced Texts in Physics. Springer Berlin Heidelberg, 2013. 1, 3

[10] Zhen-Gang Wang. 50th anniversary perspective: Polymer conformation a pedagogical review. *Macromolecules*, 50(23):9073–9114, 2017. 1, 3

[11] Alexander Yu Grosberg, Alexei R Khokhlov, H Eugene Stanley, A John Mallinckrodt, Susan McKay, et al. Statistical physics of macromolecules. *Computers in Physics*, 9(2):171–172, 1995. 3

[12] G. Gompper and M. Schick. *Soft Matter: Volume 1 - Polymer Melts and Mixtures*. Soft Matter. Wiley, 2006. 3, 25, 27, 29, 31, 59, 77, 89, 111

[13] Paul J Flory. The configuration of real polymer chains. *The Journal of Chemical Physics*, 17(3):303–310, 1949. 3

[14] Werner Kuhn. Molekülkonstellation und kristallitorientierung als ursachen kautschukähnlicher elastizität. *Colloid & Polymer Science*, 87(1):3–12, 1939. 3

[15] *Selected Works of Paul J. Flory Volume I*. Stanford University Press. 3

[16] I Bitsanis and G Hadziioannou. Molecular dynamics simulations of the structure and dynamics of confined polymer melts. *The Journal of Chemical Physics*, 92(6):3827, 1990. 3, 10, 14, 44, 59

[17] Mark R Smyda and Stephen C Harvey. The entropic cost of polymer confinement. *The Journal of Physical Chemistry B*, 116(35):10928–10934, 2012. 7, 105

[18] Hiroshi Morita, Masatoshi Toda, and Takashi Honda. Analysis of the end-segment distribution of a polymer at the interface of filler-filled material. *Polymer Journal*, 48(4):451–455, 2016. 7

[19] Isaac C Sanchez. *Physics of polymer surfaces and interfaces*. Butterworth-Heinemann, 2013. 7, 13

[20] A. Silberberg. Distribution of conformations and chain ends near the surface of a melt of linear flexible macromolecules. *Journal of Colloid And Interface Science*, 90(1):86–91, 1982. 7, 78

[21] Gerard J. Fleer. Polymers at interfaces and in colloidal dispersions. *Advances in Colloid and Interface Science*, 159(2):99 – 116, 2010. 9

[22] T. P. Lodge and M. Muthukumar. Physical chemistry of polymers: entropy, interactions, and dynamics. *The Journal of Physical Chemistry*, 100(31):13275–13292, 1996. 9

[23] Jee Hwan Jang, Rahmi Ozisik, and Wayne L. Mattice. Monte Carlo simulation on the effects of chain end modification on freely standing thin films of amorphous polyethylene melts. *Macromolecules*, 33(20):7663–7671, 2000. 9, 13

[24] Bryan B. Sauer and Gregory T. Dee. Studies of Polymer, Copolymer, and Associating Liquids by Melt Surface Tension Methods and Cahn-Hilliard Density-Gradient Theory, 1994. 9, 13, 44

[25] PG Degennes. Surface tension of molten polymers. *Comptes Rendus de l Academie des Sciences Serie II*, 307(18):1841–1844, 1988. 9

[26] TP Russell. X-ray and neutron reflectivity for the investigation of polymers. *Materials Science Reports*, 5(4):171–271, 1990.

[27] JF Elman, BD Johs, TE Long, and JT Koberstein. A neutron reflectivity investigation of surface and interface segregation of polymer functional end groups. *Macromolecules*, 27(19):5341–5349, 1994.

[28] S Affrossman, M Hartshorne, Robert Jérôme, RA Pethrick, S Petitjean, and M Rei Vilar. Surface concentration of chain ends in polystyrene determined by static secondary ion mass spectroscopy. *Macromolecules*, 26(23):6251–6254, 1993.

[29] TP Russell. The characterization of polymer interfaces. *Annual Review of Materials Science*, 21(1):249–268, 1991. 17

[30] Gregory T Dee and Bryan B Sauer. The surface tension of polymer liquids. *Advances in Physics*, 47(2):161–205, 1998.

[31] Spiros H. Anastasiadis, Irena Gancarz, and Jeffrey T. Koberstein. Interfacial Tension of Immiscible Polymer Blends: Temperature and Molecular Weight Dependence. *Macromolecules*, 21(10):2980–2987, 1988. 13, 44

[32] Claire Jalbert, Jeffrey T. Koberstein, Iskender Yilgor, Paula Gallagher, and Val Krukonis. Molecular Weight Dependence and End-Group Effects on the Surface Tension of Poly(dimethylsiloxane). *Macromolecules*, 26(12):3069–3074, 1993. 13, 44

[33] David T. Wu, Glenn H. Fredrickson, Jean Pierre Carton, Armand Ajdari, and Ludwik Leibler. Distribution of chain ends at the surface of a polymer melt: Compensation effects and surface tension. *Journal of Polymer Science Part B: Polymer Physics*, 33(17):2373–2389, 1995. 14, 15, 19, 29, 31, 44, 58, 59

[34] Chahrazed Meddah, Andrey Milchev, Sid Ahmed Sabeur, and Alexander M Skvortsov. Molecular weight effects on interfacial properties of linear and ring polymer melts: A molecular dynamics study. *The Journal of chemical physics*, 145(19):194902, 2016.

[35] A Hariharan, S K Kumar, and T P Russell. A lattice model for the surface segregation of polymer chains due to molecular weight effects. *Macromolecules*, 23(15):3584–3592, 1990. 10, 16, 65, 77

[36] Jasper Van der Gucht, N. A.M. Besseling, and G. J. Fleer. Surface segregation in polydisperse polymer melts. *Macromolecules*, 35(17):6732–6738, 2002. 10, 16, 66

[37] Venkatachala S. Minnikanti and Lynden A. Archer. Surface enrichment of branched polymers in linear hosts: Effect of asymmetry in intersegmental interactions and density gradients. *Journal of Chemical Physics*, 122(8), 2005. 16

[38] Kostas Ch. Daoulas, Doros N. Theodorou, Vagelis A. Harmandaris, Nikos Ch. Karayiannis, and Vlasis G. Mavrantzas. Self-consistent-field study of compressible semiflexible melts adsorbed on a solid substrate and comparison with atomistic simulations. *Macromolecules*, 38(16):7134–7149, 2005. 10, 107, 111, 114, 115

[39] Jörg Baschnagel, Kurt Binder, Pemra Doruker, Andrei A. Gusev, Oliver Hahn, Kurt Kremer, Wayne L. Mattice, Florian Müller-Plathe, Michael Murat, Wolfgang Paul, Serge Santos, Ulrich W. Suter, and Volker Tries. *Bridging the Gap Between Atomistic and Coarse-Grained Models of Polymers: Status and Perspectives*, pages 41–156. Springer Berlin Heidelberg, Berlin, Heidelberg, 2000. 10, 38

[40] Glenn H. Fredrickson, Venkat Ganesan, and Franois Drolet. Field-theoretic computer simulation methods for polymers and complex fluids. *Macromolecules*, 35(1):16–39, 2002. 10

[41] Florian Mller-Plathe. Coarse-graining in polymer simulation: From the atomistic to the mesoscopic scale and back. *ChemPhysChem*, 3(9):754–769, 2002. 10

[42] Marcus Müller, Birger Steinmüller, Kostas Ch. Daoulas, Abelardo Ramírez-Hernández, and Juan J. de Pablo. Polymersolid contacts described by soft, coarse-grained models. *Physical Chemistry Chemical Physics*, 13(22):10491, 2011. 10, 14, 15, 44, 59

[43] Sanat K. Kumar, Michele Vacatello, and Do Y. Yoon. Offlattice Monte Carlo simulations of polymer melts confined between two plates. *The Journal of Chemical Physics*, 89(8):5206–5215, 1988. 10, 11, 14, 15, 44, 47, 59, 70

[44] Eugene Helfand. Block copolymers, polymer-polymer interfaces, and the theory of inhomogeneous polymers. *Accounts of Chemical Research*, 8(9):295–299, 1975. 10

[45] Eugene Helfand. Theory of inhomogeneous polymers. lattice model for solution interfaces. *Macromolecules*, 9(2):307–310, 1976. 10, 35

[46] Thomas A Weber and Eugene Helfand. Theory of inhomogeneous polymers. solutions for the interfaces of the lattice model. *Macromolecules*, 9(2):311–316, 1976. 10, 13

[47] J. M. H. M. Scheutjens and G. J. Fleer. Statistical theory of the adsorption of interacting chain molecules. 1. partition function, segment density distribution, and adsorption isotherms. *The Journal of Physical Chemistry*, 83(12):1619–1635, 1979. 10, 35

[48] Doros N Theodorou. Lattice models for bulk polymers at interfaces. *Macromolecules*, 21(5):1391–1400, 1988. 10, 13, 35

[49] Doros N Theodorou. Structure and thermodynamics of bulk homopolymer solid interfaces: a site lattice model approach. *Macromolecules*, 21(5):1400–1410, 1988. 11, 13

[50] J. P. Wittmer, A. Cavallo, H. Xu, J. E. Zabel, P. Polińska, N. Schulmann, H. Meyer, J. Farago, A. Johner, S. P. Obukhov, and J. Baschnagel. *Scale-Free Static and Dynamical Correlations in Melts of Monodisperse and Flory-Distributed Homopolymers*, volume 145. 2011. 11, 64

[51] Sanat K. Kumar, Michele Vacatello, and Do Y. Yoon. Off-Lattice Monte Carlo Simulations of Polymer Melts Confined between two Plates. 2. Effects of Chain Length and Plate Separation. *Macromolecules*, 23(8):2189–2197, 1990. 11, 14, 15, 44, 59

[52] Kurt Binder and Andrey Milchev. Off-lattice monte carlo methods for coarse-grained models of polymeric materials and selected applications. *Journal of computer-aided materials design*, 9(1):33–74, 2002. 11

[53] A. Silberberg. Distribution of conformations and chain ends near the surface of a melt of linear flexible macromolecules. *Journal of Colloid And Interface Science*, 90(1):86–91, 1982. 12

[54] Jalal Sarabadani, Andrey Milchev, and Thomas A Vilgis. Structure and dynamics of polymer melt confined between two solid surfaces: A molecular dynamics study. *The Journal of chemical physics*, 141(4):044907, 2014. 12

[55] AM Skvortsov, FAM Leermakers, and GJ Fleer. Equivalence of chain conformations in the surface region of a polymer melt and a single gaussian chain under critical conditions. *The Journal of chemical physics*, 139(5):054907, 2013. 12

[56] Richard A. L. Jones, Edward J. Kramer, Miriam H. Rafailovich, Jonathon Sokolov, and Steven A. Schwarz. Surface enrichment in an isotopic polymer blend. *Phys. Rev. Lett.*, 62:280–283, Jan 1989. 12

[57] SA Schwarz, BJ Wilkens, MAA Pudensi, MH Rafailovich, J Sokolov, X Zhao, W Zhao, X Zheng, TP Russell, and RAL Jones. Studies of surface and interface segregation in polymer blends by secondary ion mass spectrometry. *Molecular Physics*, 76(4):937–950, 1992. 12

[58] L. J. Norton, E. J. Kramer, F. S. Bates, M. D. Gehlsen, R. A. L. Jones, A. Karim, G. P. Felcher, and R. Kleb. Neutron reflectometry study of surface segregation in an isotopic poly(ethylenepropylene) blend: Deviation from mean-field theory. *Macromolecules*, 28(25):8621–8628, 1995. 12

[59] Souheng Wu. *Polymer interface and adhesion*. M. Dekker, 1982. 13

[60] Gerrit ten Brinke, Dominique Ausserre, and Georges Hadziioannou. Interaction between plates in a polymer melt. *The Journal of chemical physics*, 89(7):4374–4380, 1988. 14

[61] Jiang-Sheng Wang and Kurt Binder. Enrichment of the chain ends in polymer melts at interfaces. *Journal de Physique I*, 1(11):1583–1590, 1991. 14

[62] R S Pai-Panandiker, John R Dorgan, and T Pakula. Static properties of homopolymer melts in confined geometries determined by Monte Carlo simulation. *Macromolecules*, 30(20):6348–6352, 1997. 14, 59

[63] Sanat K Kumar, Thomas P Russell, and Arvind Hariharan. Monte carlo simulations of the free surface of polymer melts. *Chemical engineering science*, 49(17):2899–2906, 1994. 14, 46

[64] Arun Yethiraj and C. K. Hall. Monte Carlo Simulation of Polymers Confined between Flat Plates. *Macromolecules*, 23(6):1865–1872, 1990. 14, 44, 59

[65] Michele Vacatello, Do Y Yoon, and Bernard C Laskowski. Molecular arrangements and conformations of liquid n-tridecane chains confined between two hard walls. *The Journal of chemical physics*, 93(1):779–786, 1990. 14

[66] M. W. Matsen and P. Mahmoudi. Segregation of chain ends to the surface of a polymer melt. *European Physical Journal E*, 37(8):1–8, 2014. 15, 28, 29, 30, 33, 44, 45, 49, 50, 56, 77, 88

[67] M. W. Matsen, J. U. Kim, and A. E. Likhtman. Finite- N effects for ideal polymer chains near a flat impenetrable wall. *European Physical Journal E*, 29(1):107–115, 2009. 15, 30

[68] Marcus Müller. Chain conformations and correlations in thin polymer films: A Monte Carlo study. *Journal of Chemical Physics*, 116(22):9930–9938, 2002. 15, 47, 70

[69] A Cavallo, M Müller, J P Wittmer, A Johner, and K Binder. Single chain structure in thin polymer films: corrections to Flory's and Silberberg's hypotheses. *Journal of Physics: Condensed Matter*, 17(20):S1697–S1709, 2005. 15

[70] David C. Morse and Glenn H. Fredrickson. Semiflexible polymers near interfaces. *Physical Review Letters*, 73(24):3235–3238, 1994. 15, 106, 110

[71] Gregory T. Dee and Bryan B. Sauer. The cohesive energy density of polymers and its relationship to surface tension, bulk thermodynamic properties, and chain structure. *Journal of Applied Polymer Science*, 134(5):1–14, 2017. 16

[72] Zhenyu Qian, Venkatachala S Minnikanti, Bryan B Sauer, Gregory T Dee, William G Kampert, and Lynden A Archer. Surface tension of polystyrene blends: Theory and experiment. *Journal of Polymer Science Part B: Polymer Physics*, 47(17):1666–1685, 2009. 16

[73] Sanat K Kumar and Ronald L Jones. Dominance of density variations in determining the molecular weight dependence of surface tensions of polymer melts. *Advances in Colloid and Interface Science*, 94(1):33–38, 2001. 16

[74] S Mostafa Sabzevari, Joshua D McGraw, and Paula Wood-Adams. Short chains enhance slip of highly entangled polystyrenes during thin film dewetting. *RSC Advances*, 6(94):91163–91170, 2016. 16

[75] Marzieh Ebrahimi, Mahmoud Ansari, Yong W. Inn, and Savvas G. Hatzikiriakos. Surface fractionation effects on slip of polydisperse polymer melts. *Physics of Fluids*, 28(9), 2016. 16

[76] Savvas G Hatzikiriakos. Wall slip of molten polymers. *Progress in Polymer Science*, 37(4):624–643, 2012. 16

[77] Sijia Li, Mingming Ding, and Tongfei Shi. Effect of bidispersity on structure and entanglement of confined polymer films. *The Journal of Physical Chemistry B*, 121(31):7502–7507, 2017. 16, 17

[78] Nicholas A Rorrer and John R Dorgan. Effects of polydispersity on confined homopolymer melts: A monte carlo study. *The Journal of chemical physics*, 141(21):214905, 2014. 16, 17

[79] Anne M. Mayes. Glass Transition of Amorphous Polymer Surfaces. *Macromolecules*, 27(11):3114–3115, 1994. 16

[80] Keiji Tanaka, Tisato Kajiyama, Atsushi Takahara, and Seiji Tasaki. A novel method to examine surface composition in mixtures of chemically identical two polymers with different molecular weights. *Macromolecules*, 35(12):4702–4706, 2002. 16, 17

[81] Keiji Tanaka, Atsushi Takahara, and Tisato Kajiyama. Effect of polydispersity on surface molecular motion of polystyrene films. *Macromolecules*, 30(21):6626–6632, 1997. 16, 17

[82] Rüdiger Stark, Michael Kappl, and Hans Jürgen Butt. Interaction of solid surfaces across binary mixtures of polymer melts. *Macromolecules*, 40(11):4088–4091, 2007. 16, 17

[83] David T. Wu and Glenn H. Fredrickson. Effect of Architecture in the Surface Segregation of Polymer Blends. *Macromolecules*, 29(24):7919–7930, 1996. 16

[84] DG Walton and AM Mayes. Entropically driven segregation in blends of branched and linear polymers. *Physical Review E*, 54(3):2811, 1996. 16

[85] Jae Sik Lee, Nam Heui Lee, Somesh Peri, Mark D. Foster, Charles F. Majkrzak, Renfeng Hu, and David T. Wu. Surface segregation driven by molecular architecture asymmetry in polymer blends. *Physical Review Letters*, 113(22):1–5, 2014. 16

[86] Chih-Yu Teng, Yu-Jane Sheng, and Heng-Kwong Tsao. Boundary-induced segregation in nanoscale thin films of athermal polymer blends. *Soft Matter*, 12(20):4603–4610, 2016. 16

[87] Zhenyu Qian, Venkatachala S Minnikanti, Bryan B Sauer, Gregory T Dee, and Lynden A Archer. Surface tension of symmetric star polymer melts. *Macromolecules*, 41(13):5007–5013, 2008. 16

[88] Venkatachala S. Minnikanti, Qian Zhenyu, and Lynden A. Archer. Surface segregation and surface tension of polydisperse polymer melts. *Journal of Chemical Physics*, 126(14), 2007. 17, 66, 85

[89] P.G. de Gennes. *Scaling Concepts in Polymer Physics*. Cornell University Press, 1979. 19

[90] G. Fredrickson. *The Equilibrium Theory of Inhomogeneous Polymers*. International Series of Monogr. OUP Oxford, 2006. 20, 25, 106

[91] D.V. Schroeder. *An Introduction to Thermal Physics*. Always learning. Pearson Education, Limited, 2013. 21, 38

[92] Donald G. Anderson. Iterative Procedures for Nonlinear Integral Equations. *Journal of the ACM*, 12(4):547–560, 1965. 26, 46, 68

[93] V Eyert. A comparative study on methods for convergence acceleration of iterative vector sequences. *Journal of Computational Physics*, 124(2):271–285, 1996. 26

[94] G. Parisi. *Statistical Field Theory*. Frontiers in Physics. Addison-Wesley, 1988. 29

[95] P Mahmoudi, WSR Forrest, TM Beardsley, and MW Matsen. Testing the universality of entropic segregation at polymer surfaces. *Macromolecules*, 2018. 35, 36, 37, 42, 60, 78, 84

[96] ON Vassiliev and MW Matsen. Fluctuation effects in block copolymer melts. *The Journal of chemical physics*, 118(16):7700–7713, 2003. 36, 40, 43

[97] D.P. Landau and K. Binder. *A Guide to Monte Carlo Simulations in Statistical Physics*. Cambridge University Press, 2013. 38, 39, 40

[98] Nicholas Metropolis, Arianna W Rosenbluth, Marshall N Rosenbluth, Augusta H Teller, and Edward Teller. Equation of state calculations by fast computing machines. *The journal of chemical physics*, 21(6):1087–1092, 1953. 40

[99] H. Gould, J. Tobochnik, and W. Christian. *An Introduction to Computer Simulation Methods: Applications to Physical Systems*. Pearson Addison Wesley, 2007. 40

[100] Jens Glaser, Pavani Medapuram, Thomas M Beardsley, Mark W Matsen, and David C Morse. Universality of block copolymer melts. *Physical review letters*, 113(6):068302, 2014. 42, 62

[101] P. Stasiak and M. W. Matsen. Efficiency of pseudo-spectral algorithms with Anderson mixing for the SCFT of periodic block-copolymer phases. *European Physical Journal E*, 34(10):110, 2011. 46

[102] Shyamal K. Nath, John D. McCoy, James P. Donley, and John G. Curro. A modified self-consistent-field theory: Application to a homopolymer melt near a hard wall. *The Journal of Chemical Physics*, 103(4):1635, 1995. 59

[103] F. Schmid. A self consistent field approach to surfaces of compressible polymer blends. *The Journal of Chemical Physics*, 104(22):9191–9201, 1996. 59

[104] David C Morse and Glenn H Fredrickson. Semiflexible polymers near interfaces. *Physical review letters*, 73(24):3235, 1994. 77, 89

[105] Nobuhiko Saitô, Kunihiko Takahashi, and Yasuo Yunoki. The statistical mechanical theory of stiff chains. *Journal of the Physical Society of Japan*, 22(1):219–226, 1967. 77, 89, 105, 106

[106] Jacob A Hill, Kevin J Endres, Pendar Mahmoudi, Mark W Matsen, Chrys Wesdemiotis, and Mark D Foster. Detection of surface enrichment driven by molecular weight disparity in virtually monodisperse polymers. *ACS Macro Letters*, 7:487–492, 2018. 89

[107] MW Matsen. Melts of semiflexible diblock copolymer. *The Journal of chemical physics*, 104(19):7758–7764, 1996. 105, 107

[108] Chandralekha Singh, Mark Goulian, Andrea J Liu, and Glenn H Fredrickson. Phase behavior of semiflexible diblock copolymers. *Macromolecules*, 27(11):2974–2986, 1994. 105

[109] Ying Jiang and Jeff ZY Chen. Influence of chain rigidity on the phase behavior of wormlike diblock copolymers. *Physical review letters*, 110(13):138305, 2013. 105

[110] Wendi Song, Ping Tang, Feng Qiu, Yuliang Yang, and An-Chang Shi. Phase behavior of semiflexible-coil diblock copolymers: a hybrid numerical scft approach. *Soft Matter*, 7(3):929–938, 2011. 105

[111] Shiben Li, Ying Jiang, and Jeff ZY Chen. Phase transitions in semiflexible–rod diblock copolymers: a self-consistent field theory. *Soft Matter*, 10(44):8932–8944, 2014. 105

[112] Jiuzhou Tang, Ying Jiang, Xinghua Zhang, Dadong Yan, and Jeff ZY Chen. Phase diagram of rod–coil diblock copolymer melts. *Macromolecules*, 48(24):9060–9070, 2015. 105

[113] Raul Cruz Hidalgo, DE Sullivan, and Jeff ZY Chen. Smectic ordering of homogeneous semiflexible polymers. *Physical Review E*, 71(4):041804, 2005. 105

[114] AN Semenov and Alexei Removich Khokhlov. Statistical physics of liquid-crystalline polymers. *Physics-Uspekhi*, 31(11):988–1014, 1988. 105

[115] Ian MacKay. *Self-Consistent Field Theory for Smectic Ordering of Semiflexible Homo-polymers*. PhD thesis, 2014. 105

[116] Qiang Wang. Theory and simulation of the self-assembly of rod–coil block copolymer melts: recent progress. *Soft Matter*, 7(8):3711–3716, 2011. 105

[117] Wendi Song, Ping Tang, Hongdong Zhang, Yuliang Yang, and An-Chang Shi. New numerical implementation of self-consistent field theory for semiflexible polymers. *Macromolecules*, 42(16):6300–6309, 2009. 105

[118] Raul Cruz Hidalgo, DE Sullivan, and Jeff ZY Chen. Smectic phases in rod–coil diblock copolymers. *Journal of Physics: Condensed Matter*, 19(37):376107, 2007. 105

[119] Roland R Netz and M Schick. Liquid-crystalline phases of semiflexible diblock copolymer melts. *Physical review letters*, 77(2):302, 1996. 105

[120] Wenlin Zhang, Enrique D Gomez, and Scott T Milner. Surface-induced chain alignment of semiflexible polymers. *Macromolecules*, 49(3):963–971, 2016. 105

[121] Jeff ZY Chen and DE Sullivan. Free energy of a wormlike polymer chain confined in a slit: crossover between two scaling regimes. *Macromolecules*, 39(22):7769–7773, 2006. 105

[122] JZY Chen, DE Sullivan, and X Yuan. Model for wormlike polymers confined between hard walls. *EPL (Europhysics Letters)*, 72(1):89, 2005. 105

[123] Jeff ZY Chen. Theory of wormlike polymer chains in confinement. *Progress in Polymer Science*, 54:3–46, 2016. 105, 106, 108

[124] Shiwei Ye, Pingwen Zhang, and Jeff ZY Chen. Surface-induced phase transitions of wormlike chains in slit confinement. *Soft Matter*, 12(11):2948–2959, 2016. 105

[125] Hsiao-Ping Hsu, Wolfgang Paul, and Kurt Binder. Breakdown of the kratky-porod wormlike chain model for semiflexible polymers in two dimensions. *EPL (Europhysics Letters)*, 95(6):68004, 2011. 105

[126] Hsiao-Ping Hsu, Wolfgang Paul, and Kurt Binder. Polymer chain stiffness vs. excluded volume: A monte carlo study of the crossover towards the worm-like chain model. *EPL (Europhysics Letters)*, 92(2):28003, 2010. 105

[127] Jörg Baschnagel, Hendrik Meyer, Joachim Wittmer, Igor Kulić, Hervé Mohrbach, Falko Ziebert, Gi-Moon Nam, Nam-Kyung Lee, and Albert Johner. Semiflexible chains at surfaces: Worm-like chains and beyond. *Polymers*, 8(8):286, 2016. 105, 106

[128] O Kratky and G Porod. Röntgenuntersuchung gelöster fadenmoleküle. *Recueil des Travaux Chimiques des Pays-Bas*, 68(12):1106–1122, 1949. 106

[129] Eugene Helfand and Yukiko Tagami. Theory of the interface between immiscible polymers. ii. *The Journal of chemical physics*, 56(7):3592–3601, 1972. 107

[130] Friederike Schmid and Marcus Mueller. Quantitative comparison of self-consistent field theories for polymers near interfaces with monte carlo simulations. *Macromolecules*, 28(25):8639–8645, 1995. 107, 111

[131] Ying Jiang and Jeff ZY Chen. Self-consistent field theory and numerical scheme for calculating the phase diagram of wormlike diblock copolymers. *Physical Review E*, 88(4):042603, 2013. 108

[132] Qin Liang, Jianfeng Li, Pingwen Zhang, and Jeff ZY Chen. Modified diffusion equation for the wormlike-chain statistics in curvilinear coordinates. *The Journal of chemical physics*, 138(24):244910, 2013. 108

[133] MG Bawendi and Karl F Freed. A wiener integral model for stiff polymer chains. *The Journal of chemical physics*, 83(5):2491–2496, 1985. 108

[134] Jolanta B Lagowski, Jaan Noolandi, and Bernie Nickel. Stiff chain modelfunctional integral approach. *The Journal of chemical physics*, 95(2):1266–1269, 1991. 108

[135] Andrew J Spakowitz and Zhen-Gang Wang. End-to-end distance vector distribution with fixed end orientations for the wormlike chain model. *Physical Review E*, 72(4):041802, 2005. 109

[136] Semjon Stepanow and Gunter M Schütz. The distribution function of a semiflexible polymer and random walks with constraints. *EPL (Europhysics Letters)*, 60(4):546, 2002. 109

[137] Shafigh Mehraeen, Bariz Sudhanshu, Elena F Koslover, and Andrew J Spakowitz. End-to-end distribution for a wormlike chain in arbitrary dimensions. *Physical Review E*, 77(6):061803, 2008. 109

[138] Jan Wilhelm and Erwin Frey. Radial distribution function of semiflexible polymers. *Physical review letters*, 77(12):2581, 1996. 109

[139] NB Becker, A Rosa, and R Everaers. The radial distribution function of worm-like chains. *The European Physical Journal E*, 32(1):53–69, 2010. 109

[140] Xiangyu Bu and Xinghua Zhang. Scattering and gaussian fluctuation theory for semiflexible polymers. *Polymers*, 8(9):301, 2016. 109

[141] Xinghua Zhang, Ying Jiang, Bing Miao, Yunlin Chen, Dadong Yan, and Jeff ZY Chen. The structure factor of a wormlike chain and the random-phase-approximation solution for the spinodal line of a diblock copolymer melt. *Soft Matter*, 10(29):5405–5416, 2014. 109

[142] Erwin Kreyszig. *Advanced engineering mathematics*. John Wiley & Sons, 2010. 113, 114

[143] Blaber S, Mahmoudi P, Spencer R, and Matsen M.W. work in progress. 2018. 117, 118

Appendices

Appendix A

Convolution integral for infinitely long chains

As seen in equation 2.25, the propagator is determined through a convolution integral, which will be the case for $N \to \infty$ as well. Using the notation defined before, the integral will now be

$$G_\infty(z) = h_\infty(z) \int g(Z) G_\infty(z - Z) \mathrm{d}Z \ . \tag{A.1}$$

By noting that the coordinate is placed on discrete points, this integral is actually a sum. Hence, with a change of variables, $z - Z = z'$, it becomes

$$G_\infty(z) = h_\infty(z) \sum_{z'} g(z - z') G_\infty(z') = \sum_{z'} h_\infty(z) g(z - z') G_\infty(z') \ . \tag{A.2}$$

The previous equation is seen to be similar to a matrix equation, *i.e* if $G_\infty(z) = X$ and $A(z, z') = h_\infty(z) g(z - z')$, we have $X = AX$. As this is not seen to be symmetric, a few alterations should provide us with a symmetric matrix that will make the calculations much more efficient. After rewriting the previous equation as follows,

$$\frac{G_\infty(z)}{\sqrt{h_\infty(z)}} = \sum_{z'} \sqrt{h_\infty(z)} \sqrt{h_\infty(z')} g(z - z') \frac{G_\infty(z')}{\sqrt{h_\infty(z')}} \ , \tag{A.3}$$

we get

$$\frac{G_\infty(z)}{\sqrt{h_\infty(z)}} = A \frac{G_\infty(z')}{\sqrt{h_\infty(z')}} \ , \tag{A.4}$$

where A is a symmetric real matrix given by $A(z, z') = g(z - z') \sqrt{h_\infty(z)} \sqrt{h_\infty(z')}$. By using this method, G_∞ can be determined from solving $X = AX \Rightarrow (A - I)X = 0$, where $X = G_\infty(z)/\sqrt{h_\infty(z)}$ is the eigenvector corresponding to an eigenvalue of 1.

Appendix B

Wormlike Chain model

Polymers are not all completely flexible and in fact possess a degree of rigidity in their backbone due to factors such as the chemistry of the constituent monomers, the type of bonds or steric effects. These chains cannot be accurately described with the models presented thus far and require a representation with the ability to incorporate stiffness of the chains. The worm-like chain model developed by Saito *et al.* [105] can provide the means for a more realistic consideration of these chains, as it takes their local bending into account. Chain stiffness has been seen to affect various aspects regarding the properties of chains such as the phase behavior of copolymers [107, 108, 109, 110, 111, 112] and homopolymers [113, 114, 115], the structures they form [116, 117, 118, 119], as well as chain alignment [120] and the response to confinement [17, 121, 122, 123, 124] to name a few. Due to the additional parameter considered in this model for chain rigidity, which is usually given by a bending modulus, $\mathcal{K}$, it does involve extra layers of complexity with respect to its calculations compared to the other models mentioned thus far. Consequently, a considerably lower number of theoretical works have utilized it in their studies and even then, some have opted to facilitate the calculations by looking at the systems in the limits of high/low flexibility for which the theory can be simplified.

Despite the clear advantages offered by this model, there have been some issues raised towards its applicability in certain cases, such as its treatment of polymers in good solvents where excluded volume interactions find importance [125, 126, 127]. While taking these shortcomings into consideration, there is no doubt of it providing a clear advantage over the older models utilized, due to the higher degree of accuracy and tunability in its representation of the polymer chains. This widespread applicability of the worm-like chain model in providing a more realistic representation of various systems, ensures the pursuit towards the exploitation of all its available features. In terms of methods used for incorporation of this model into studies, both simulations as well as theoretical attempts have contributed to the available insight from literature. A number of simulations have looked

at the behavior of semi-flexible chains, due to their high technological and industrial importance, using lattice MC methods for which detailed reviews are outside the scope of the current document and have been addressed elsewhere [127]. It is worth noting that these attempts still dealt with the problem of having an artificial lattice present, as was outlined in the previous chapters. In this light, evidently the focus needs be shifted to off-lattice models which include MC simulations, MD methods in addition to theoretical work. We will choose to focus on the theoretical developments made thus far, for which a review will be presented, followed by the consideration of extending our previous study to incorporate this model.

B.1 Literature review

The initial model proposed in 1949 by Kratky and Porod [128] was based on a discrete representation of a polymer chain with a bending penalty, which later on lead to the establishment of a continuous counterpart denoted as the worm-like chain model [123] presented by Saito *et al.* [105] in 1967. In this work, they obtained the average end-to-end distances for stiff chains of both constant and variant lengths, by first enforcing and then relaxing the condition for the tangent vector to be a unit vector in each respective scenario. The comparison of their results to the limits of flexible (Gaussian) as well as rigid chains, for which the end-to-end distances are well known, is used to confirm the validity of their results. They also looked at obtaining the scattering function of this model before providing insight on the motion of these chains. For comparing the results of the worm-like chain to both the very rigid and very flexible limits, there are two length scales of the chain that find significance. The flexibility of polymer chains can be considered in terms of the ratio of their contour length, l_c, which is the total length of the chain, to the persistence length, l_p, that is the distance along the contour over which orientational correlations decay [5, 90]. When $l_c/l_p \gg 1$, the chain is flexible on the large scales and rigid on scales smaller than l_p. If however l_p becomes comparable to the bond length b, the chain is mostly flexible [127] and when $l_c/l_p \ll 1$ the chains are fairly rigid.

Morse *et al.* [70] applied a self-consistent field theory approach to find the equilibrium properties of the interfaces formed from semi-flexible polymeric components. They utilized the worm-like chain model, focusing on the two limits of completely rigid (high $\mathcal{K}$) as well flexible chains (Gaussian limit at low $\mathcal{K}$). In this light, they could compare the results obtained using this model to other well known calculations for each case, prior to focusing on intermediate rigidity and its effects. Their chain Hamiltonian contained a term allocated to the bending energy as well as a field representing the interaction of each

monomer with the average environment, as is the case in the mean-field treatment. To calculate average monomer densities, the propagators require evaluation which are seen to satisfy a generalized diffusion equation that is solved subject to an initial condition. For the worm-like chain model, the resultant concentration is seen to be a function of not only the position, but the orientation of the chains as well. Their results focused on the chains with dimensions much larger than their persistence length, $l_p = \mathcal{K}b$, with b giving the bond length. From these assumptions, they simplified the equation required for the determination of the propagator, which was solved numerically for the large N limit. They also evaluated the surface tension for various rigidity of chains, which was seen to agree with the flexible chain limit [129] as $\mathcal{K}$ was reduced.

In the work of Schmid *et al.* [130], they use the rigidity constraint from the worm-like chain model to look at the interfaces of a blend of homopolymers. Additionally, they include the formalism for the Gaussian chain limit of their system, such that comparisons can be made between both models. For obtaining the solution for the semiflexible chains, they expand the orientational dependence of the propagator in terms of Legendre polynomials and present the resultant form after incorporating the simplifications stemming from this expansion. The consideration of the distribution of chain ends at the interface leads to the conclusion of there being an entropic preference for them to reside in their vicinity, which results in the chains adopting a parallel orientation in that region. Their results for chains of various rigidities are compared to MC simulations as well as the Gaussian chain limit, whereby both the advantages and the downfalls of SCFT are noted. Another instance of incorporating the worm-like chain model using SCFT was subsequently developed by Matsen [107] some years later. He uses this model to account for the effect of rigidity on the order-disorder transition (ODT) of block copolymer melts, whereby the rigidity of chains is pointed out to be influential for microstructures formed by the molecules, specially when l_p is comparable to the interfacial width ξ. In this work, periodically ordered structures are being considered, which motivates expansions for both the spatial and orientational dependence of the partition function required for solving the diffusion equation. In terms of results, a shift is seen in the ODT as the rigidity changes, which is attributed to reductions in conformational entropy.

Some years later, Daoulas [38] *et al.* utilized this worm-like chain model to study the behavior of polymers at solid interfaces. In the adsorption problem being considered, they mention rigidity to be influential in determining the entropic penalty of the polymer being close to the surface, which is in competition with the enthalpic gain. They noted the fact that with the chain stiffness being incorporated in only the worm-like model, comparing its results to those obtained from the Gaussian chain will result in a significance difference in observations for the system. With this in mind, they mention the advantage of the

worm-like chain model to stem from its incorporation of an additional length scale, *i.e.* l_p, which results in its enhanced capability in predicting key properties exhibited from the chains. They develop the formalism for the polymer adsorption problem using SCFT for a worm-like chain as well as the Gaussian chain model and compare their results to atomistic simulations to test their accuracy. For finding the propagators, they choose to expand the orientational dependence in terms of Legendre polynomials. After pointing out the lack of an extensive consideration on the numerical methods required to solve this equation for the problem of polymers at an interface, they present the details for the implementation of the calculation as well as the stability criterion. In this work they observe better agreement between the atomistic results and the worm-like chain model compared to the Gaussian chain, which shows the superior capabilities of the former model. Nonetheless, the results of both are said to converge for high molecular weights since the effects of local chain structure on global chain conformations are seen to decrease.

As is discernible from the aforementioned literature, there is a distinct lack of theoretical works using the worm-like chain model, owing from the difficulties involved in obtaining its solutions. The majority this model's applications consist of considering the structures formed by diblock copolymers by incorporating different persistence lengths in each block or altering the rigidity of the copolymer chains, or looking at the effect of changing the polymer concentration in solutions in order to obtain the phase behavior of these molecules [131]. There are additional considerations pointed out for the worm-like chain model, such as the ease of evaluating some problems in curvilinear coordinates [132], having the right boundary conditions at the walls adjacent to these melts [123] as well as difficulties arising from the constraint of having the tangent vector scaled to be a unit vector. Attempts at relaxing the latter restriction mentioned have been conducted using alternative implementations, which in some instances are observed to cause undesirable effects [133, 134]. Evidently, there is a distinct gap in considering the behavior of neat melts using this model, which is what we hope to achieve and contribute to. With the entropic effect being considered in the prior chapters, the presence of a surface was seen to affect the conformational entropy of the system, hence resulting in certain components being enriched there. For the monodisperse melt, we have observed an enrichment of chain ends at the surfaces of these melts, as was also noted in the work mentioned above. In hopes of expanding and strengthening our understanding of this phenomenon, as well as previous literature which have suggested chain stiffness to play a vital role in these entropic effects, the additional parameter of chain rigidity is incorporated into the calculations. We will highlight the extension of the previous theoretical steps to include this new model and note the numerical methods that will be required to find the solution for it in the following sections.

B.2 Theory

The statistics of worm-like chains are not as readily determined as the flexible ones, hence the determination of quantities such as the distribution function for their end-to-end distance has been the focus of various studies [135, 136, 137, 138, 139]. As noted previously, the inextensibility constraint of this model results in difficulties and challenges for obtaining the statistics throughout the range of rigidities possible. Nevertheless, it has been incorporated into the majority of works utilizing the worm-like chain model due to the results having a higher degree of accuracy. By having good knowledge on the statistical behavior of these systems, quantities such as the single chain structure function can be determined. This quantity has great value in that it can be readily compared to experimental results obtained using scattering techniques, which give great insight into local and global structural details of the system at various length scales. The methods used to obtain the structure function for the worm-like chain as well as their developments are well summarized in recent reviews [140, 141] and obtained for any dimensionality in ref [137].

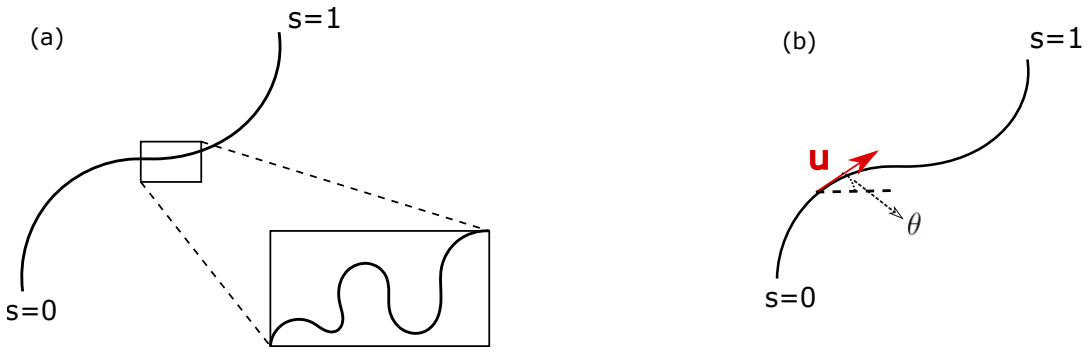

Figure B.1: Schematic of the (a) Gaussian and the (b)worm-like chains

For introducing the theory for the worm-like chain, it is useful to provide comparisons to state how it differs from the well known Gaussian model, hence schematics for both are presented in figure B.1. For the Gaussian chain, there is an energy penalty for local stretching but none for local bending, whereas the latter is taken into account in the worm-like chain model. The smallest characteristic length scale in the Gaussian chain is the statistical segment length, a, whereas for the worm-like chain it is the segment bond length, b, which is taken to be a constant in the method being applied here. This last constraint results in a constant total chain contour length $l_c = Nb$ where N is the

number of monomers as before. Both models have a space curve $\boldsymbol{r}_\alpha(s)$ where $s \in [0,1]$ gives the position along the chain backbone and α specifies each of the n chains in the system. In addition, the worm-like chain has a tangent vector $\mathbf{u}_\alpha(s) \equiv \dfrac{1}{bN}\dfrac{d}{ds}\mathbf{r}_\alpha(s)$ which is constrained to be a unit vector $|\mathbf{u}_\alpha(s)| = 1$. We are considering a monodisperse melt here with n polymers each containing N monomers and the total volume $V = nN/\rho_0$. With these definitions, the propagators are not only a function of the chain position, $\boldsymbol{r}_\alpha(s)$, as well as the placement along the contour length, s, but the orientation at that position determined by the tangent vector as well. In other words, compared to the Gaussian chain which would have $G(\boldsymbol{r}, s)$, for the model at hand we have $G(\boldsymbol{r}, \mathbf{u}, s)$. As before, we need to find the propagators, in order to determine the total partition function and subsequently, the concentration. To this end, a modified diffusion equation bearing resemblance to the one required for the calculation of the Gaussian chain propagators, must be solved.

We shall be looking at the surface behavior of the ends of these polymer chains which will have an excess followed by a depletion in the bulk. This depletion will be compared to the universal form we have for the Gaussian chain limit, which should hold in the flexible limit of the worm-like chain model ($l_c \gg l_p$ or $\mathcal{K} \to 0$). It will be interesting to see how the chain stiffness affects this entropic excess of ends since real polymer chains exhibit rigidity in their backbones. The surface of this melt will once more be created by having a sigmoidal target profile of a given width (ξ) and adjusting the field such that the concentration conforms to this shape. Before stepping into the equations at hand, it is worth mentioning what the independent parameters of the study are. A multitude of length scales are needed here which are not all separate and uncorrelated from one another. The ones required for the study are l_p , l_c and ξ. We will look at the results in terms of the ratios l_p/ξ and l_c/ξ for a defined surface width, which are seen to fully define the system. Moreover, separate studies using the Gaussian chain model will be conducted, for which we will use the length scale of the rms end-to-end length scaled by the interfacial width R_0/ξ to compare. For the Gaussian chain, which will also be the flexible limit of the worm-like chain, we have

$$R_0 = a\sqrt{N} \xrightarrow{a=b\sqrt{2\mathcal{K}} \quad [70]} \sqrt{2b^2\mathcal{K}N} = \sqrt{2l_p l_c} \quad , \tag{B.1}$$

which helps clarify the relationship between these different length scales.

Calculations

As recurrently shown in the theoretical sections of this work, we need to find the propagators from which the total partition function can be found and the concentration subsequently determined. The total concentration will be compared to the target shape and the field, w, adjusted if necessary. After the completion of the aforementioned steps, we will be interested in determining the concentrations of end monomers at the surfaces of these monodisperse melts in order to observe the effect of chain rigidity on the amount of entropic excess at the surface. The process of evaluating the propagators for the worm-like chain model presented here will be seen to be more involved than what is required for the Gaussian chain. The details of the latter will not be covered in this section in sake of brevity, as well as in-depth elaborations presented for it elsewhere [12, 38, 130]. To look at the more general case, the worm-like chain is first considered in 3d whereby determining the propagator $G(\mathbf{r}, \mathbf{u}, s)$ would allow the evaluation of the single chain partition function from

$$Q = \int \mathrm{d}\mathbf{r}\, \mathrm{d}\mathbf{u}\, G(\mathbf{r}, \mathbf{u}, s) G^{\dagger}(\mathbf{r}, \mathbf{u}, s) \ , \tag{B.2}$$

with G given by the modified diffusion equation

$$\frac{\partial G}{\partial s} + bN\mathbf{u} \cdot \nabla_r G = \frac{N}{2\mathcal{K}} \nabla_u^2 G - w(\mathbf{r}) G \ . \tag{B.3}$$

By considering $l_c = Nb$ and $l_p = \mathcal{K}b$, the equation is seen to be defined in terms of only these two length scales as mentioned before

$$\frac{\partial G}{\partial s} + l_c\mathbf{u} \cdot \nabla_r G = \frac{l_c}{2l_p} \nabla_u^2 G - w(\mathbf{r}) G \ . \tag{B.4}$$

Similar to the previous chapters, the propagator for the other end of the chain for a homopolymer is given by $G^{\dagger}(\mathbf{r}, \mathbf{u}, s) = G(\mathbf{r}, -\mathbf{u}, 1-s)$. The total concentration could then be determined from

$$\phi(\mathbf{r}) = \frac{1}{Q} \int_0^1 \mathrm{d}s \int \mathrm{d}\mathbf{u}\, G(\mathbf{r}, \mathbf{u}, s) G(\mathbf{r}, -\mathbf{u}, 1-s) \ . \tag{B.5}$$

As in our previous theoretical calculations, when a surface is placed at the origin of the z coordinate and there is spatial invariance in the other two directions, the field only depends on one coordinate and hence becomes $w(z)$ in place of $w(\mathbf{r})$. In this sense we have $G(z, u_z, s)$ instead of $G(\mathbf{r}, \mathbf{u}, s)$ where $u_z = |\mathbf{u}| \cos\theta = \cos\theta$ with the angle being defined with respect to the z axis, as seen in figure B.1. With these simplifications, equation B.4 becomes

$$\frac{\partial G}{\partial s} + l_c u_z \frac{\partial G}{\partial z} = \frac{l_c}{2l_p} \nabla_u^2 G - w(z) G \ , \tag{B.6}$$

which will give the concentration by

$$\phi(z) = \frac{1}{Q} \int_0^1 \mathrm{d}s \int_{-1}^1 \mathrm{d}u_z \, G(z, u_z, s) G(z, -u_z, 1-s) \ , \tag{B.7}$$

with

$$Q = \int_0^L \mathrm{d}z \int_{-1}^1 \mathrm{d}u_z \, G(z, u_z, s) G(z, -u_z, 1-s) \ . \tag{B.8}$$

Here the size of the system in the z direction, L, is chosen to be suitably large so as to allow bulk properties to be obtained far away from the surface. The problem now comes down to solving equation B.6 for which there have been a few approaches, as noted in the literature review. In this work, we choose to expand the orientational dependence of $G(z, u_z, s)$ using Legendre polynomials which will simplify the modified diffusion equation. Moreover, the properties of these polynomials give us a relatively simpler form for the aforementioned equation, which aid the development of a straightforward numerical method of calculation. Let us first determine what the propagator expansion will look like.

$$G(z, u_z, s) = \sum_{l=0}^{\infty} \underbrace{G_l(z, s)}_{\text{independent of } u} \overbrace{P_l(u_z)}^{\text{function of } \cos\theta} \ . \tag{B.9}$$

As seen in the equation above, the dependence on direction has been separated from the two other variables, which will prove to be useful in the subsequent equations. By determination of the propagator in this manner, the derivatives required for solving equation B.6 can be written accordingly. That is to say, they become

$$\frac{\partial G}{\partial s} = \sum_l \frac{\partial G_l}{\partial s} P_l(u) \ , \tag{B.10}$$

$$\frac{\partial G}{\partial z} = \sum_l \frac{\partial G_l}{\partial z} P_l(u) \ , \tag{B.11}$$

$$\nabla_u^2 G = \sum_l G_l \nabla_u^2 P_l(u) \ . \tag{B.12}$$

Before insertion of these forms into equation B.6, we note two properties of Legendre polynomials that will be useful for further simplification, which are $\nabla_u^2 P_l(u) = -l(l+1)P_l(u)$ and $P_1(u_z) = u_z$. By taking these into account, the form of the modified diffusion equation becomes

$$\sum_l \frac{\partial G_l}{\partial s} P_l(u) + l_c P_1(u) \sum_l \frac{\partial G_l}{\partial z} P_l(u) = -\frac{l_c}{2l_p} \sum_l G_l l(l+1) P_l(u) - w(z) \sum_l G_l P_l(u) \ , \tag{B.13}$$

which evidently requires further simplification. By noting the orthogonality of Legendre polynomials [142], it would seem that we could benefit from the multiplication of the equation above by a Legendre polynomial of a different degree which would evidently be followed by an integration. The expression for the aforementioned orthogonality relation of the Legendre polynomials is given below, by noting their weighting function to be 1. As for the norm, which corresponds to the evaluation of the integral when the order of the two polynomials are identical, the value is obtained from concepts outlined in detail by mathematical texts [142]. Thus, we observe the following for the integral of two Legendre polynomials

$$\int \mathrm{d}u_z P_l(u_z) P_{l'}(u_z) = \frac{2}{2l+1} \delta_{ll'} \ . \tag{B.14}$$

By consideration of equation B.13 in conjunction with equation B.14 there is a clear opportunity for simplification. That is to say, it would appear that we could make the latter relation show up in the former by multiplying equation B.13 by $P_{l'}$ and integrating over the dependent variable. This will give

$$\begin{aligned} \sum_l \frac{\partial G_l}{\partial s} \int \mathrm{d}u \, P_l(u) P_{l'}(u) + l_c \sum_l \frac{\partial G_l}{\partial z} \int \mathrm{d}u \, P_1(u) P_l(u) P_{l'}(u) \\ = -\frac{l_c}{2l_p} \sum_l G_l l(l+1) \int \mathrm{d}u \, P_l(u) P_{l'}(u) - w(z) \sum_l G_l \int \mathrm{d}u \, P_l(u) P_{l'}(u) \ , \end{aligned} \tag{B.15}$$

such that it simplifies to

$$\frac{\partial G_l}{\partial s} + \frac{l_c(2l+1)}{2} \sum_{l'} \frac{\partial G_{l'}}{\partial z} \Gamma_{1ll'} = -\frac{l_c}{2l_p} G_l l(l+1) - w(z) G_l \ , \tag{B.16}$$

where $\Gamma_{1ll'} = \int \mathrm{d}u\, P_1 P_l(u) P_{l'}(u)$. This remaining integral is another well known property of these polynomials [142]. It is shown to be

$$\Gamma_{1ll'} = \int \mathrm{d}u_z\, u_z P_l(u_z) P_{l'}(u_z) = \begin{cases} \dfrac{2(l+1)}{(2l+1)(2l+3)}\ , & \text{for } l' = l+1 \\ \\ \dfrac{2l}{(2l-1)(2l+1)}\ , & \text{for } l' = l-1 \end{cases}$$

which means that the sum over l' in equation B.16 only contains two non zero terms, which further simplifies it to be

$$\begin{aligned} \frac{\partial G_l}{\partial s} + \frac{l_c(2l+1)}{2}\left[\frac{\partial G_{l+1}}{\partial z}\Gamma_{1l(l+1)} + \frac{\partial G_{l-1}}{\partial z}\Gamma_{1l(l-1)}\right] &= -\frac{l_c}{2l_p} G_l l(l+1) - w(z) G_l \Rightarrow \\ \frac{\partial G_l}{\partial s} + l_c\left[\frac{\partial G_{l+1}}{\partial z}\frac{l+1}{2l+3} + \frac{\partial G_{l-1}}{\partial z}\frac{l}{2l-1}\right] &= -\frac{l_c}{2l_p} G_l l(l+1) - w(z) G_l\ . \end{aligned} \tag{B.17}$$

By expanding the propagators in this manner and using the properties of Legendre polynomials, we have gone from finding the solution for equation B.6 to determining the answer to equation B.17. This is now the point where we will have to introduce a suitable boundary condition for the propagator, as well as a numerical method of solving each of the remaining derivatives. As seen in equation B.9, $G_l(z,s)$ is a function of two variables and will need to be determined in terms of each. For the initial point of the chain contour we have $G_l(z, s=0) = \delta_{l,0}$, which signifies the system being isotropic as well as homogeneous since there is no preference for the orientation or the position of the end. As for the direction in space, reflecting boundary conditions are considered. For the evaluation of the derivatives, as well as the method to solve the equation such that it is stable, we follow the mannerism proposed in [38], an outline of which will be the focus of the subsequent section.

Numerics

We have derivatives in equation B.17 that require evaluation, one with respect to the direction in space and the other with respect to the chain contour variable. These derivatives will need to be evaluated numerically, for which the chosen methods are identical to the ones utilized by Daoulas *et al.* [38] due to the similarities of the problems being considered. For the derivative with respect to s, they applied a first-order forward method and a second-order central for the one with respect to z, which will give

$$\frac{\partial G}{\partial s} \approx \frac{G(s+\Delta s) - G(s)}{\Delta s} \,, \tag{B.18}$$

$$\frac{\partial G}{\partial z} \approx \frac{G(z+\Delta z) - G(z-\Delta z)}{2\Delta z} \,, \tag{B.19}$$

with Δs and Δz denoting the discretized steps taken along the chain length and in the z direction, respectively. The leading order term for the error involved is mentioned to be $-\frac{\Delta s}{2}\frac{\partial^2 G_l}{\partial s^2}$ which needs to be added to the right hand side of equation B.17. To evaluate this term, equation B.17 should be differentiated with respect to s, which gives

$$\frac{\partial^2 G_l}{\partial s^2} + l_c\left[\frac{l+1}{2l+3}\frac{\partial^2 G_{l+1}}{\partial s \partial z} + \frac{l}{2l-1}\frac{\partial^2 G_{l-1}}{\partial s \partial z}\right] = -\frac{l_c}{2l_p} l(l+1)\frac{\partial G_l}{\partial s} - w(z)\frac{\partial G_l}{\partial s} \,. \tag{B.20}$$

As noted by the aforementioned work [38] and in light of the multitude of equations involved, the notation can be simplified by utilizing D to show the derivatives which would make equation B.20 become

$$D_{ss}G_l + l_c\left[\frac{l+1}{2l+3}D_{sz}G_{l+1} + \frac{l}{2l-1}D_{sz}G_{l-1}\right] = -\frac{l_c}{2l_p} l(l+1)D_s G_l - w(z)D_s G_l \,. \tag{B.21}$$

In order for $D_{ss}G_l$ to be obtained from equation B.21, we require knowledge on $D_{sz}G_{l+1}$ and $D_{sz}G_{l-1}$. We can determine the first derivatives of these two terms with respect to s from equation B.17 by changing l to $l+1$ and $l-1$, respectively. If we differentiate these expressions with respect to z, we obtain the quantities needed for the calculation. Hence, first by writing equation B.17 for these two indices we have

$$D_s G_{l+1} + l_c \left[\frac{l+2}{2l+5} D_z G_{l+2} + \frac{l+1}{2l+1} D_z G_l \right] = -\frac{l_c}{2l_p}(l+1)(l+2)G_{l+1} - w(z)G_{l+1} \ , \tag{B.22}$$

$$D_s G_{l-1} + l_c \left[\frac{l}{2l+1} D_z G_l + \frac{l-1}{2l-3} D_z G_{l-2} \right] = -\frac{l_c}{2l_p}(l-1)(l)G_{l-1} - w(z)G_{l-1} \ . \tag{B.23}$$

Now taking the derivative with respect to z we obtain

$$\begin{aligned} D_{zs} G_{l+1} + l_c \left[\frac{l+2}{2l+5} D_{zz} G_{l+2} + \frac{l+1}{2l+1} D_{zz} G_l \right] &= -\frac{l_c}{2l_p}(l+1)(l+2)D_z G_{l+1} \\ &\quad - w(z)D_z G_{l+1} - G_{l+1} D_z w(z) \end{aligned} \tag{B.24}$$

$$\begin{aligned} D_{zs} G_{l-1} + l_c \left[\frac{l}{2l+1} D_{zz} G_l + \frac{l-1}{2l-3} D_{zz} G_{l-2} \right] &= -\frac{l_c}{2l_p}(l-1)(l)D_z G_{l-1} \\ &\quad - w(z)D_z G_{l-1} - G_{l-1} D_z w(z) \end{aligned} \tag{B.25}$$

A summary of the equations requiring evaluation is

$$D_s G_l \quad + l_c \left[\frac{l+1}{2l+3} D_z G_{l+1} \ + \frac{l}{2l-1} D_z G_{l-1} \right] = -\frac{l_c}{2l_p} G_l l(l+1) - w(z)G_l + \frac{\Delta s}{2} D_{ss} G_l \tag{B.26}$$

$$D_{ss} G_l \quad + l_c \left[\frac{l+1}{2l+3} D_{sz} G_{l+1} + \frac{l}{2l-1} D_{sz} G_{l-1} \right] = -\frac{l_c}{2l_p} l(l+1) D_s G_l - w(z) D_s G_l \tag{B.27}$$

$$\begin{aligned} D_{zs} G_{l+1} + l_c \left[\frac{l+2}{2l+5} \ D_{zz} G_{l+2} + \frac{l+1}{2l+1} \ D_{zz} G_l \right] &= -\frac{l_c}{2l_p}(l+1)(l+2)D_z G_{l+1} \\ &\quad - w(z)D_z G_{l+1} - G_{l+1} D_z w(z) \end{aligned} \tag{B.28}$$

$$\begin{aligned} D_{zs} G_{l-1} + l_c \left[\ \frac{l}{2l+1} D_{zz} G_l + \frac{l-1}{2l-3} D_{zz} G_{l-2} \right] &= -\frac{l_c}{2l_p}(l-1)(l)D_z G_{l-1} \\ &\quad - w(z)D_z G_{l-1} - G_{l-1} D_z w(z) \end{aligned} \tag{B.29}$$

The order of the calculation will be as follows. Initially equations B.29 and B.28 require evaluation such that $D_{ss}G_l$ can be determined from equation B.27. This in turn, will allow the calculation of the propagator for the next step in the contour from equation B.26 since we know what it will be at $s = 0$ from the condition set for this boundary. By following this methodology, we will require derivatives which are first order with respect to s as well as first and second order for z. The first two are evaluated using the schemes given by equations B.18 and B.19, the last one is determined through a second order central method given by

$$D_{zz}G = \frac{\partial^2 G}{\partial z^2} \approx \frac{G(z + \Delta z) - 2G(z) + G(z - \Delta z)}{(\Delta z)^2} \ . \tag{B.30}$$

For the implementation of the method, a certain number of Legendre polynomials are required to represent the orientation dependence. Hence, there will be a value at which l will be truncated, for which the equations above will need to be solved up to that point. Furthermore, the coefficients are only dependent on system parameters as well as this value of the polynomial order, which grants us the ability to calculate them *a priori*. As mentioned in the theory section, through the governing equations we have confirmed l_c and l_p as influential lengths of the system. The interfacial width of the surface shape needs to be known, so that the target profile is defined and can be compared to the total concentration obtained. Hence, by knowing l_c/ξ as well as l_p/ξ for a chosen value of the width, *e.g.* $\xi = 1$, we will have all the information required to complete the study. We will conclude the section by presenting some preliminary results as obtained through collaborative work in our group led by Steven Blaber [143]. Furthermore, results for the Gaussian chain model were obtained for the same system and provided by Dr Russell Spencer from the group, which shall be compared to the flexible chain limit of our model.

Results

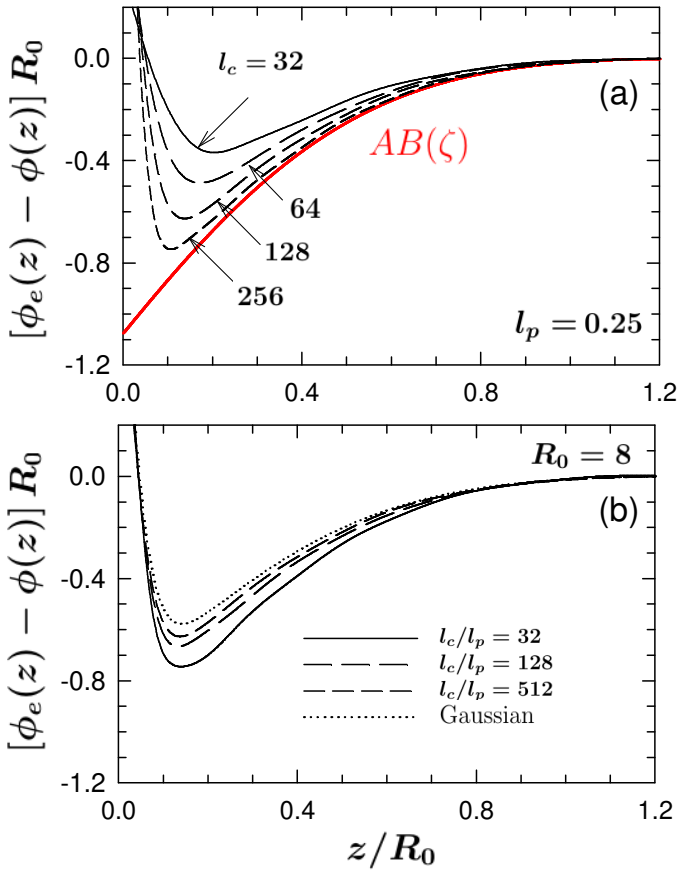

Figure B.2: Depletion of ends in the bulk for (a) constant persistence length $l_p = 0.25$ and (b) constant end-to-end length $R_0 = 8$

We conclude this chapter by presenting some preliminary results from our current work in progress [143]. This graph focuses on the depletion of ends in the bulk, which results from there being an excess of them at the surface. In previous chapters, we observed good agreement from comparing our semi-analytical predictions for this end depletion to off-lattice mean-field results in figure 3.6 as well as the lattice model mean-field and simulation results seen in figure 3.11. If these predictions are truly universal, they should also become valid as the worm-like chain approaches the Gaussian chain limit which is what is being investigated in figure B.2a. In this plot, for a small constant value of the persistence length, $l_p = 0.25$, compared to the width which is set to be $\xi = 1$ we see the

results from the worm-like chain model calculations for various values of the chain contour length, l_c. The red curve in this plot is the quantity $AB(\zeta)$, which was the prediction from the semi-analytical calculation for the end depletion as obtained in the previous chapters. As we would expect, with an increase in the chain contour lengths for a constant persistence length, l_c/l_p increases and chains become more Gaussian. In this light, we observe good agreement with the prediction shown by the red curve at high values of chain length. In part (b) the rms end-to-end distance, R_0, is kept to be the same hence by decreasing l_p, l_c needs to be increased such that as noted from equationB.1, which gave $R_0 = \sqrt{2l_p l_c}$, it is kept constant. Here, the dotted curve denotes results obtained from the Gaussian chain model from a separate calculation, which we see the worm-like chain results approach as the ratio l_c/l_p is increased.

From both of these plots we observe the worm-like chain results approaching the Gaussian chain ones, as the chain is made to be more flexible. This is in-line with our expectations as well as previous works that have considered this model. In addition, from the change observed in the amount of this bulk depletion as the chain stiffness is altered, the effect of rigidity on this entropic surface excess becomes apparent. This is as we had postulated in the previous chapters and provides evidence for the effectiveness of this new model for further exploration of these phenomena in the near future.